博士論文

The changes of elastic wave propagation in the process of rainfall induced slope surface failure

（斜面が豪雨によって表層崩壊する過程の弾性波伝播の変化）

Shangning TAO
陶尚寧

Student ID 17DE008

A thesis submitted to Saitama University in partial fulfillment of
the requirements for the degree of
Doctor of Philosophy
in
Civil Engineering

March, 2020

Department of Civil and Environmental Engineering

Saitama University, Tokyo, Japan

ABSTRACT

Rainfall-induced landslides commonly occur in mountainous areas and cause severe human and infrastructural damage around the world. Most of the previous landslides have occurred at shallow depths, generally less than 3 m, and the average thickness of the failed surface layer was 1.2 m. To mitigate damage caused by rainfall-induced landslides, physical countermeasures such as retaining walls, ground anchors and dewater systems are common, however, they are not economically feasible for the amount of potentially unstable slope. Therefore, landslide early warning systems are an alternative soft countermeasure that can provide an efficient and economical way to reduce the damage of landslides. A typical landslide early warning system is based on monitoring of soil moisture and pore pressure, or on measuring mass movement events by linear displacement transducers, inclinometers or extensometers, or measuring both the soil moisture and the displacement by soil moisture sensors and tilt sensors. These methods have recently been used because they are simple and easy to install in the slope surface layer. However, they can only sense the local area surrounding the position of the sensor. To cover a wide area of unstable slope, many sensors are required.

Elastic wave propagation in soil as a non-destructive monitoring technique has received considerable attention in recent years. The application of elastic wave propagation in soil has been developed by many researchers, for example, shear waves were measured in laboratory specimens by means of piezoelectric transducers, and recently, both shear wave (S-wave) and compression wave (P-wave) velocities were designed to measure the unsaturated soil. It was found that both P-wave and S-wave velocities decreased by nearly half when soil saturation was increased from 20% to 80% in laboratory triaxial experiments. A series of model experiments found that elastic wave velocities continuously decreased in response to moisture content and deformation.

In this study, a method of evaluating slope shear deformation and soil moisture by elastic wave is presented. Elastic wave devices include an exciter and several receivers

that are laid out within the slope surface layer to cover a relatively deep and wide area. To extend the former research, three main points have been improved in this study. Firstly, an exciter has been developed that can automatically generate clear and powerful elastic wave signals to propagate more than 1 m in soil. Secondly, an algorithm has been developed that can process the huge number of wave signals, and automatically detect the travel time and calculate the wave velocities. Thirdly, a full-scale multi-layer shear model was used to simulate the process of slope failure and observe the wave propagation. The detailed behavior of elastic wave propagation in soil over a wide range of soil moisture, shear stress, and shear deformation, can be explored. A series of tests were designed to reproduce the slope failure. The factors affect on elastic wave velocity have been confirmed.

In this study, not only the elastic wave velocities but also the wave attenuation has been investigated. A method using wave attenuation is presented to monitor slope deformations and soil moisture variations. It is an application of geometric spreading, which is as the wave moves away from the source, the area that the wave energy covers become larger and thus wave intensity decreases, and wave energy loss due to inelastic material behavior or internal friction during wave propagation. Laboratory experiments using a Multi-layer shear model were conducted, wave attenuation affected by shear forces corresponding with deformations on every layer, and the soil moistures in wet and dry processes have been analyzed.

To investigate the behavior of elastic wave propagation in the natural slope surface layer, elastic wave monitoring has been conducted at a slope located at Aso-shi, Kumamoto, Japan. This slope was suffered from the 2016 Kumamoto Earthquakes and some big cracks appeared on the slope surface. It is a typically unstable slope. The elastic wave monitoring devices include a fully automatic to generate elastic wave by the exciter, measure the wave signal by receivers. The layout of sensors and exciter underground and the monitoring parameters such as velocities, soil moisture, deformation from the tilt sensor are shown in detail. Elastic wave velocities and attenuation behaviors with

soil moisture on-site is similar to laboratory experiments.

These findings show that monitoring the wave propagation in a slope surface layer can indicate the status of soil moisture content and shear deformation. Slope instabilities may be predicted based on the historical record. Monitoring the changes in elastic waves in the slope surface layer is valuable and can be applied to an early warning system.

Keywords: *Slope failure; Early warning; Wave propagation; Compression wave velocity; Wave attenuation; Shear deformation; Multi-layer shear model, Unsaturated soil*

ACKNOWLEDGEMENT

I would like to express my greatest gratitude to my supervisor **Prof. Uchimura Taro**, for your practical advice and good ideas not only helped me to continue to think and conduct this research but also helped me to think how to settle the difficult problems in real-world along with the over three years' time. From the laboratory experiments and On-site investigation, processing the data, to the presentation, the discussions with Uchimura sensei helped me verify my research idea, help me to improve the abilities of the thinking and action in scientific research.

My appreciation and gratitude are extended to members of my research advisory committee **Prof. Jiro KUWANO, Prof. Masahiko OSADA** and **Prof. Yasunao MATSUMOTO** for their enlightening discussions and constructive comments on my research in general and this thesis in particular. I am grateful that they took time out of their busy schedules to be part of the evaluation committee.

Special appreciation is extended to the administrative staff of Department of Civil and Environmental Engineering and Foreign Student Officers for their consistent guidance and support during my study. I would like to thank Ms. Nara, secretary Geotechnical Laboratory, who took care of several administrative matters related to my research.

I really enjoy the time with Dr. Ho Manh Hung, Ali Murtaza Rasool, Aung Aung Soe, Tang Junfeng, Makoto Fukuhara, Pradeep Pokhrel, Albano Acacio Ajuda, Shah Syed Kamran Hussain, and Khola Iqbal, who have graduated and new join, and Dr. Chen Yulong and Huang Dong who suggested me to perform experiments. The relatives, teachers, and friends that could not be listed here all are thankful.

Best thanks to my wife and family for their endless love and supports throughout my life.

I gratefully acknowledge the financial supports provided by Grants-in-Aid for Scientific Research of Japan Society for the Promotion of Science (JSPS), Grant-in-Aid for JSPS Fellows (DC2).

I would like to keep this three-year experience, the people, the work, and the challenges as one of the best treasures in my mind.

Shangning Tao
March 2020
Tokyo, Japan

TABLE OF CONTENTS

List of Figures

List of Tables

CHAPTER 1

DISSERTATION OVERVIEW

The early warning system aims to save the life of people who live near the danger area of slope failure. This thesis presents my research and development of the method to evaluate soil moisture and shear deformation by elastic wave propagation in a shallow slope surface layer.

The objective is to develop an elastic wave measure system includes newly designed exciter, receivers and the Akaike's information criterion algorithm, which can automatically calculate the elastic wave travel time with accuracy and reliability, to investigate factors affect on the elastic wave and develop a method to predict the instabilities of slope by the elastic wave.

1.1 INTRODUCTION

Rainfall-induced landslides commonly occur in mountainous areas and cause severe human and infrastructural damage around the world. For example, in Europe, a total of 1370 deaths and 784 injuries were reported resulting from 476 landslides in the studied period 1995~2014, average economic loss per year in Europe is approximately 4.7 billion Euros (Haque et al., 2016). In the United States, every year landslides cause 25~50 fatalities and approximately 3.5 billion dollars of infrastructure damage (Lynn Highland, 2004). In Canada, thousands of landslides occur, damage to infrastructure and secondly loss properly exceeds $200 million annually (Brooks, 2001). Death tolls in less developed, populated regions are higher (e.g. Ancash, Peru, 1970, 18,000 deaths; Layte, Phillipines, 2006, 1,800 fatalities)(Mosher, 2008). In Japan, a statistical study on 19035 cases of landslides from 1972 to 2007 shows that 93% of those landslides were

caused by heavy rainfall. (Nobutomo et al., 2009). Therefore, the demand of countermeasures for landslides and slope instabilities induced by rainfall is on the rise in every country. Retaining walls and ground anchors are widely used as the typical mechanical countermeasures. However, they are not an economical solution for the amount of potential risk slopes. The early warning system is monitoring the slope by sensors, if it detects unstable status, inform people safely escape from the dangerous area as an alternative economic method. This study attempts to improve the existing landslide early warning system by developing a new technique to predict the instabilities of slope by elastic wave propagation in soil.

1.2 MOTIVATION & SIGNIFICANCE

Landslide is one of the most serious geological disasters. It is described as an outward and downward slope movement of an abundance of slope-forming materials including rock, soil, artificial, or even a combination of these things. According to the statistics of 132 landslides between 1999 and 2017, around 53% were triggered by rainfall (www.glidenumber.net). Rainfall induced landslides have caused substantial damage in many areas such as Japan(Okada et al., 2004), Hong Kong (Brand, 1981), USA (Baum and Godt, 2010), and Italy(Aleotti, 2004). Most of the previous landslides have occurred at shallow depths, generally less than 3 m, and the average thickness of the failed surface layer was 1.2 m, about 500,000 potentially dangerous slopes exist(Uchimura et al., 2015). To mitigate damage caused by rainfall-induced landslides, physical countermeasures (Popescu and Sasahara, 2008) such as retaining walls (Conte et al., 2017), ground anchors (Hutchinson, 1984) and dewater systems (Conte and Troncone, 2018) are common, however, they are not economically feasible for the amount of potentially unstable slope. Because rainfall-induced landslides spread usually very large areas (Uchimura et al., 2010), the protective measures also need to cover this large area (Figure 1.1). As a result, these physical measures are not feasible and economical. Therefore, landslide early warning systems are an alternative soft countermeasure that can provide an efficient and economical way to reduce the damage of landslides. Compared to physical countermeasures, although landslide early warning system may not be able to prevent landslide, but at least it can timely inform people in its surrounding to leave the dangerous area. It can take necessary countermeasures to

prevent the landslide if the warning comes early enough. Even if early warning systems may not be prevented the infrastructure to avoid the damage from landslide, yet it can save human lives, so it is a great enough contribution to invest in this field.

(**a**) (**b**)

Figure 1.1 Typical landslide protection works: (a) A physical countermeasures on an unstable slope (Kamakura, Kanagawa, Japan) (b) A larger prevention area of slope failure (Kanagawa, Japan)

1.3 PROBLEM STATEMENT

A typical landslide early warning system is based on monitoring of soil moisture and pore pressure (Baum and Godt, 2010), or on measuring mass movement events by linear displacement transducers (Arnhardt et al., 2007), inclinometers (Lollino et al., 2002) or extensometers (Angeli et al., 2000), or measuring both the soil moisture and the displacement by soil moisture sensors and tilt sensors (Uchimura et al., 2010). These methods have recently been used because they are simple and easy to install in the slope surface layer. However, they can only sense the local area surrounding the position of the sensor. To cover a wide area of the unstable slope, many sensors are required (Wang et al., 2018).

Elastic wave propagation in soil as a non-destructive monitoring technique has received considerable attention in recent years. The application of elastic wave propagation in soil has been developed by many researchers, for example, shear waves were measured in laboratory specimens by means of piezoelectric transducers (Brignoli et al., 1996),

and recently, both shear wave (S-wave) and compression wave (P-wave) velocities were designed to measure the unsaturated soil (Irfan and Uchimura, 2016). It was found that both P-wave and S-wave velocities decreased by nearly half when soil saturation was increased from 20% to 80% in laboratory triaxial experiments (Irfan et al., 2017). A series of model experiments found that elastic wave velocities continuously decreased in response to moisture content and deformation (Chen et al., 2017).

In this paper, a method of evaluating slope shear deformation and soil moisture by elastic wave is presented. Elastic wave devices include an exciter and several receivers that are laid out within the slope surface layer to cover a relatively deep and wide area, as shown in Figure 1.2. Laboratory experiments using a multi-layer shear model were conducted to reproduce the slope failure and to investigate soil moisture and shear deformation by elastic wave propagation in a shallow slope surface layer.

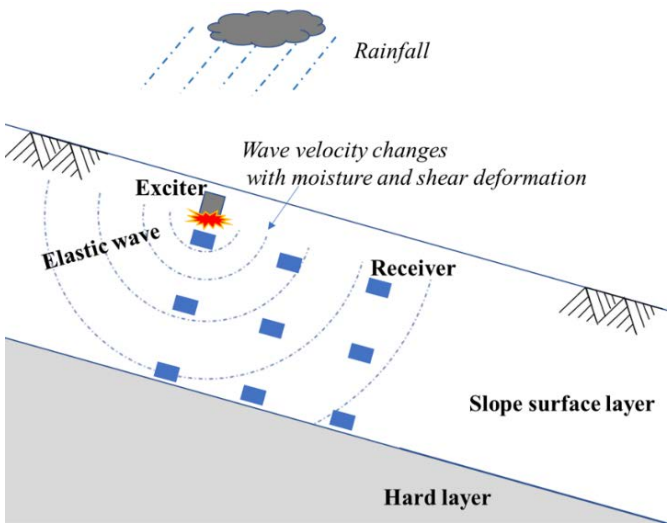

Figure 1.2 The typical layout of the sensors to determine the soil moisture and shear deformation by elastic wave propagation in a slope surface layer.

1.4 AIMS & OBJECTIVES

This research is aimed towards developing the fundamental understanding of elastic wave propagation in soils with reference to shallow slope unstable conditions. Clear and comprehensive understanding of characteristics of elastic wave changing during

rainfall and shear deformation until slope failure. In general, the main objectives of this study can be outlined as follows;

- Explore factors effect on elastic wave velocities in the process of shallow slope failure.
- Explore the frequency characteristics of elastic wave in different soil moisture and shear deformation.
- Explore the changes of elastic wave signals in different depth by a multiple sensor array. which includes developing of:
    a. An exciter that can automatically generate clear and powerful elastic wave signals to propagate more than 1 m in soil.
    b. An algorithm that can automatically pick up wave travel time based on AIC Model.

- A full-scale multi-layer shear model was used to simulate the process of slope failure and observe the wave propagation. The detailed behavior of elastic wave propagation in soil over a wide range of soil moisture, shear stress, and shear deformation, can be explored.
- Explore the behavior of elastic wave propagation in a natural slope surface layer by an on-site elastic wave monitoring.

1.5 SCOPE OF WORK AND LIMITATIONS

The scope of this research encompasses comprehensive studies to explore the variation of elastic wave velocities and attenuation with soil saturation, and with shear deformation. The objective of this research is to explore the factors affecting on elastic wave variation in the process of slope failure. During a rainfall event, rainwater infiltrates into the ground surface, with the increasing of the soil moisture, the normal stress, and shear stress increase. Hence, it is desired to explore the effects of normal stress and soil moisture effect on wave velocities. When more and more water infiltrates into the ground, near the sliding surface there is high moisture. The high soil moisture makes the soil strength decrease, makes the ground loose and cracks occur. These processes lead the slope to start to move. Normal stress, soil moisture, shear stress, and

displacement are the parameters related to slope stability, a separate study is required to explore the effects of these parameters on elastic wave during slope failure, for example, keeping constant water content conditions and increase the shear strength, on the other hand, keeping constant shear strength and increase the water content conditions. The laboratory experimental plan was defined to explore the effects of soil normal stress in the initial state, which at constant soil moisture, no shear force applied. And then another series of experiments was conducted to reproduce slope failure, and wave velocities and attenuation were examined during actual slope failure conditions. On-site elastic wave monitoring is an attempt to verify the results of laboratory experiments.

Due to the limitation of time, findings of this research could not be expanded to other conditions such as the groundwater level and soil types. This study is however limited to exploring the behavior of elastic wave velocities during landslides by means of laboratory model tests and one On-site test only. The validity of said findings in actual slope failure conditions is yet to be done.

1.6 UNIT SYSTEM

The International System of Units (abbreviated as "SI"), known as the modern form of the metric system and the most widely used system of measurement, was used in this research. Following the usual sign convention adopted in soil mechanics, variables just as stresses and strains in compression were represented as positive, whereas those in tension were marked as negative.

1.7 TIME SCALE AND LOCATION OF RESEARCH

The research and all laboratory tests were conducted in Geotechnical Engineering Laboratory of Saitama University located at 255 Shimo-Okubo, Sakura-ku, Saitama City, Saitama 338-8570, JAPAN. during April 2017-March 2020.

1.8 THESIS ORGANIZATION

The thesis is arranged in nine chapters providing a detailed overview of the work done and the main findings of this research program. The outline of the thesis is organized as follows:

Chapter 1 shows an introduction to this research and a brief synopsis of this research. The problem statement and its significance, objectives and specific aims, as well as the scope of work and its limitations, are discussed.

Chapter 2 provides a brief review of previous studies related to rainfall-induced landslides and landslide protection approaches such as physical countermeasures and early warning systems.

Chapter 3 presents a detailed description of the physical properties of the test material and experimental setup employed for this study.

Chapter 4 describes the overall research methodology. The detailed experimental plan and step by step procedure for the performance of each type of experiment are outlined in this chapter.

In Chapter 5, the factors affect on elastic wave velocities using the multi-layer shear model are studied. A detailed description of elastic wave velocities changing with the normal stress, volumetric water content, shear stress, and displacement is outlined in this chapter.

Chapter 6 summarizes the results of elastic wave energy attenuation during a series of tests concerning different soil moisture and shear conditions. The detail frequency characteristic, energy density of elastic wave during rain and drain events, and shear deformation are outlined.

In Chapter 7, the application of elastic wave propagation in soil to monitoring natural unstable slope is discussed.

Finally, Chapter 8 summarizes the conclusions drawn from this research along with the associated recommendations for future studies.

1.9 REFERENCES

Aleotti, P., 2004. A warning system for rainfall-induced shallow failures. Eng. Geol. 73, 247–265. https://doi.org/10.1016/j.enggeo.2004.01.007

Angeli, M.G., Pasuto, A., Silvano, S., 2000. A critical review of landslide monitoring experiences. Eng. Geol. 55, 133–147. https://doi.org/10.1016/S0013-7952(99)00122-2

Arnhardt, C., Asch, K., Azzam, R., Bill, R., Fernandez-Steeger, T.M., Homfeld, S.D., Kallash, a., Niemeyer, F., Ritter, H., Toloczyki, M., Walter, K., 2007. based Landslide Early Warning System -- SLEWS. Development of a geoservice infrastructure as basis for early warning systems for landslides by integration of. Geotechnol. Sci. Report. Early Warn. Syst. Earth Manag. Kick-Off-Meeting 10 Oct. 2007 Tech. Univ. Karlsruhe 75–88.

Baum, R.L., Godt, J.W., 2010. Early warning of rainfall-induced shallow landslides and debris flows in the USA. Landslides 7, 259–272. https://doi.org/10.1007/s10346-009-0177-0

Brand, E.W., 1981. Some thoughts on rain-induced slope failures. Proc. Int. Conf. Soil Mech. Found. Eng. 3, 373–376.

Brignoli, E.G.M., Gotti, M., Stokoe, K.H., 1996. Measurement of shear waves in laboratory specimens by means of piezoelectric transducers. Geotech. Test. J.

Brooks, G., 2001. A synthesis of geological hazards in Canada. https://doi.org/10.4095/212210

Chen, Y., Uchimura, T., Irfan, M., Huang, D., Xie, J., 2017. Detection of water infiltration and deformation of unsaturated soils by elastic wave velocity. Landslides 14, 1715–1730. https://doi.org/10.1007/s10346-017-0825-8

Conte, E., Troncone, A., 2018. A performance-based method for the design of drainage trenches used to stabilize slopes. Eng. Geol. 239, 158–166. https://doi.org/10.1016/j.enggeo.2018.03.017

Conte, E., Troncone, A., Vena, M., 2017. A method for the design of embedded cantilever retaining walls under static and seismic loading. Géotechnique Vol. 67, 1081–1089. https://doi.org/10.1680/jgeot.16.p.201

Haque, U., Blum, P., da Silva, P.F., Andersen, P., Pilz, J., Chalov, S.R., Malet, J.P., Auflič, M.J., Andres, N., Poyiadji, E., Lamas, P.C., Zhang, W., Peshevski, I., Pétursson, H.G., Kurt, T., Dobrev, N., García-Davalillo, J.C., Halkia, M., Ferri, S., Gaprindashvili, G., Engström, J., Keellings, D., 2016. Fatal landslides in Europe. Landslides 13, 1545–1554. https://doi.org/10.1007/s10346-016-0689-3

Hutchinson, J.N., 1984. Landslides in Britain and their countermeasures. Landslides 21, 1–25. https://doi.org/10.3313/jls1964.21.1

Irfan, M., Uchimura, T., 2016. Modified triaxial apparatus for determination of elastic wave velocities during infiltration tests on unsaturated soils. KSCE J. Civ. Eng. 20, 197–207. https://doi.org/10.1007/s12205-015-0404-2

Irfan, M., Uchimura, T., Chen, Y., 2017. Effects of soil deformation and saturation on elastic wave velocities in relation to prediction of rain-induced landslides. Eng. Geol. 230, 84–94. https://doi.org/10.1016/j.enggeo.2017.09.024

Lollino, G., Arattano, M., Cuccureddu, M., 2002. The use of the automatic inclinometric system for landslide early warning: The case of Cabella Ligure (North-Western Italy). Phys. Chem. Earth 27, 1545–1550. https://doi.org/10.1016/S1474-7065(02)00175-4

Lynn Highland, 2004. Landslide Types and Processes. Highw. Res. Board Spec. Rep. 1–4. https://doi.org/Fact Sheet 2004-3072

Mosher, D., 2008. Submarine Mass Movememts in Canada: Geohazards with far-reaching implications. 4th Can. Conf. Geohazards (Laval Univ., 2008) 594.

Nobutomo, O., Yoko, T., Kazuya, A., Tomoaki, M., 2009. Realty of cliff failure disaster, CHNICAL NOTE of National Institute for Land and Infrastructure Management. NILIM.

Okada, Y., Ochiai, H., Furuya, G., Okura, Y., Matsui, T., Sammori, T., Terajima, T., Sassa, K., 2004. A fluidized landslide on a natural slope by artificial rainfall. Landslides 1, 211–219. https://doi.org/10.1007/s10346-004-0030-4

Popescu, M.E., Sasahara, K., 2008. Engineering Measures for Landslide Disaster Mitigation. Landslides – Disaster Risk Reduct. 609–631. https://doi.org/10.1007/978-3-540-69970-5_32

Uchimura, T., Towhata, I., Anh, T.T.L., Fukuda, J., Bautista, C.J.B., Wang, L., Seko, I., Uchida, T., Matsuoka, A., Ito, Y., Onda, Y., Iwagami, S., Kim, M.S., Sakai, N., 2010. Simple monitoring method for precaution of landslides watching tilting and water contents on slopes surface. Landslides 7, 351–357. https://doi.org/10.1007/s10346-009-0178-z

Uchimura, T., Towhata, I., Wang, L., Nishie, S., Yamaguchi, H., Seko, I., Qiao, J., 2015. Precaution and early warning of surface failure of slopes using tilt sensors. Soils Found. 55, 1086–1099. https://doi.org/10.1016/j.sandf.2015.09.010

Wang, L., Nishie, S., Su, L., Yamaguchi, H., Yamamoto, S., Uchimura, T., Tao, S.N., 2018. An early warning monitoring of Earthquake-induced slope failures by monitoring inclination changes in multi-point tilt sensors 19, 251–256.

Irfan, M. (2014). Elastic wave propagation through unsaturated soils concerning early warning of rain-induced landslides. PhD Thesis, Univeristy of Tokyo, Japan.

CHAPTER 2

LITERATURE REVIEW

2.1 INTRODUCTION

This chapter presents a brief overview of previous literature related to the mechanism rain-induced slope failures, the currently available landslide early warning systems and elastic wave propagation in soil. Several kinds of landslide early warning systems currently in practice are introduced, and their limitations are also discussed. Previous research has been conducted to explore the shear and compressive waves in saturated soils and unsaturated soils by element test and model test. However, little information is available about the prediction of slope failure by elastic wave velocities in unsaturated soils. A thorough understanding of elastic wave propagation in unsaturated soils is very necessary and important in this study. Therefore, a comprehensive review of existing literature related to the response of elastic waves in unsaturated soils is presented.

2.2 RAIN-INDUCED SLOPE FAILURES

Rainfall-induced slope failure occurred commonly in mountainous areas and caused severe human and infrastructure damages like China(Brand, 1981), Japan(Uchimura et al., 2015), USA (Baum and Godt, 2010), and Italy (Peruccacci et al., 2017). Most of the Rainfall-induced slope failure occurs at shallow depths, generally less than 3 m(Anderson and Sitar, 1996)(NG and PANG, 2000). In Japan the average depth is 1.2m, 90% is under 2.5m, 500,000 potentially dangerous slopes exist(ONODERA et al., 1974)(Uchimura et al., 2015).

2.3 MECHANISM OF RAIN-INDUCED LANDSLIDES

The mechanism of rain-induced landslides has been concluded by several researchers(Anderson and Sitar, 1996; Brand, 1981; FAROOQ et al., 2004; Sorbino and Nicotera, 2013). Soil moisture is the key factor of a slope's stability in the context of rainfall-induced slope failure. When rainwater infiltrates unsaturated soil, the soil moisture will increase. This will lead to a decrease in soil matric suction, resulting in the soil losing its strength. The changes in soil moisture content can be expressed by the changes in matric suction; high soil moisture content means lower matric suction. The decreasing matric suction reduces the effective normal stress acting along the potential failure plane, which in turn diminishes the available shear strength to a point when equilibrium can no longer be sustained hence induces slope failure.

2.4 LANDSLIDE EARLY WARNING SYSTEMS

To prevent rainfall-induced slope failure, Traditional approaches (Popescu and Sasahara, 2008) such as retaining walls (Conte et al., 2017), ground anchors (Hutchinson, 1984) and dewater systems (Conte and Troncone, 2018) are common, however, they are not economically feasible for the amount of potentially unstable slope. Therefore, landslide early warning systems are an alternative soft countermeasure that can provide an efficient and economical way to reduce the damage of slope failure. A typical landslide early warning system is based on monitoring of soil moisture and pore pressure (Baum and Godt, 2010), or on measuring mass movement events by linear displacement transducers (Arnhardt et al., 2007), inclinometers (Lollino et al., 2002) or extensometers (Angeli et al., 2000), or measuring both the soil moisture and the displacement by soil moisture sensors and tilt sensors (Uchimura et al., 2010). These methods have recently been used because they are simple and easy to install in the slope surface layer. However, they can only sense the local area surrounding the position of the sensor. To cover a wide area at an unstable slope, many sensors are required (Wang et al., 2018).

Elastic wave propagation in soil as a non-destructive monitoring technique has received considerable attention in recent years. The application of elastic wave propagation in

soil has been developed by many researchers, for example, shear waves were measured in laboratory specimens by means of piezoelectric transducers (Brignoli et al., 1996), and recently, both shear wave (S-wave) and compression wave (P-wave) velocities were designed to measure the unsaturated soil (Irfan and Uchimura, 2016). It was found that both P-wave and S-wave velocities decreased by nearly half when soil saturation was increased from 20% to 80% in laboratory triaxial experiments (Irfan et al., 2017). This study is to find out a method to evaluate slope shear deformation and soil moisture by elastic wave velocities. Elastic wave devices include an exciter and several receivers that are laid out within the slope surface layer to cover a relatively deep and wide area.

2.5 ELASTIC WAVE PROPAGATION IN SOIL

The elastic waves propagating through soil in forms of body waves involve ground dilation and distortion. Body waves travel through the interior of the soil along paths controlled by the material properties in terms of density and modulus (stiffness). There are two types of body waves, P-waves and S-waves, shown in Figure 2.1. In P-waves (also known as primary waves, longitudinal or compression waves), particle vibrations are in the direction of wave propagation. In S-waves (also known as secondary waves or shear waves), the vibration of particles is perpendicular to the direction of propagation. Elastic wave has been widely used to investigate the mechanically stressed geomaterials.

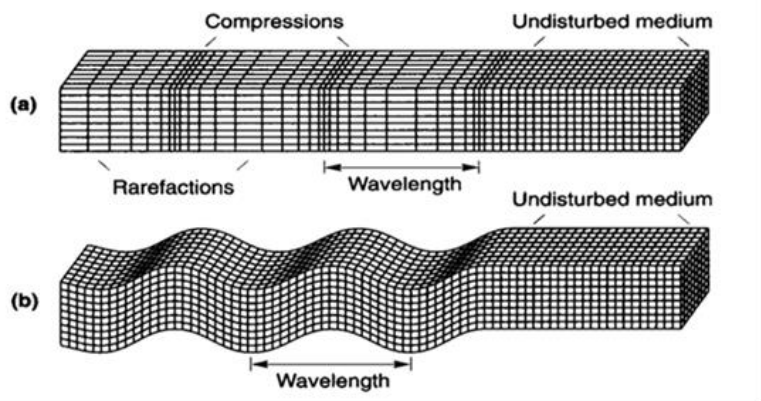

Figure 2.1 Particle motions of (a) Compression waves; (b) Shear waves (Kramer 1996)

However, most of the studies are focused on shear wave velocity, which is supposed to be related to the material's shear modulus (Hardin and Richart 1963, Ohta and Goto 1978, Brignoli et al. 1996, Mancuso et al. 2002).

2.6 FACTORS AFFECTING ELASTIC WAVE PROPAGATION IN SOIL

Early Studies of soil behavior by elastic wave velocity to understand the effective stress-strain relation for soils for small, nearly elastic, strains. The shear wave velocity and the compression wave velocity can be expressed as (Hardin, 1978; Hardin and F. E. Richart, 1963) ;

$$Vs = Cs \cdot \sqrt{F(e)} \cdot \left(\frac{\sigma'_o}{P_a} \right)^n \tag{2.1}$$

$$Vp = Cp \cdot \sqrt{F(e)} \left[\frac{\sigma'_0}{P_a} \right]^n \tag{2.2}$$

where V_s *is* shear wave velocity, V_p is compression wave velocity, respectively. σ'_o is effective isotropic stress, C_s, C_p, and n are constants reflecting soil type, grain properties, and fabric. P_a represents the atmospheric pressure which is in the same units as σ'_o, and $F(e)$ is the void ratio function.

2.6.1 Effective Stress State

Some of the earliest studies on the effects of effective stress state on shear wave velocities were performed by (Hardin and F. E. Richart, 1963), (Hardin and Black, 1968), and (Hardin and Drnevich, 1972). Figure 2.2 shows the relationship between shear wave velocity and confining pressure (Hardin and F. E. Richart, 1963). Other researchers (Marcuson, William F; Harvey E. Wahls, 1972),(IWASAKI, TOSHIO; TATSUOKA, FUMIO; TAKAGI, 1978); (Kokusho, 1980); (T.C. Kim, 1981); also found the similar findings for various other types of soils.

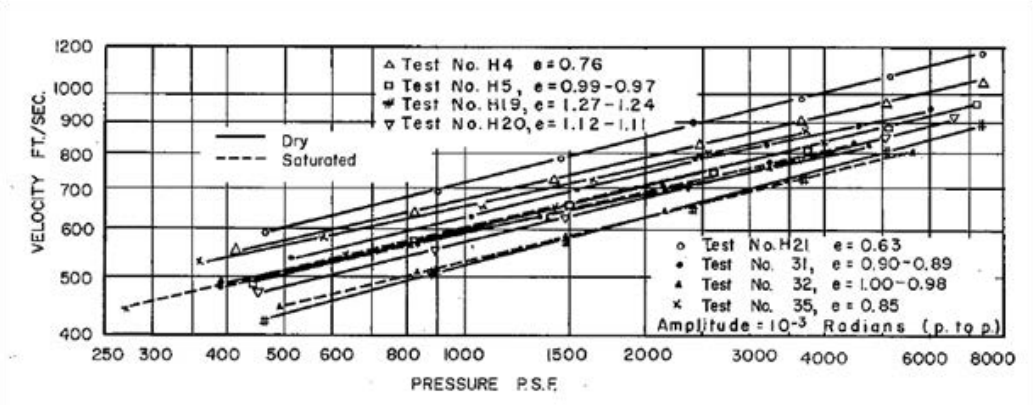

Figure 2.2 Variation of shear wave velocity with confining pressure and void ratio for saturated and dry crushed quartz sand (Hardin and F. E. Richart, 1963).

More recent studies have shown that the elastic wave behavior is dependent on the principal stress directions (Bellotti et al., 1996; Roesler, 1979; STOKOE, 1991). The compression wave velocity only depends on the stress state in the direction of wave propagation, while the shear wave velocity is found to be dependent on the state of stress in the direction of wave propagation as well as particle vibration (Stokoe and Santamarina, 2000; STOKOE, 1991).

2.6.2 Void Ratio

The void ratio had been recognized that it was a role affecting elastic wave velocity by Some of the earliest studies. (B. O. Hardin & Richart, 1963; B. Hardin & Black, 1968; Iwasaki et al., 1978). Figure 2.3 shows the relationship between shear wave velocity and void ratio from resonant-column experiments(Bobby O. Hardin, F. E. Richart, 1963).

Wave velocities can be normalized by using Eq. 2.1 for the varying stress conditions in Figure 2.3. Shear wave velocities normalized for isotropic stress level show a nearly linear decrease with the increase of the void ratio (Figure 2.4).

During triaxial compression experiments, elastic wave velocities affect by the change in void ratio, which caused by the changes in stress level and/or other parameters. Void ratio function, *F(e)*, defined in Eq 2.1 and 2.2, is therefore used to normalize wave velocities for any changes in void ratio.

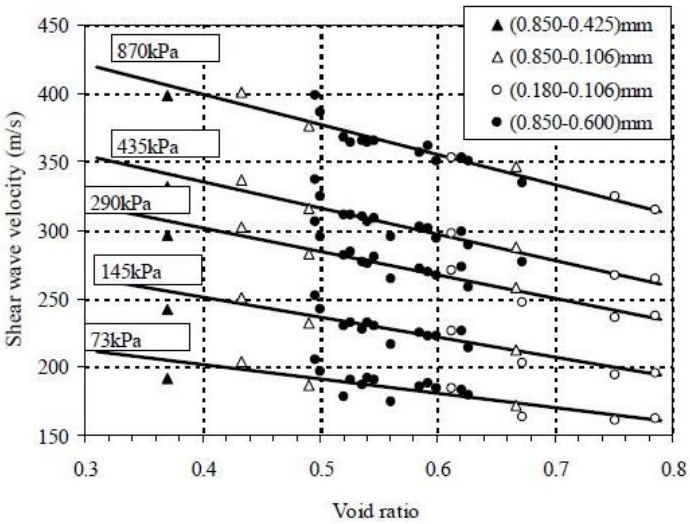

Figure 2.3 Shear wave velocity variation with the void ratio for different stress states (Hardin and F. E. Richart, 1963)

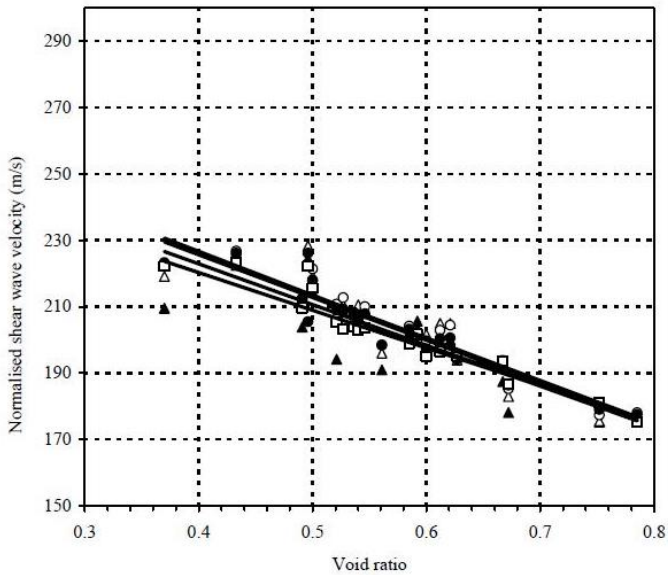

Figure 2.4 Shear wave velocity variation with void ratio. Wave velocities normalized by using Eq. 2.1 to cancel the effect of stress state(Hardin and F. E. Richart, 1963)

2.6.3 Degree of Saturation

The propagation of the shear wave is dependent on the shear stiffness of soil skeleton whereas the compression wave is influenced by both of the pore fluid and soil skeleton (Stokoe and Santamarina, 2000). A resonant column was used to study the response of

shear wave velocities in low saturation ranges (0% ~ 50% saturation) (Qian et al., 1991). The shear wave velocity was expressed in terms of small strain shear modulus, G, of soil. The presence of a certain peak in shear modulus with soil saturation was observed. This peak of G/G_{dry} was dependent upon external confining pressure and the percentage of fines. However, the peak of G/G_{dry} was not affected by the particle size of soil(Figure 2.5).

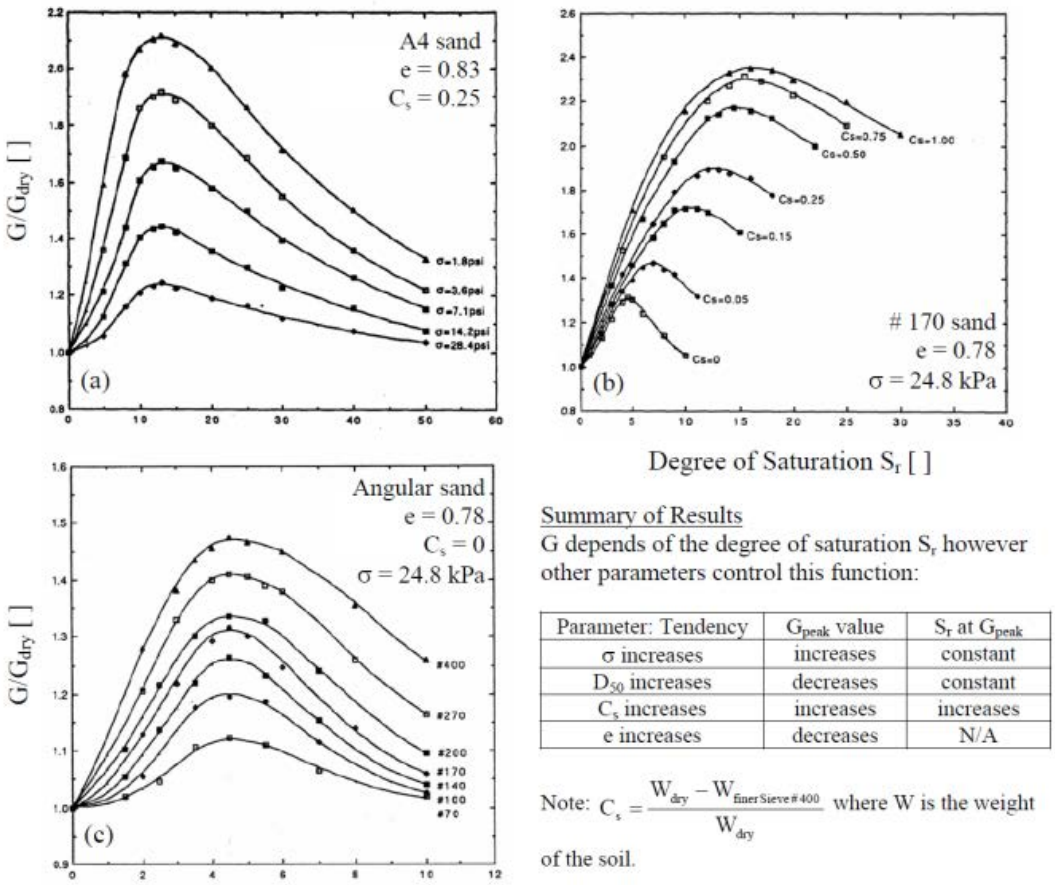

Figure 2.5 Shear stiffness of unsaturated soils versus (a) degree of saturation and confining pressure, (b) degree of saturation and fine content, and (c) degree of saturation confining pressure as tested in a resonant column device. (Qian et al., 1991)

The small strain behavior of an unsaturated compacted silty sand had been investigated by a resonant column – torsional shear cell fitted with a suction control assembly (Mancuso et al., 2002). The shear wave velocities were expressed in terms of initial shear stiffness, *Go*. It was explained based on the progressive change from bulk-water regulated soil response, observed close to saturation state, to a menisci-water regulated

soil response which was observed at relatively drier stages of the experiment, as shown in Figure 2.6. The suction values higher than 200 kPa, shear stiffness mainly depended on the net stress level only.

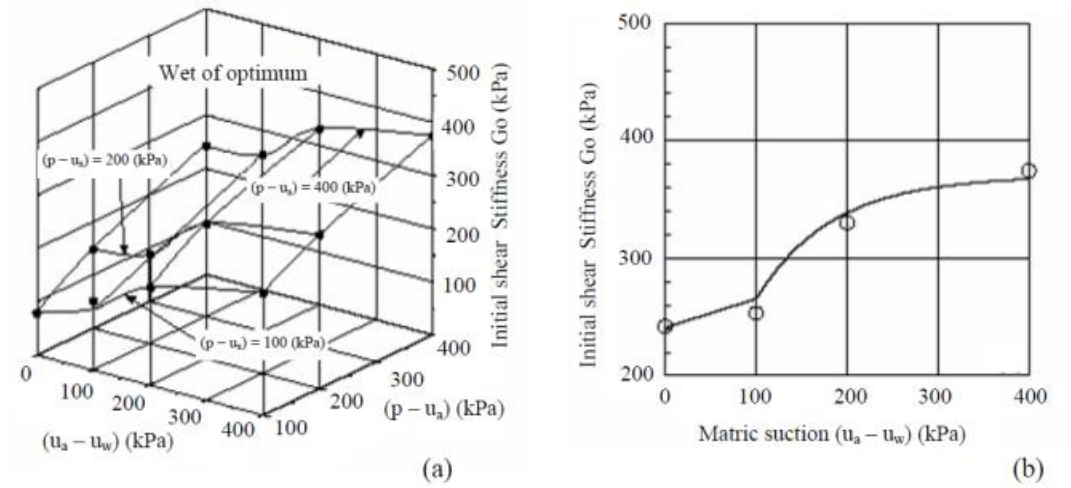

Figure 2.6 (a) Initial shear stiffness in controlled-suction resonant column tests. (b) Response of shear stiffness to suction at a mean net stress of 400 kPa(Mancuso et al., 2002).

To examine the variation of shear wave velocity with soil saturation, bender element tests on various cohesive soil specimens had been conducted (Cho and Santamarina, 2001). Shear wave velocities were measured at various saturation ratios from saturated state to the specimens dried, a gradual increase in shear wave velocities was observed as shown in Figure 2.7. Based on the increased bonding between fine-grained soil particles with drying, the wave velocity increase.

(Alramahi et al., 2010) also found that S-wave velocity and P-wave velocity increases as the degree of saturation decreases when measured wave velocity on clay and silt at different degrees of saturation, as shown in Figure 2.8.

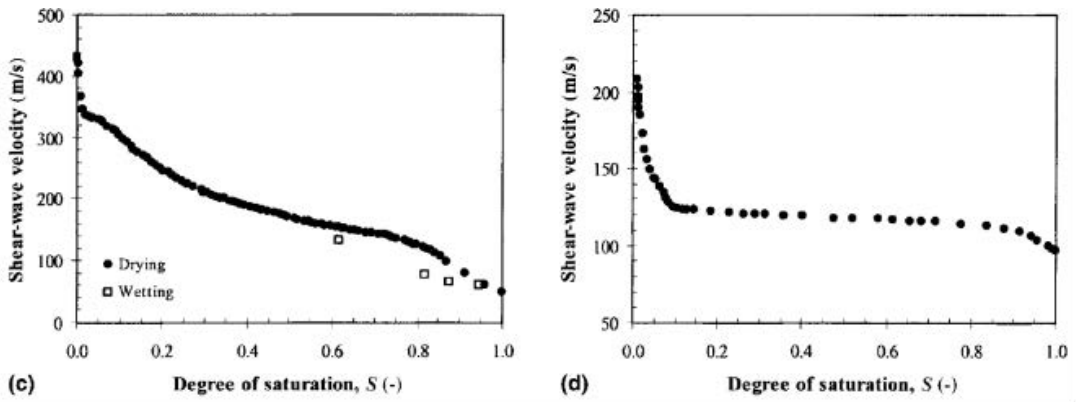

Figure 2.7 Shear wave velocity versus degree of saturation; (a) Granite Powder; (b) Sandboil sand. (Cho and Santamarina, 2001).

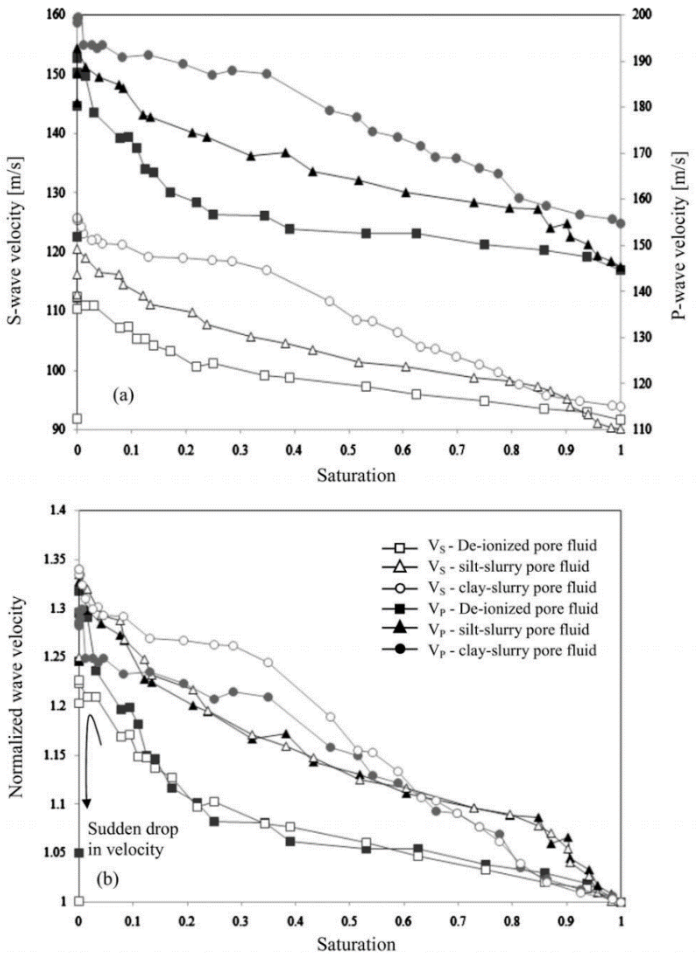

Figure 2.8 S and P wave velocities and normalized velocity profiles for the three drying experiments caused. (Alramahi et al., 2010).

Triaxial tests had been conducted on Edosaki sand under constant water injection conditions, the results showed that both P-wave and S-wave velocities decrease before failure initiation was mainly due to water infiltration (Irfan et al., 2017), as shown in Figure 2.9.

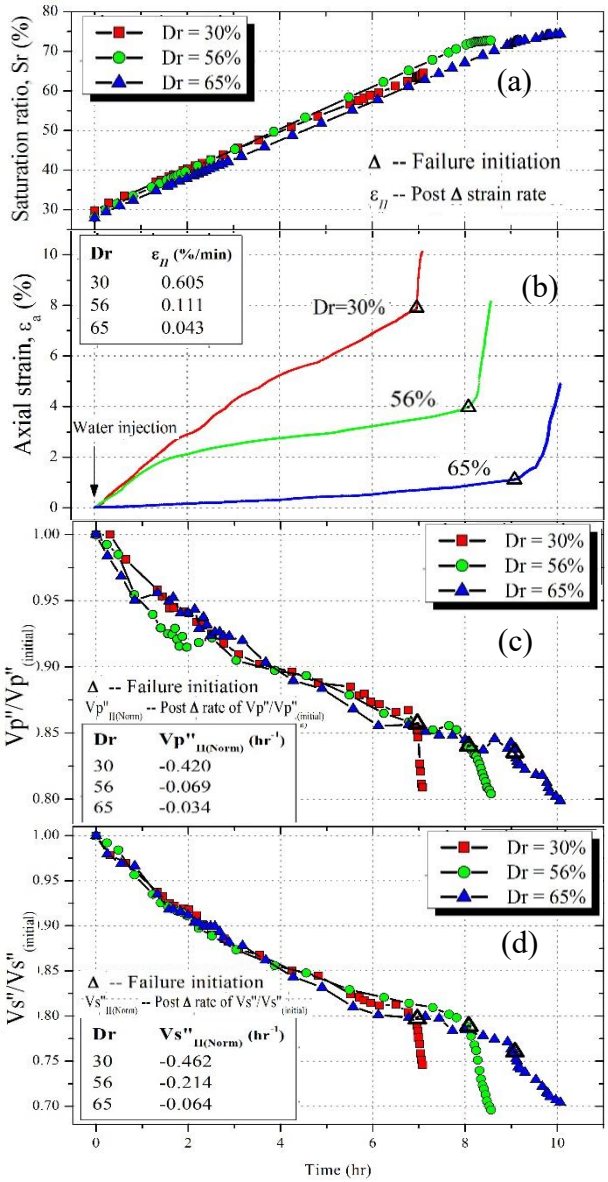

Figure 2.9 Variation of (a) Saturation ratio; (b) Axial strain; (c) Normalized compression wave velocities, and (d) Normalized shear wave velocities, with time series.

2.7 WAVE ATTENUATION

Elastic wave has been widely applied for investigation of mechanically stressed geomaterials. However, the majority of geotechnical laboratory studies are focused on shear wave velocity, which is supposed to be linked with the material's shear modulus(Hardin and F. E. Richart, 1963; Roesler, 1979; Stokoe and Santamarina, 2000).

The propagation of elastic wave is geometric spreading, which is as the wave moves away from the source, the area that the wave energy covers becomes larger and thus wave intensity decreases, and wave energy loss due to inelastic material behavior or internal friction during wave propagation, these effects are called wave attenuation. The wave attenuation is usually expressed in terms of the dimensionless quality factor Q,(Bormann et al., 2012),

$$Q = 2\pi\ E/\Delta E \qquad (2\text{-}3)$$

with ΔE the dissipated energy per cycle. Large energy loss means low Q and vice versa, i.e., Q is inversely proportional to the attenuation.

The energy density E contained in a seismic wave may be expressed as the sum of kinetic (Ekin) and potential (E_{pot}) energy densities,

$$E = E_{kin} + E_{pot} \qquad (2\text{-}4)$$

$E_{kin} = E_{pot}$ in case of anisotropic stress-strain relationship in a non-dispersive (closed) system for the average energy density

$$E = 1/2\ \rho\ A^2\ \omega^2. \qquad (2\text{-}5)$$

where ρ is the density of the material,

$A\ \omega \cos(\omega t - kx)$ is the ground-motion particle velocity,

with A is wave amplitude,

ω is angular frequency $2\pi f$ and k is the wavenumber.

The signal attenuation is a wide range application in Acoustic Emission, a kind of elastic wave. The other defined of the attenuation of a wave signal can be expressed using the following equation (Koerner et al., 1981).

$$\alpha = \frac{20}{x}\log\frac{A_1}{A_2} \tag{2-6}$$

Where α = attenuation coefficient in dB/distance,

x =distance between pickup points,

A_1 = amplitude of first wave, and

A_2 = amplitude of second wave.

The attenuation of wave not only depends on the signal frequency but also the propagating medium. As can be seen in Figure 2.10, iron and steel have a much lower rate of attenuation compared with sands whereas the dry sand has a higher rate of attenuation.

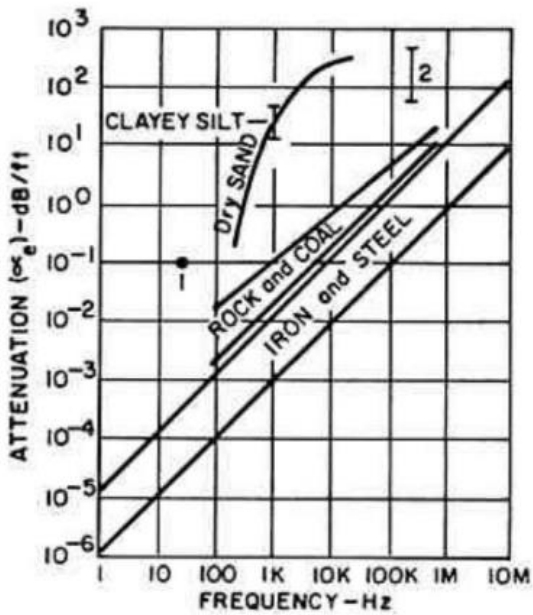

Figure 2.10 Wave attenuation as a function of frequency of various materials. (Koerner et al., 1981)

2.8 CASE STUDY OF MONITORING SHEAR DEFORMATION ON-SITE

(Smith et al., 2014) presented monitoring the stability of soil slopes by AE (Acoustic emission), a field trial at a reactivated soil slope in North Yorkshire, UK. This slope continuous deformation during somedays. They confirmed that AE rates generated were directly proportional to slope movement, and demonstrated the performance of AE monitoring of active waveguides to provide continuous information on slope displacements from the measurements (Figure 2.11 Change in shape of SAA3 depth profile at the end of each slope displacement event at cluster 3(Smith et al.,2014).

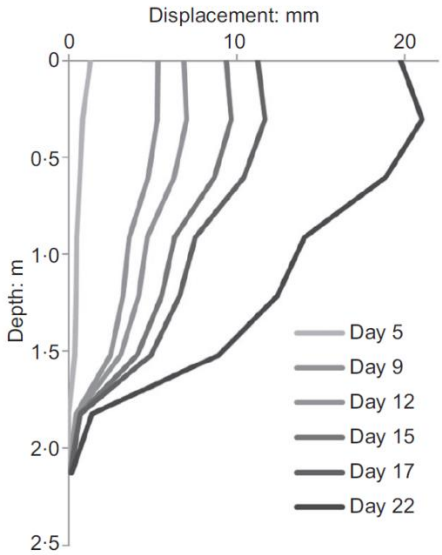

Figure 2.11 Change in shape of SAA3 depth profile at the end of each slope displacement event at cluster 3(Smith et al.,2014)

2.9 SUMMARY

In this chapter, the fundamental concepts which form the backbone of this study are discussed. The overall discussion presented is categorized in two broad fields; *(i)* rainfall-induced landslides, and *(ii)* elastic wave propagation in soil. In the first section, the basic mechanism of rain-induced is discussed. Several kinds of landslide early warning systems include their merits and demerits are analyzed. Since the main aim of

this study is to find out a method based on elastic waves to predict landslide, thus the second half of this chapter was focus on presenting a comprehensive overview of elastic wave propagation in soils.

2.10 REFERENCES

Alramahi, B., Alshibli, K.A., Asce, M., Fratta, D., 2010. Effect of Fine Particle Migration on the Small-Strain Stiffness of Unsaturated Soils. J. Geotech. Geoenvironmental Eng. 136, 620–628. https://doi.org/10.1061/(ASCE)GT.1943-5606.0000244

Anderson, B.S.A., Sitar, N., 1996. Analysis of rainfall-induced debris flows. Int. J. Rock Mech. Min. Sci. Geomech. Abstr. 33, A106. https://doi.org/10.1016/0148-9062(96)86891-4

Angeli, M.G., Pasuto, A., Silvano, S., 2000. A critical review of landslide monitoring experiences. Eng. Geol. 55, 133–147. https://doi.org/10.1016/S0013-7952(99)00122-2

Arnhardt, C., Asch, K., Azzam, R., Bill, R., Fernandez-Steeger, T.M., Homfeld, S.D., Kallash, a., Niemeyer, F., Ritter, H., Toloczyki, M., Walter, K., 2007. based Landslide Early Warning System -- SLEWS. Development of a geoservice infrastructure as basis for early warning systems for landslides by integration of. Geotechnol. Sci. Report. Early Warn. Syst. Earth Manag. Kick-Off-Meeting 10 Oct. 2007 Tech. Univ. Karlsruhe 75–88.

Baum, R.L., Godt, J.W., 2010. Early warning of rainfall-induced shallow landslides and debris flows in the USA. Landslides 7, 259–272. https://doi.org/10.1007/s10346-009-0177-0

Bellotti, R., Jamiolkowski, M., Lo Presti, D.C.F., O'Neill, D.A., 1996. Anisotropy of small strain stiffness in Ticino sand. Geotechnique 46, 115–131. https://doi.org/10.1680/geot.1996.46.1.115

Bormann, P., Engdahl, E., Kind, R., 2012. Seismic Wave Propagation and Earth models. p. p36. https://doi.org/10.2312/GFZ.NMSOP-2_ch2

Brand, E.W., 1981. Some thoughts on rain-induced slope failures. Proc. Int. Conf. Soil Mech. Found. Eng. 3, 373–376.

Brignoli, E.G.M., Gotti, M., Stokoe, K.H., 1996. Measurement of shear waves in laboratory specimens by means of piezoelectric transducers. Geotech. Test. J.

Cho, G.-C., Santamarina, J., 2001. Unsaturated particulate materials—particle-level studies. J. Geotech. Geoenvironmental Eng. 127, 84–96. https://doi.org/10.1061/(asce)1090-0241(2001)127

Conte, E., Troncone, A., 2018. A performance-based method for the design of drainage trenches used to stabilize slopes. Eng. Geol. 239, 158–166. https://doi.org/10.1016/j.enggeo.2018.03.017

Conte, E., Troncone, A., Vena, M., 2017. A method for the design of embedded cantilever retaining walls under static and seismic loading. Géotechnique Vol. 67, 1081–1089. https://doi.org/10.1680/jgeot.16.p.201

FAROOQ, K., ORENSE, R., TOWHATA, I., 2004. RESPONSE OF UNSATURATED SANDY SOILS UNDER CONSTANT SHEAR STRESS DRAINED CONDITION. SOILS Found. 44, 1–13. https://doi.org/10.3208/sandf.44.2_1

Hardin, B., Black, W., 1968. Vibration Modulus of Normally Consolidated Clay. J. Soil Mech. Found. Div.

Hardin, B.O., 1978. The Nature of Stress-Strain Behavior for Soils. Earthq. Eng. Soil Dyn. 3–90.

Hardin, B.O., Drnevich, V.P., 1972. Shear modulus and damping in soils: Design equations and curves. Geotech. Spec. Publ. 1459–1484.

Hardin, B.O., F. E. Richart, J., 1963. Elastic Wave Velocities in Granular Soils. J. Soil Mech. Found. Div. 89, 33–65.

Hutchinson, J.N., 1984. Landslides in Britain and their countermeasures. Landslides 21, 1–25. https://doi.org/10.3313/jls1964.21.1

Irfan, M., Uchimura, T., 2016. Modified triaxial apparatus for determination of elastic wave velocities during infiltration tests on unsaturated soils. KSCE J. Civ. Eng. 20, 197–207. https://doi.org/10.1007/s12205-015-0404-2

Irfan, M., Uchimura, T., Chen, Y., 2017. Effects of soil deformation and saturation on elastic wave velocities in relation to prediction of rain-induced landslides. Eng. Geol. 230, 84–94. https://doi.org/10.1016/j.enggeo.2017.09.024

IWASAKI, TOSHIO;TATSUOKA, FUMIO;TAKAGI, Y., 1978. Shear Moduli of Sands under Cyclic Torsional Shear Loading. Soils Found. 18, 39–56. https://doi.org/https://doi.org/10.3208/sandf1972.18.39

Koerner, R.M., McCabe, W.M., Lord, A.E., 1981. Acoustic Emission Behavior and Monitoring of Soils, in: Drnevich, V.P., Gray, R.E. (Eds.), Acoustic Emissions in Geotechnical Engineering Practice. ASTM International, West Conshohocken, PA, pp. 93–141. https://doi.org/10.1520/STP28343S

Kokusho, T., 1980. Cyclic Triaxial Test of Dynamic Soil Properties for Wide Strain Range. 3, 305–312. https://doi.org/10.1016/0148-9062(81)91053-6

Lollino, G., Arattano, M., Cuccureddu, M., 2002. The use of the automatic inclinometric system for landslide early warning: The case of Cabella Ligure (North-Western Italy). Phys. Chem. Earth 27, 1545–1550. https://doi.org/10.1016/S1474-7065(02)00175-4

Mancuso, C., Vassallo, R., D'Onofrio, A., 2002. Small strain behavior of a silty sand in controlled-suction resonant column - Torsional shear tests. Can. Geotech. J. 39, 22–31. https://doi.org/10.1139/t01-076

Marcuson, William F;Harvey E. Wahls, 1972. Time Effects on Dynamic Shear Modulus of Clays. J. Soil Mech. Found. Div. 98, 1359–1373.

NG, C.W.W., PANG, Y.W., 2000. Influence of Stress State on Soil-Water Characteristics and Slope Stability. J. Geotech. Geoenvironmental Eng. 126, 157–166.

ONODERA, T., YOSHINAKA, R., KAZAMA, H., 1974. SLOPE FAILURES CAUSED BY HEAVY RAINFALL IN JAPAN. J. Japan Soc. Eng. Geol. 15, 191–200. https://doi.org/10.5110/jjseg.15.191

Peruccacci, S., Brunetti, M.T., Gariano, S.L., Melillo, M., 2017. Geomorphology Rainfall thresholds for possible landslide occurrence in Italy. Geomorphology 290, 39–57. https://doi.org/10.1016/j.geomorph.2017.03.031

Popescu, M.E., Sasahara, K., 2008. Engineering Measures for Landslide Disaster Mitigation. Landslides – Disaster Risk Reduct. 609–631. https://doi.org/10.1007/978-3-540-69970-5_32

Qian, X., Gray, D., Woods, R., 1991. Resonant Column Tests on Partially Saturated Sands. Geotech. Test. J. 14, 266–275. https://doi.org/10.1520/GTJ10571J

Roesler, S.K., 1979. Anisotropic Shear Modulus due to Stress Anisotropy. J. Geotech. Eng. Div. 105, 871–880.

Smith, A., Dixon, N., Meldrum, P., Haslam, E., Chambers, J., 2014. Acoustic emission monitoring of a soil slope: Comparisons with continuous deformation measurements. Proc. Inst. Civ. Eng. Struct. Build. 4, 255–261. https://doi.org/10.1680/geolett.14.00053

Sorbino, G., Nicotera, M.V., 2013. Unsaturated soil mechanics in rainfall-induced flow landslides. Eng. Geol. 165, 105–132. https://doi.org/10.1016/J.ENGGEO.2012.10.008

Stokoe, K.H., Santamarina, J., 2000. Seismic-wave-based testing in geotechnical engineering. GeoEng 2000 1490–1536.

STOKOE, K.H.I.I., 1991. Characterization of soil in calibration chambers with seismic waves. Proc. Int. Symp. Calibration Chamb. Testing, Clarkson Univ. 2, 363–376.

T.C. Kim, M.N., 1981. Dynamic properties of some cohesive soils of Ontario. Can. Geotech. J. 18, 371–389. https://doi.org/https://doi.org/10.1139/t81-044

Uchimura, T., Towhata, I., Anh, T.T.L., Fukuda, J., Bautista, C.J.B., Wang, L., Seko, I., Uchida, T., Matsuoka, A., Ito, Y., Onda, Y., Iwagami, S., Kim, M.S., Sakai, N., 2010. Simple monitoring method for precaution of landslides watching tilting and water contents on slopes surface. Landslides 7, 351–357. https://doi.org/10.1007/s10346-009-0178-z

Uchimura, T., Towhata, I., Wang, L., Nishie, S., Yamaguchi, H., Seko, I., Qiao, J., 2015. Precaution and early warning of surface failure of slopes using tilt sensors. Soils Found. 55, 1086–1099. https://doi.org/10.1016/j.sandf.2015.09.010

Wang, L., Nishie, S., Su, L., Yamaguchi, H., Yamamoto, S., Uchimura, T., Tao, S.N., 2018. An early warning monitoring of Earthquake-induced slope failures by monitoring inclination changes in multi-point tilt sensors 19, 251–256.

CHAPTER 3

EXPERIMENTAL SETUP

3.1 INTRODUCTION

The purpose of this study is to investigate the changes in elastic wave propagation in soil in the process of slope failure. Evaluate soil moisture and shear deformation by elastic wave in a shallow slope is the main task. A variety of laboratory experiments were conducted to explore the characterization of the elastic wave propagation in soil. Both shear wave (S-wave) and compression wave (P-wave) velocities were designed to measure the unsaturated soil (Irfan and Uchimura, 2016). It was found that both P-wave and S-wave velocities decreased by nearly half when soil saturation was increased in laboratory triaxial experiments (Irfan et al., 2017). A series of model experiments found that elastic wave velocities continuously decreased in response to moisture content and deformation (Chen et al., 2017).

Distinct from the previous studies, this research focuses on elastic wave changes in different depth of soil in the process of slope failure, due to soil moisture, shear stress, and shear displacement, which are different in depth of the ground. Therefore, a full-scale multi-layer shear model was used to simulate the process of slope failure. An exciter has been developed that can automatically generate clear and powerful elastic wave signals to propagate more than 1 m in soil. A detailed description of apparatuses, as well as the elastic wave instrumentations for activity monitoring, are discussed in this chapter.

3.2 MODEL EXPERIMENT

3.2.1 The Concept of Multi-layer Shear Model

The testing apparatus used in this study is a multi-layer shear model. The concept of a multi-layer shear model is shown in Figure 3.1. The size of the model is based on an investigation of slope failure in Japan, which shows that the average depth of shallow slope failure was 1.2 m (Nobutomo et al., 2009). The model can be visualized as a part of the soil cut out from an infinitely long slope surface layer. Assuming that the slope angle is θ, the horizontal direction force can be expressed by $\tan\theta$ times the weight of the soil. If this 1 m model is divided into a multi-layer model and horizontal force is loaded on every layer, every layer can undergo shear deformation independently.

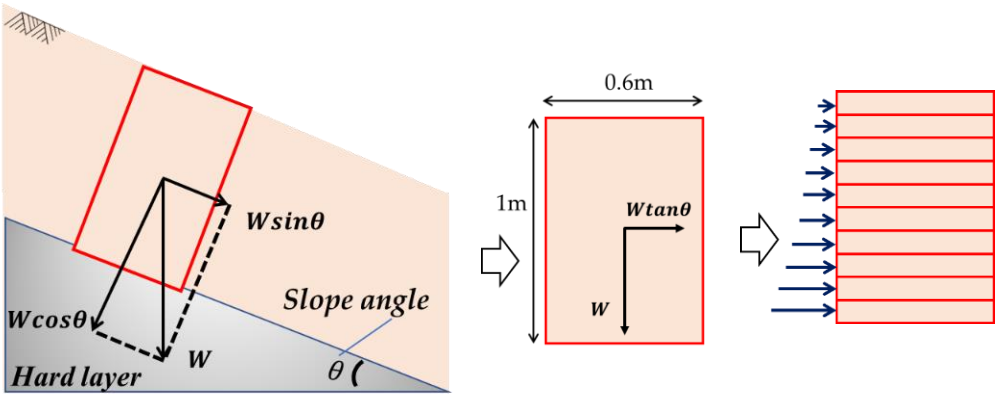

(a) (b) (c)

Figure 3.1 The concept of the multi-layer shear model used in the lab experiment. (a) A part of the soil cut out from an infinitely long slope surface layer. The horizontal direction force can be expressed by $\tan\theta$ times the weight of the soil. (b) The force ratio is the same as it turned to the horizontal direction. (c) The 1 m model is divided into the multi-layer model, the horizontal force is loaded on every layer, and every layer can undergo shear deformation independently.

3.2.2 Multi-layer Shear Model

The multi-layer shear model is shown in Figure 3.3. It includes 20 layers with a total height of 1 m, where each layer is an independent frame with a height of 0.05 m, length of 0.6 m and width of 0.54 m. Each frame is equipped with wheels and is movable under the horizontal shear force (Figure 3.2). Shear force is applied on every frame by an air cylinder to simulate the shear force corresponding to the slope angle.

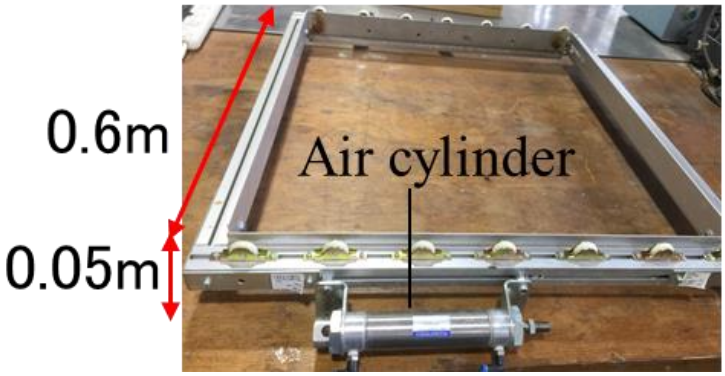

Figure 3.2 An independent frame of the multi-layer shear model

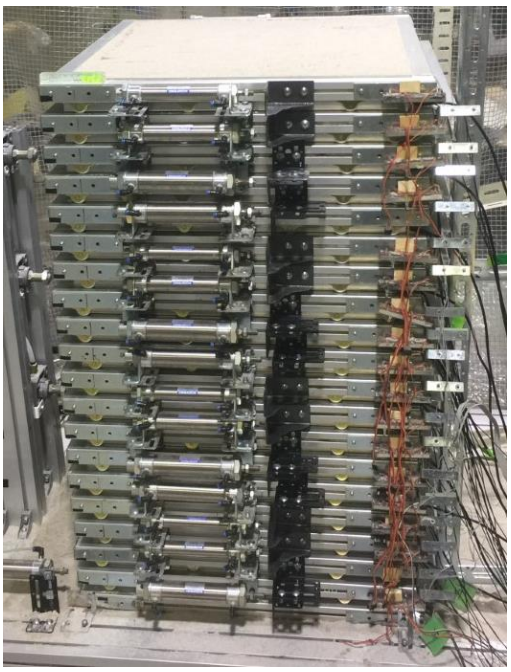

Figure 3.3 A photo overview of the multi-layer shear model

3.2.3 Sensors Layout

The sensors layout in the soil and at the frame are shown in Figure 3.4. Displacement meters are also placed at every layer. Dis1~Dis19 are the displacement meters used to record the shear displacement. A total of 10 exciters and 30 receivers are set in the specified position in the soil. E1~E10 are the exciters used to generate elastic waves; CH01~CH30 are the receivers used to sense the elastic waves. Ten soil moisture sensors were set up in the soil, with a vertical interval of 100 mm, to measure the soil moisture distribution with depth.

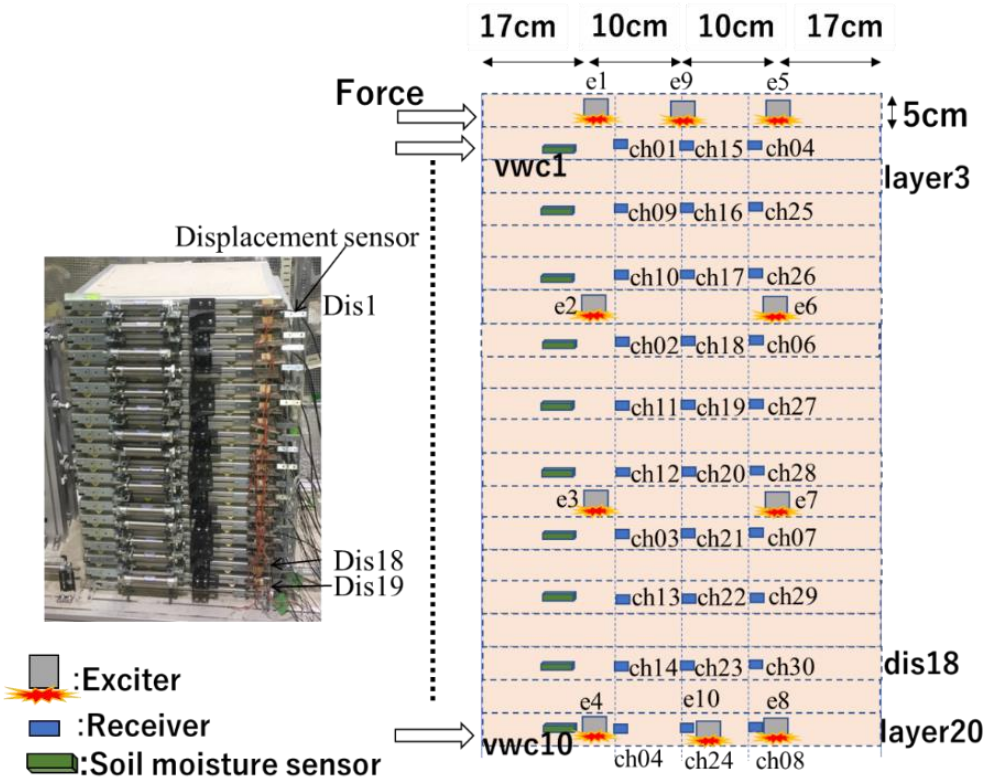

Figure 3.4 Sensors layout in the soil and at the frame.

3.2.4 Data Acquisition System

The data of elastic wave, Volumetric Water Content, loadcell (shear force), and displacement (shear deformation) are collected by the data acquisition system, shown in Figure 3.5 and Figure 3.6. The analog elastic wave signals are converted to digital data by Keyence (NR-500 and NR-HA08) and transferred to the personal computer, which controlled by the application WAVE LOGGER. The Volumetric Water

Content is measured by a total of 10 EC-5 sensors, converted and stored in HOBO RX3000. The shear force is applied by air cylinder, measured by a total of 40 loadcell, converted by A/D converter (MSP430f169 and HX711). A total of 40 channels are assigned to the displacement sensors, converted by the A/D converter in the MSP430f169.

Figure 3.5 Photo of data logger

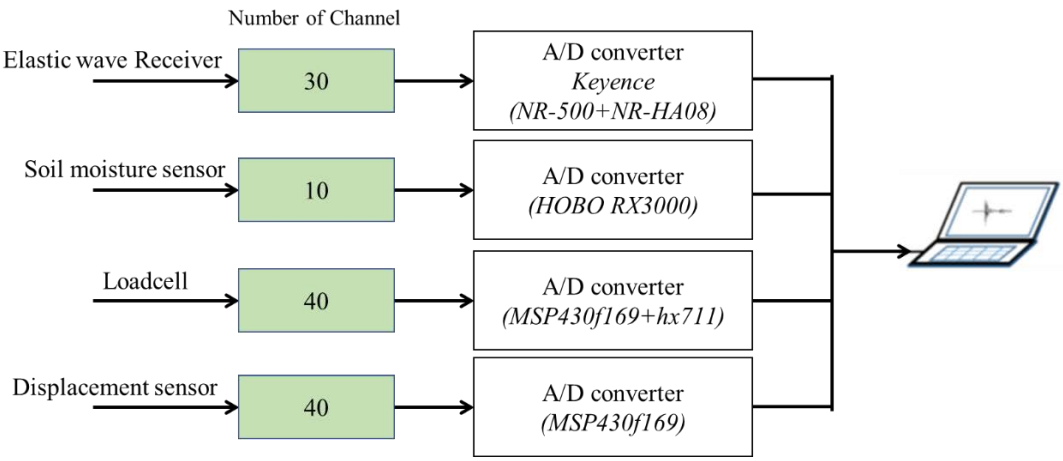

Figure 3.6 Schematic description of the data acquisition system in laboratory experiment

3.2.5 Measuring Devices

3.2.5.1 Newly designed exciter

The newly designed exciter is used to generate pulse elastic waves, as shown in Figure 3.7. It has a height of 33 mm, and a diameter of 25 mm. It has a steel ball inside that weighs 16.95 g. It can be pulled up by an electromagnet and then freefalls from a height of 8.3 mm when the electromagnet is released. The electromagnet is controlled by the Micro Controller(Figure 3.8).

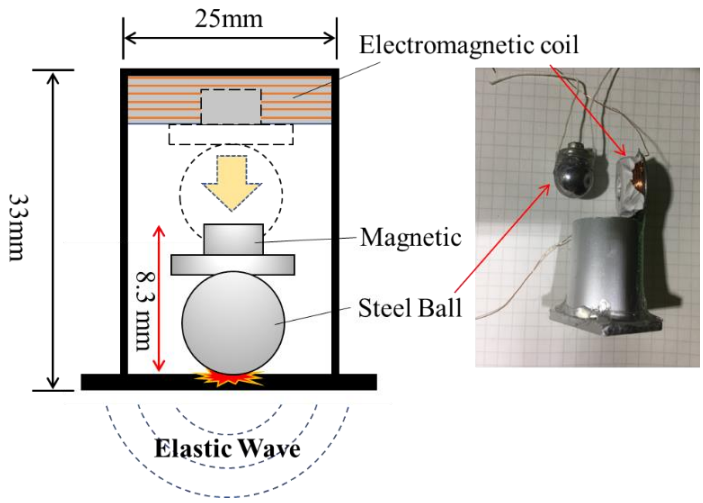

Figure 3.7 The newly designed exciter.

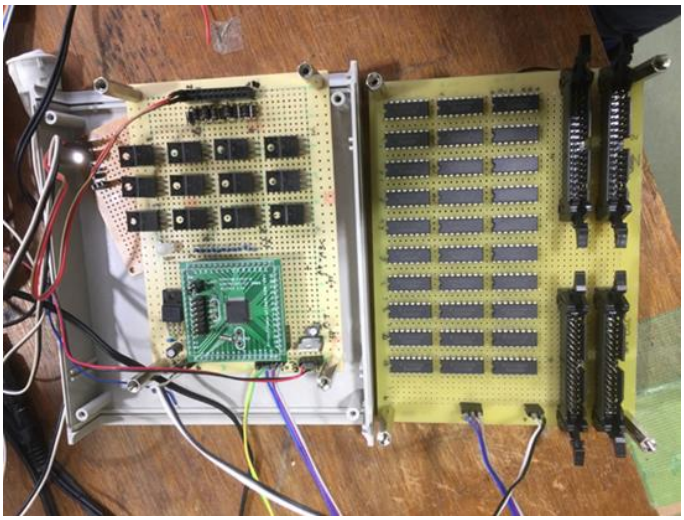

Figure 3.8 Micro Controller for the exciters.

3.2.5.2 Newly designed receiver

The receiver is used to sense the pulse elastic waves, as shown in Figure 3.9. It has a height of 5 mm, length of 22 mm, and a width of 12 mm. It has a MEMS sensor inside, named ADXL354 (Analog Devices, Norwood, MA), which is a high sensitivity, ultralow noise density, low drift 3-axis accelerometer.

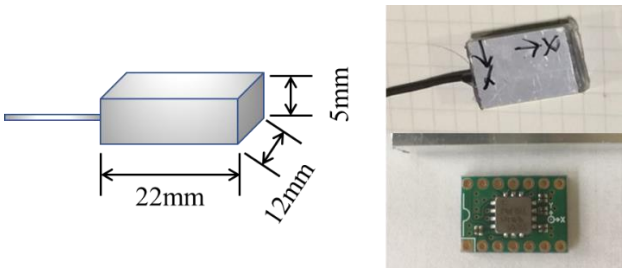

Figure 3.9 Receiver is 3- axis MEMS accelerometers (ADXL354)

Table 3.1 Specification of the receiver (ADXL354)

No	Parameter	Typical	Unit
1	Output Full-Scale Range	±2	g
2	Resonant Frequency	2.4	kHz
3	Sensitivity at XOUT, YOUT, ZOUT	400	mV/g
4	Sensitivity Change due to Temperature	±0.01	%/°C
5	Noise Density	20	µg/√Hz
6	Bandwidth	1500	Hz

3.2.5.3 Analog to digital converter

Analog to digital converter is a high-performance analog to digital converter (*Keyence NR-500*), manufactured by KEYENCE CORPORATION, shown in Figure 3.10.

Figure 3.10 Analog to digital converter (Keyence NR-500)

The elastic wave signals from the receivers (ADXL354) are converted to digital data by *NR-500. The* digital data is sent personal computer by the USB interface. A software named *WAVE LOGGER (NR-HA08)* controls the *NR-500*. *NR-500* can convert 32 channel's analog signals to digital data at the same time with a sampling rate of 100 kHz.

3.2.5.4 Geophone

The Geophone (*Geospace GS-11D*) is a high output, rotating coil geophone, manufactured by Geospace, is shown in Figure 3.11.

Figure 3.11 Geophone GS-11D

The Natural frequencies are 4.5Hz, with a standard coil resistance of 380 ohms. The feathers of Geophone *GS-11D* are listed in Table 3.2.

Table 3.2 Specification of Geophone GS-11D

No	Parameter	Value	Unit
1	Frequency	4.5	Hz
2	Coil Resistance	380	Ohms
3	Sensitivity	0.32	V/cm/sec
4	Damping Constant	762	-
5	Open Circuit Damping	0.34 ± 20%	-
6	Height	3.35	cm
6	Diameter	3.18	cm
8	Weight	111	g

3.2.5.5 Data logger (OMRON mobile data recorder ZR-MDR10)

Data logger (*OMRON mobile data recorder ZR-MDR10*) is a mobile data recorder, manufactured by *OMRON*.

Figure 3.12 Datalogger ZR-MDR10 (OMRON)

The signals of *Geophones (GS-11D)* are converted to digital data and recorded by *ZR-MDR10. ZR-MDR10* has a 16bit analog-to-digital converter, can convert 8 channel's analog signal to digital data at the same time with a sampling rate of 10 kHz. The recorded data can be analyzed by software named *SmartViewer*. Feathers of *ZR-MDR10* are listed in Table 3.3.

Table 3.3 Specification of ZR-MDR10

No	Parameter	Typical	Unit
1	Channel	8	-
2	Sampling rate	1~1000k	Hz
3	Analog-to-digital Converter	16	bit
4	Input range	±10	V
5	Maximum Sampling rate	1M	Hz
6	Frequency feature	−3～＋0.5	dB

3.2.5.6 Soil moisture sensor (ECH2O EC-5)

The soil moisture sensor (ECH2O EC-5 (METER Group, Inc., Pullman, WA, USA)) determines the volumetric water content of the soil shown in Figure 3.13. The specifications of EC-5 is shown in Table 3.4,

Figure 3.13 Soil moisture content sensor EC-5 (Decagon Devices)

Table 3.4 Specification of EC-5

No	Parameter	Typical	Unit
1	Accuracy (with soil specific calibration)	±1-2%	-
2	Resolution (mineral soil)	0.1%	-
3	Range (with polynomial equation)	0-100%	-
4	Dimension	8.9 x 1.8 x 0.7	cm
5	Measurement time	10	ms
6	Power	2.5 - 3.6 V DC @ 10 mA	-
7	Temperature	-40 to +50	°C

3.2.5.7 Soil moisture data logger (HOBO RX3000)

Data logger (*HOBO RX3000*) is manufactured by Onset Computer Corporation, shown in Figure 3.14.

Figure 3.14 HOBO RX3000 (Onset Computer Corporation)

The signals of the Soil moisture content sensor (EC-5) are converted to digital data and recorded by HOBO RX3000. HOBO can convert 10 channel's analog signal to digital data at the same time with a sampling rate of 1Hz. The specification of HOBO RX3000 is shown in Table 3.5.

Table 3.5 Specification of HOBO RX3000

No	Parameter	Typical	Unit
1	Data channel	10	-
2	Fastest Logging Rate	1	Hz
3	Memory	32M	Byte
4	Size	18.6 x 18.1 x 11.8	cm
5	Operating Range	-40 to +60	°C

3.2.5.8 Displacement sensor

Displacement sensor SL4515N-B100K is used to measure the shear displacement. It is a production of Supertech Electronic Co., Ltd. Figure 3.15 shows the photo of SL4515N-B100K, its Specification is summarized in Table 3.6

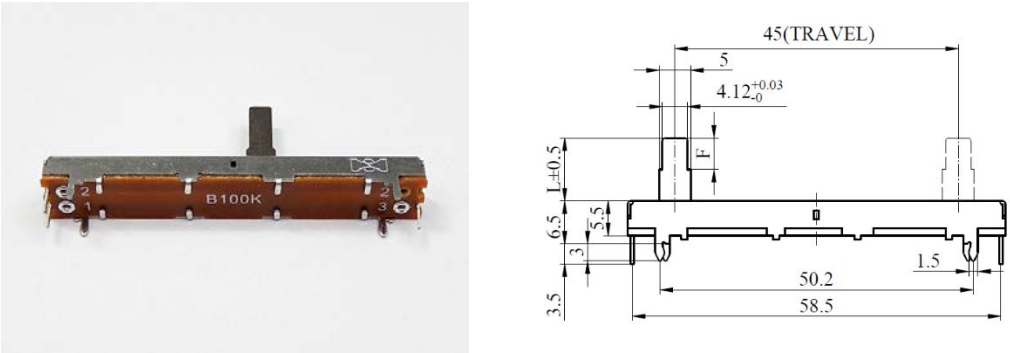

(a) (b)

Figure 3.15 photo of SL4515N-B100K; (b) Size (mm)

Table 3.6 Specification of SL4515N-B100K

Parameter	Typical	Unit
Operating temperature	1 0 ℃ ~ + 7 0	℃
Total resistance	100k	Ω
Resistance tolerance	20%	-
Sliding noise	Less than 100 mV at 20mm/sec	-
Residual resistance	≤20	Ω
Lever Travel	60	mm
Operating Force	3 0 ~ 2 0 0	gf.cm

Lever Stopper Strength	5	Kgf.cm

3.2.5.9 Load cell

Load Cell (SC902) is used to measure the shear force. It is a production of Sensor and Control Company Limited. Figure 3.16 shows the photo of Half Bridge Micro Load Cell (SC902), the Specification is summarized in Table 3.7.

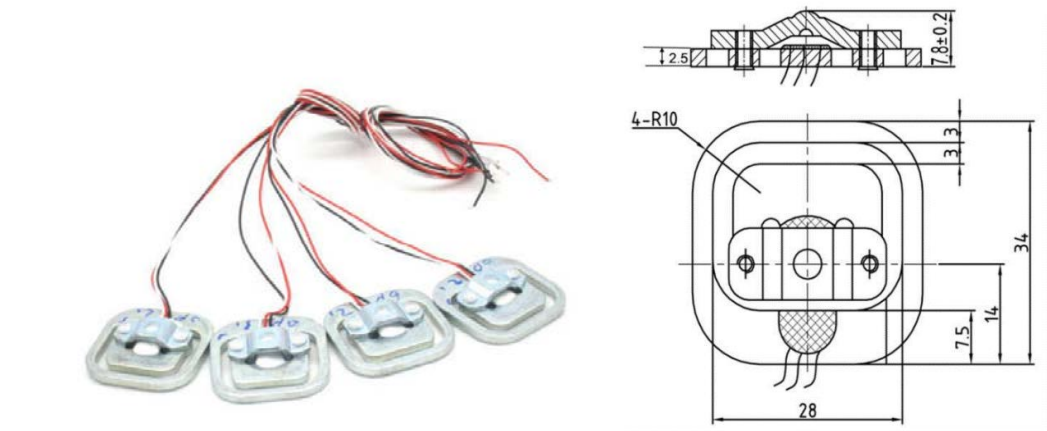

(**a**) (**b**)

Figure 3.16 a) photo of Half Bridge Micro Load Cell (SC902); b) size(mm). Sensor and Control Company Limited.

Table 3.7 Specification of SC902

Parameter	Typical	Unit
Capacity	50	kg
Comprehensive error	0.2% FS	-
Rated output	1.0±0.15	mV /V
Non-linearity	0.2% FS	-
Hysteresis	0.2% FS	-
Repeatability	0.15% FS	-
Creep	0.15%FS/10MIN	-
Zero balance	±0.3	mV /V
Input resistance	1090±10	Ω
output resistance	1000±10	Ω
Insulation resistance	≥2000M	Ω
Excitation voltage	3~10	VDC
Use temperature	-20~+55	ºC

3.2.5.10 Model AN-500

Model AN-500 is a production of Japan Instrumentation System Co., Ltd. Model AN-500 is used to calibrate the loadcell.

Figure 3.17 Model AN-500

3.2.6 Rainfall Simulation System

The artificial rainfall system includes an air compressor, pressure regulator, water tank, pipeline, and hydraulic spray nozzle. The water tank cover is airtight, and the air pressure is applied above the water surface. A pipeline is connected to the bottom of the tank and the nozzle at the end of the pipeline. Water sprays out under the applied air pressure. A uniform rainfall intensity of 60 mm/h was used in this study. The nozzle is an SSXP series manufactured by H. IKEUCHI and Co., Ltd., Osaka, Japan. Rainwater infiltrates into the top layer and then into sublayer, and finally drains from the bottom of the model. Figure 3.19 shows the rainfall simulation system used for the experiments where the nozzle is highlighted.

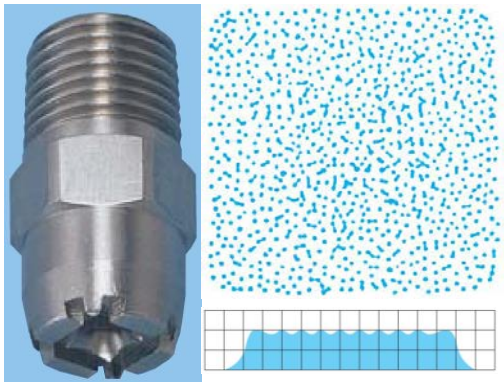

Figure 3.18 Square Spray Nozzle (SSXP)

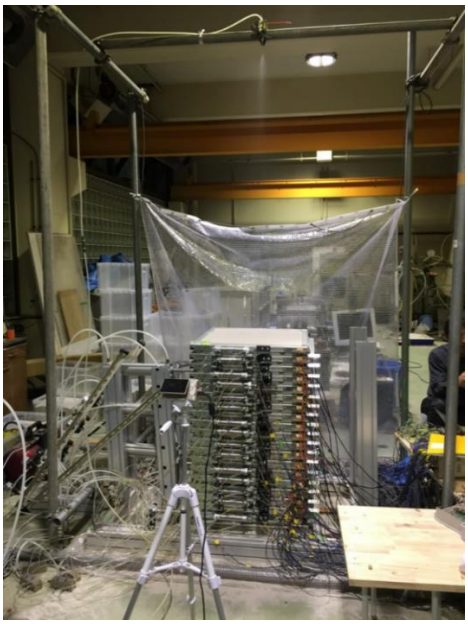

Figure 3.19 Rainfall simulation system.

3.2.7 Calibration of Soil Moisture Sensor

Soil moisture sensors (EC-5) were used to determine volumetric water content (VWC). Soil-Specific calibration is recommended for the best possible accuracy in volumetric water content measurements. Calibration of the EC-5 sensors has been shown to result in increased accuracy of 1%–2% for all soils with soil-specific calibration (Cobos and Chambers, 2005). Research has indicated that soil-specific calibration of soil moisture sensors achieves a good performance (Czarnomski et al., 2005). For the purpose of attaining a higher accuracy, all of the EC-5 sensors were calibrated with the test material.

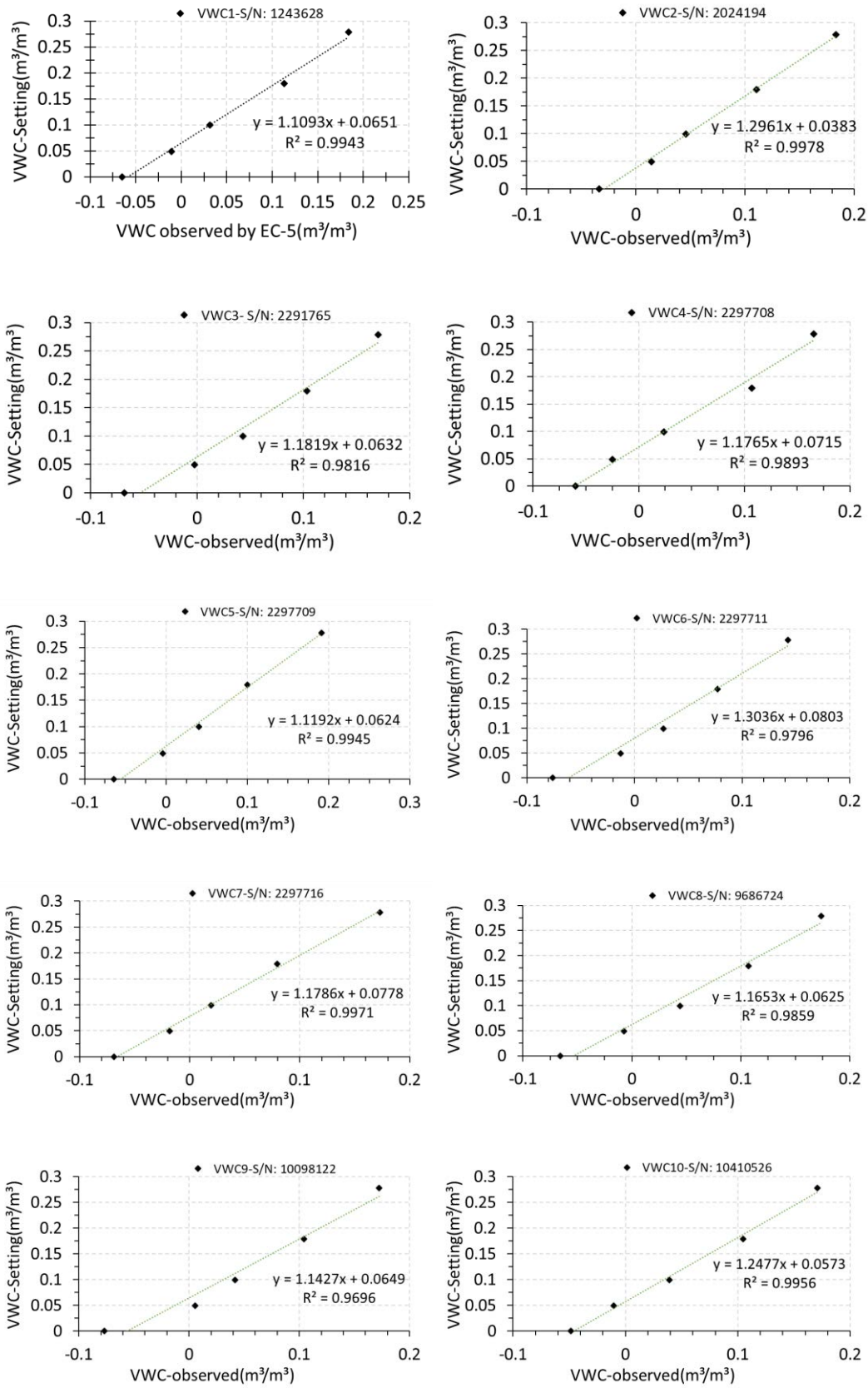

Figure 3.20 The calibration of soil moisture.

3.3 ELASTIC WAVE MONITORING SYSTEM ON-SITE

Investigate the elastic wave propagation in soil not only in laboratory experiments using the Multi-layer shear model but also in a natural slope surface layer. Figure 3.21 shows the schematic description of the elastic wave monitoring system On-site. It includes a microcontroller, signal amplifier, exciter, receivers, and battery. Under the command from the microcontroller, the elastic wave can be automatically generated by the exciter, measured the wave signal by receivers, and save to the SD card.

The microcontroller is using MSP432P4111, which includes an integrated 16-bit precision ADC, 2MB flash and 256kB SRAM and a 48MHz Arm® Cortex®-M4F processor. It is a low-power operation and suitable for developing high-precision sensor node applications (Figure 3.22).

Figure 3.23 shows the receivers using On-site. ADXL354 is inside, the same sensor using in laboratory experiments. An amplifier is designed because of the high wave attenuation propagation in soil. Figure 3.24 shows the exciter, a solenoid is inside.

The elastic wave monitoring system installed on an unstable slope, shown in Figure 3.25, and a case of senor layout underground, shown in Figure 3.26.

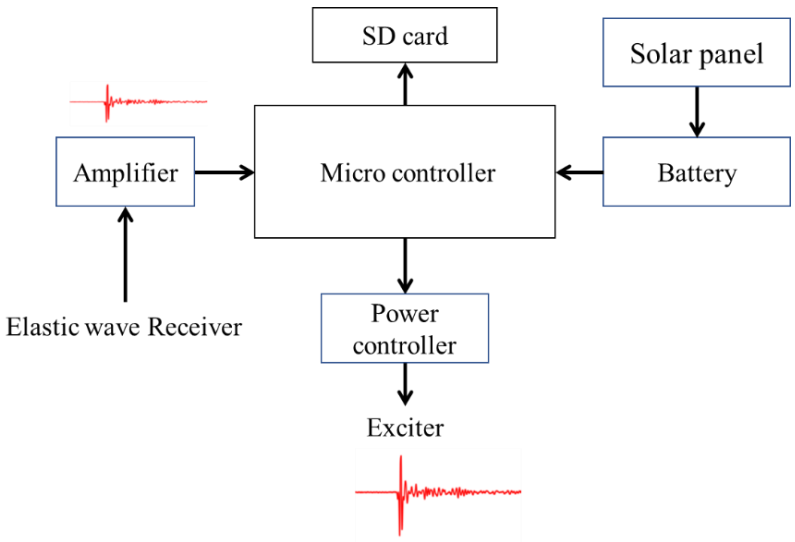

Figure 3.21 Schematic description of the elastic wave monitoring system On-site

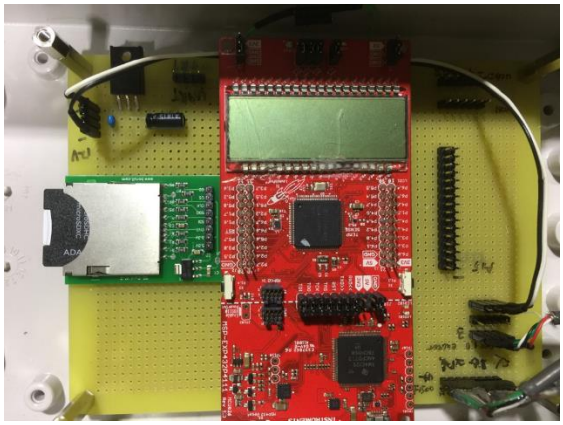

Figure 3.22 micro controller is MSP-EXP432P4111

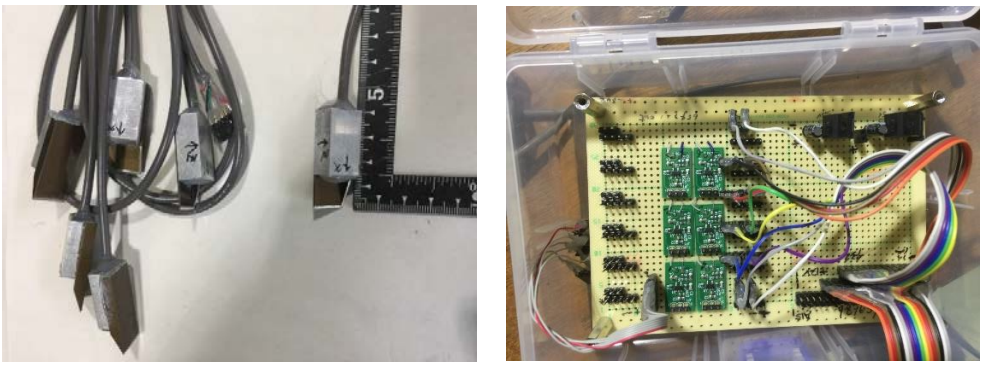

(**a**) (**b**)

Figure 3.23 The receivers using On-site. a) Receivers, ADXL354 inside. b) Amplifier

(**a**) (**b**)

Figure 3.24 The exciter using On-site. a) Exciter, a solenoid inside. b) Power controller for the exciter.

(**a**) (**b**)

Figure 3.25 elastic wave monitoring system installed on an unstable slope. (a) kumamoto, 2018/05/10; (b) kumamoto, 2019/08/04

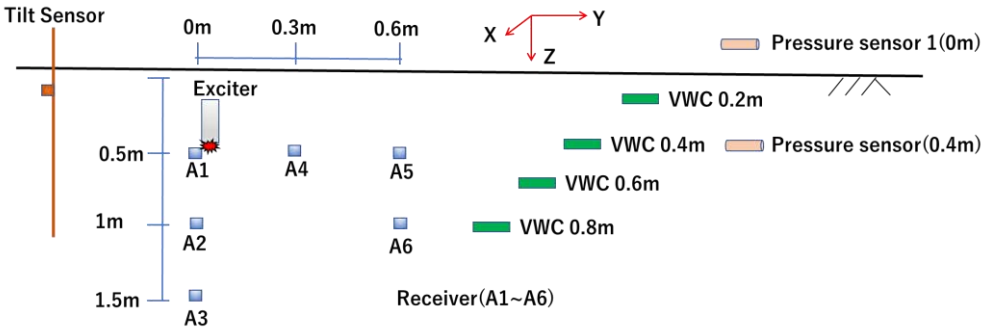

Figure 3.26 A case of senor layout underground

3.4 SUMMARY

This chapter discusses the details of the experimental apparatus used for this research. The functional description of the multi-layer shear model, shear force control system, rainfall simulation system, as well as the elastic wave instrumentation, the elastic wave monitoring system on-site assembly have been presented in detail by means of photographs and schematic illustrations.

3.5 REFERENCES

Chen, Y., Uchimura, T., Irfan, M., Huang, D., Xie, J., 2017. Detection of water infiltration and deformation of unsaturated soils by elastic wave velocity. Landslides 14, 1715–1730. https://doi.org/10.1007/s10346-017-0825-8

Cobos, D., Chambers, C., 2005.Calibrating ECH 2 O Soil Moisture Sensors Application Note 1–5.

Czarnomski, N.M., Moore, G.W., Pypker, T.G., Licata, J., Bond, B.J., 2005. Precision and accuracy of three alternative instruments for measuring soil water content in two forest soils of the Pacific Northwest 1876, 1867–1876. https://doi.org/10.1139/X05-121

Irfan, M., Uchimura, T., 2016. Modified triaxial apparatus for determination of elastic wave velocities during infiltration tests on unsaturated soils. KSCE J. Civ. Eng. 20, 197–207. https://doi.org/10.1007/s12205-015-0404-2

Irfan, M., Uchimura, T., Chen, Y., 2017. Effects of soil deformation and saturation on elastic wave velocities in relation to prediction of rain-induced landslides. Eng. Geol. 230, 84–94. https://doi.org/10.1016/j.enggeo.2017.09.024

Nobutomo, O., Yoko, T., Kazuya, A., Tomoaki, M., 2009. Realty of cliff failure disaster, CHNICAL NOTE of Natonal Institute for Land and Infrastructure Management. NILIM.

CHAPTER 4

MATERIALS & METHODOLOGY

4.1 TESTED MATERIAL

The test material used in this study was composed of silica sand No. 4, No. 5, No. 7 and No. 8 mixed at a ratio of 1:1:3:1 to closely resemble the particle size distribution in the natural soil of the slope. It had a dry density of around 1.481 g/cm3. Its minimum and maximum dry density were found to be 1.308 g/cm3 and 1.707 g/cm3. The relative density (Dr) was 50% and the volume water content was 7.4% at the initial state (all tests were conducted according to Japanese Geotechnical Society (JGS) standards; JGS 0161 test method for minimum and maximum densities of sands (JIS A1224)). Figure 4.1 shows the grain size accumulation curve of the test material. A nature soil showed Figure 4.1 is sampled from a slope in Aso-shi, Kumamoto, Japan.

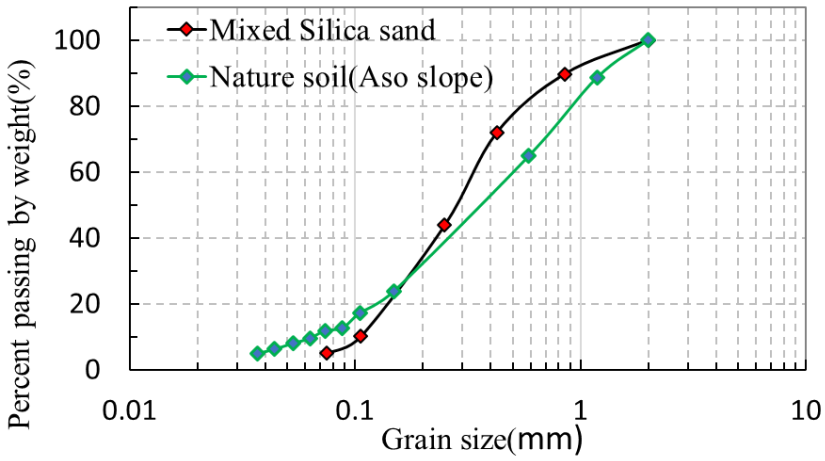

Figure 4.1 Grain size accumulation curve of the material.

4.1.1 Physical Properties of Tested Material

Table 4.1 Physical properties of the tested material

No	Test material	Silica sand No4,5,7,8	Silica sand 7
1	Dry density (ρ_d)	$1.481 g/cm^3$	$1.373\ g/cm^3$
2	Maximum dry density (ρ_{dmax})	$1.707 g/cm^3$	$1.523\ g/cm^3$
3	Minimum dry density (ρ_{dmin})	$1.308 g/cm^3$	$1.196\ g/cm^3$
4	Relative density (D_r)	50%	60%
5	Volume Water Content (initial)	7.4%	7.4%

4.1.2 Determine Soil Strength by Direct Shear Test

It is meaningful to investigate the shear strength of soil in the unsaturation condition, especially in the process of rainfall-induced slope failure. In geotechnical fields, the general shear strength parameters of soil known as cohesion c and internal friction angle φ. The criterion of Mohr-Coulomb is expressed by

$$\tau = \sigma * \tan(\varphi) + c \tag{4-1}$$

Where τ shear stress, σ is vertical stress, φ is friction, c is cohesion.

Box shear apparatus is shown in Figure 4.2, the vertical pressure is applied by air cylinder, keeping constant by manual during the shear test. The shear force is driven by a motor with a shear rate of 0.0275mm/sec. The vertical pressure and the shear force are measured by loadcells, the horizontal displacement (Dh) and vertical displacement(Dv) are measured by displacement sensors(Figure 4.3, Figure 4.4). The loadcells and displacement sensors are calibrated before the experiments (Figure 4.5).

The direct shearing process was including 6 different vertical loadings which start from 10kPa, 20kPa, 30kPa,50kPa, and 70kPa for one VWC. Each shearing stage took about 7 minutes to reach a shear displacement of 10mm. The test case of the direct shear test is shown in Table 4.1, The relative density (Dr) is 50%.

The friction is 42 digress, which are summarized by the series experiments (Figure 4.6). Figure 4.7 ~Figure 4.14 are the detail results.

The friction is the reference values used by the multi-layer shear test.

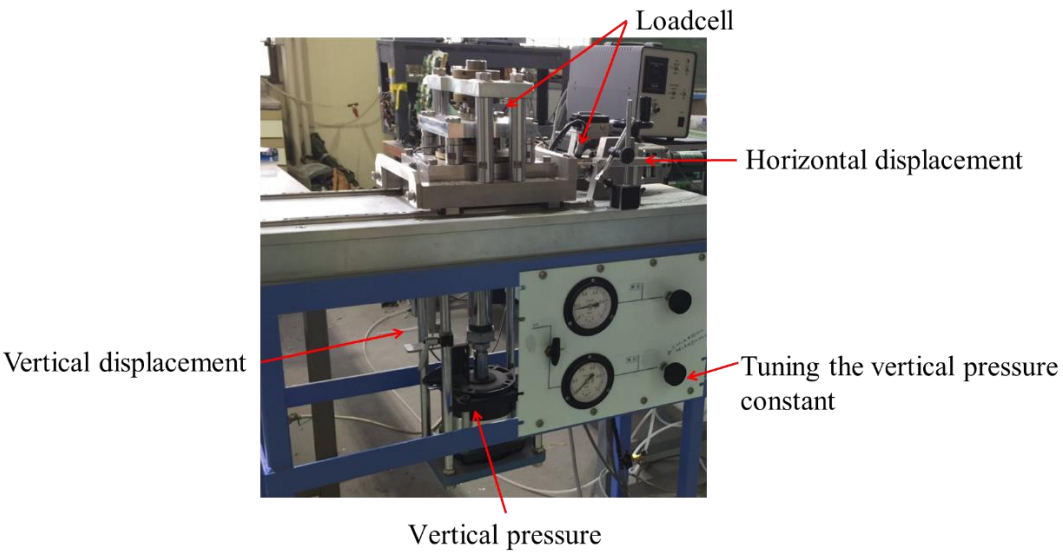

Figure 4.2 Box shear apparatus with a single shear surface

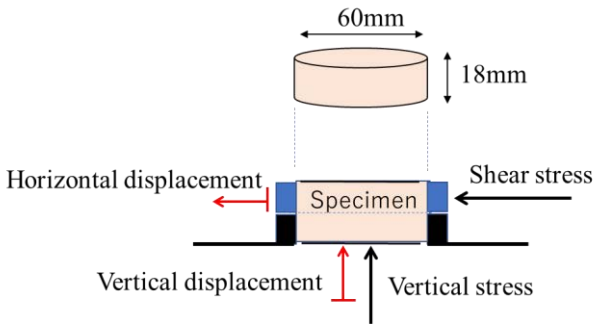

Figure 4.3 The specimen setup in the direct shear test.

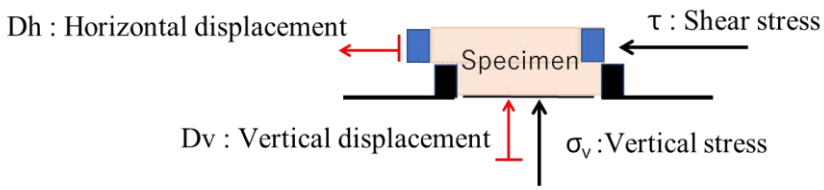

Figure 4.4 The specimen after the direct shear test.

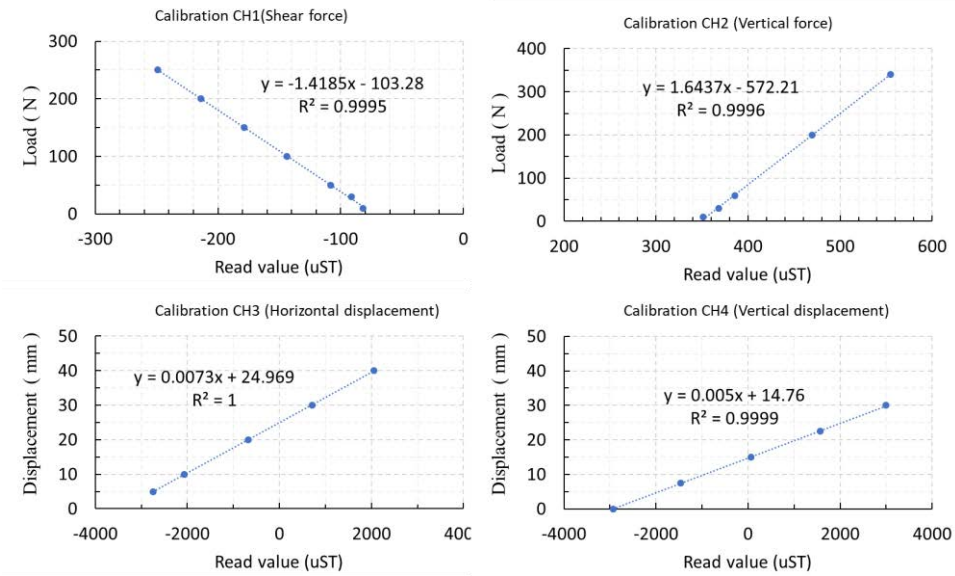

Figure 4.5 Calibration of the load cells and displacement sensors.

Table 4.2 Test cases of direct shear test

VWC	σ(kPa)	σ(kPa)	σ(kPa)	σ(kPa)	σ(kPa)
0.05	10	20	30	50	70
0.10	10	20	30	50	70
0.15	10	20	30	50	70
0.20	10	20	30	50	70
0.25	10	20	30	50	70
0.30	10	20	30	50	70
0.35	10	20	30	50	70
0.40	10	20	30	50	70

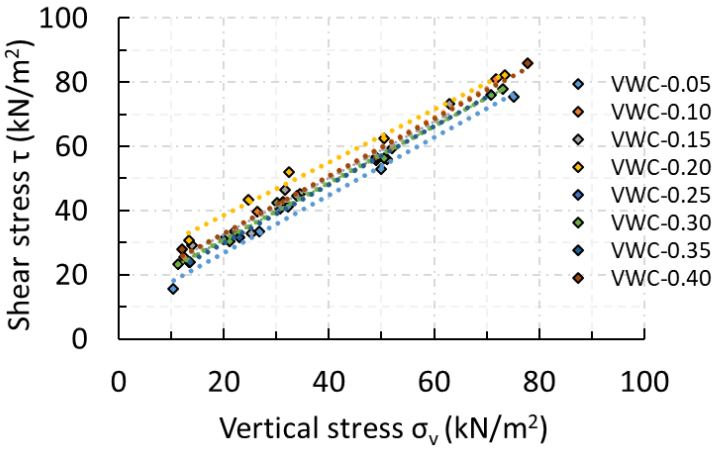

Figure 4.6 Shear stress versus vertical stress in various VWC (φ = 42)

VWC = 0.05

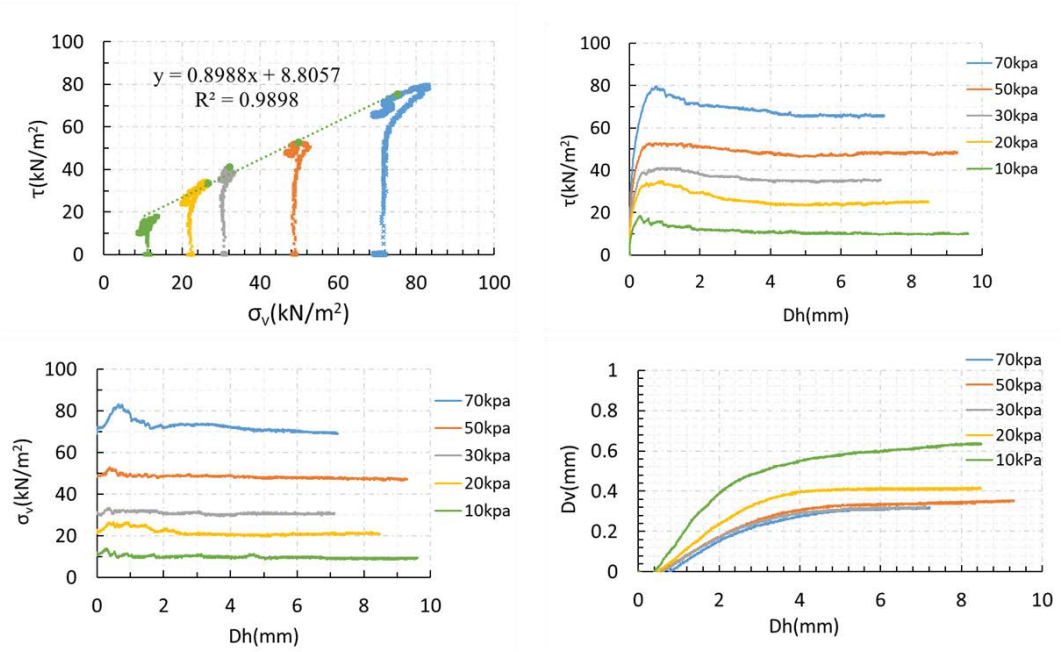

Figure 4.7 The relationship between shear stress, vertical stress, and displacement when VWC = 0.05.

VWC = 0.10

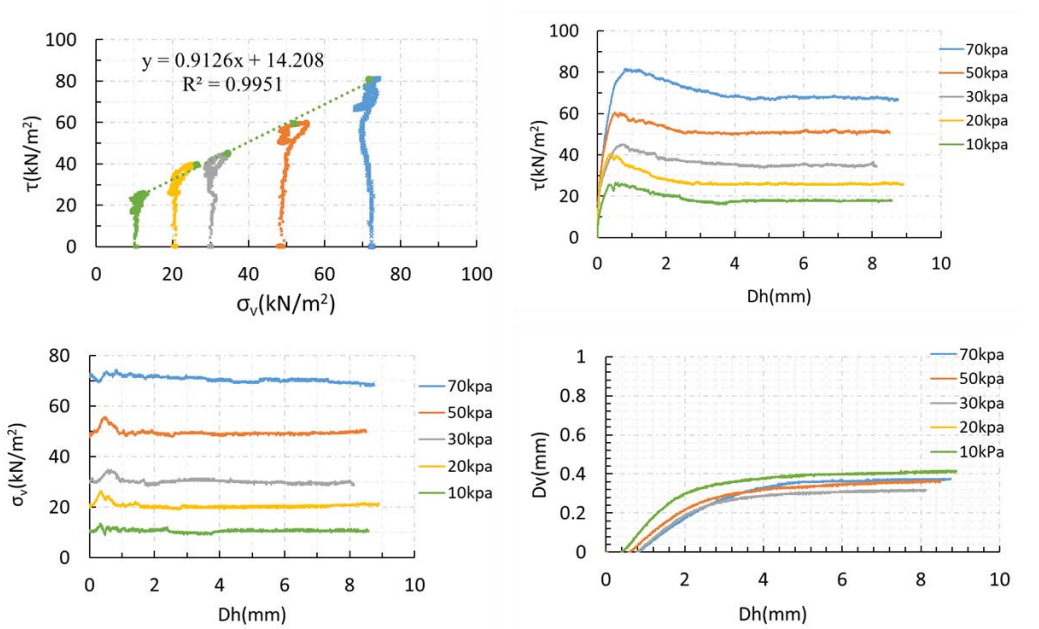

Figure 4.8 The relationship between shear stress, vertical stress, and displacement when VWC = 0.10.

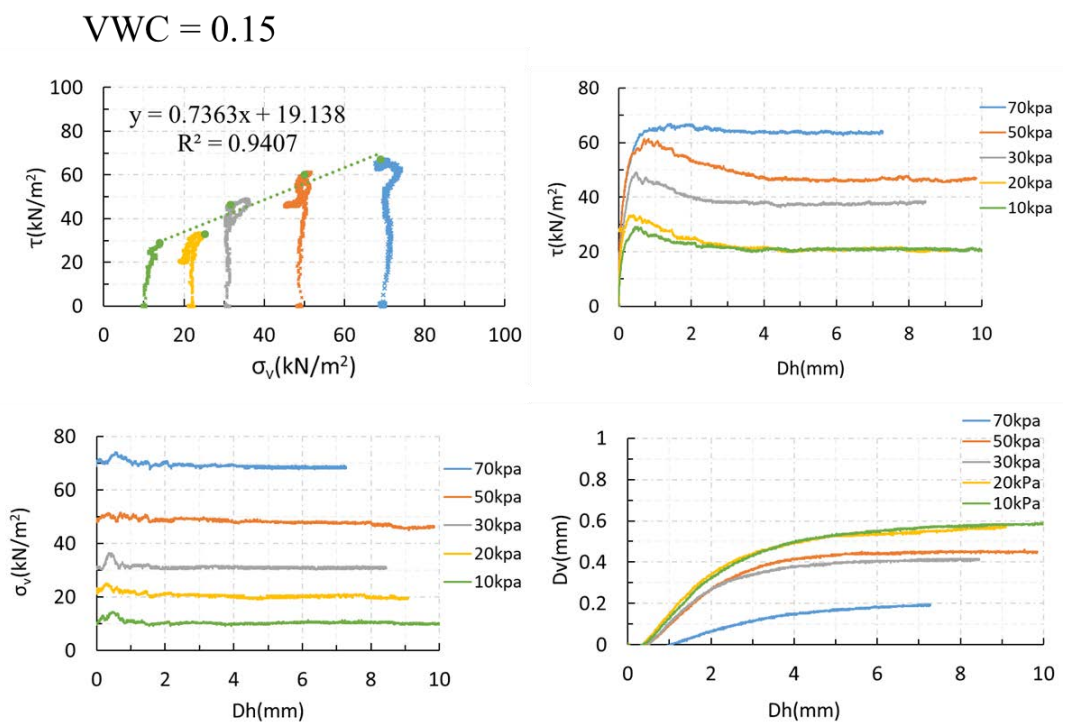

Figure 4.9 The relationship between shear stress, vertical stress, and displacement when VWC = 0.15.

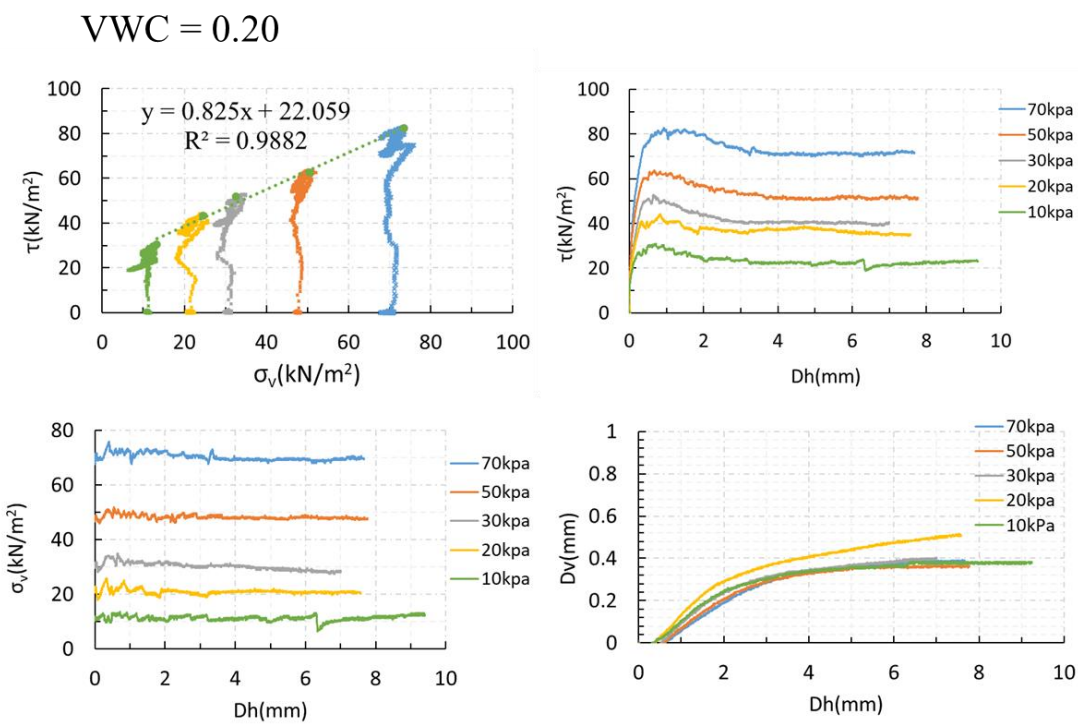

Figure 4.10 The relationship between shear stress, vertical stress, and displacement when VWC = 0.20.

VWC = 0.25

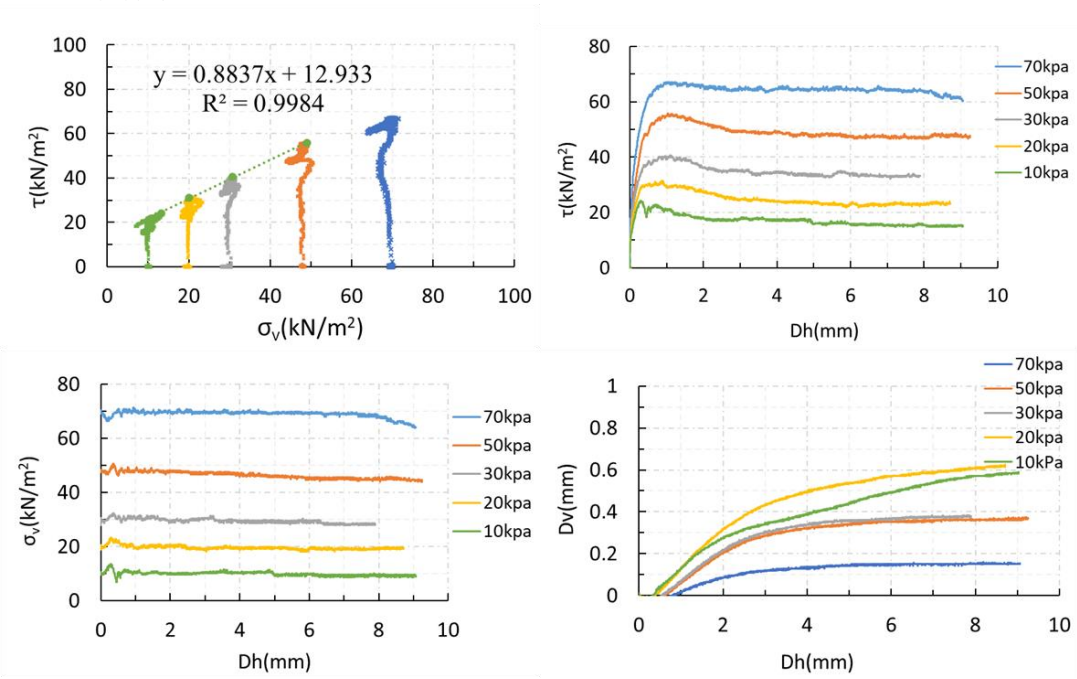

Figure 4.11 The relationship between shear stress, vertical stress, and displacement when VWC = 0.25.

VWC = 0.30

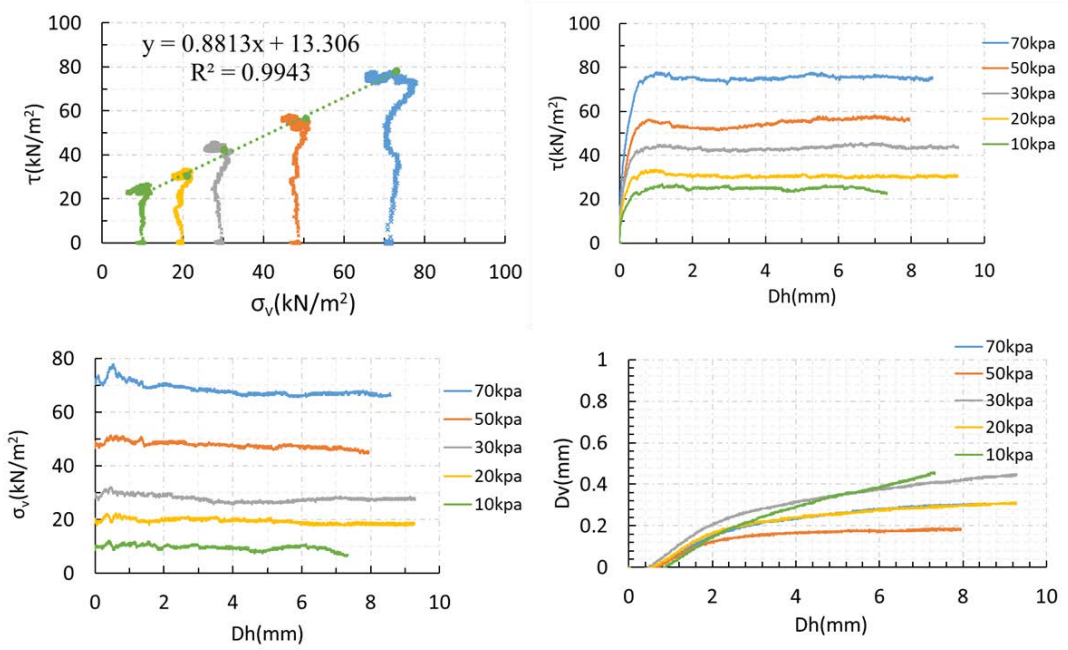

Figure 4.12 The relationship between shear stress, vertical stress, and displacement when VWC = 0.30.

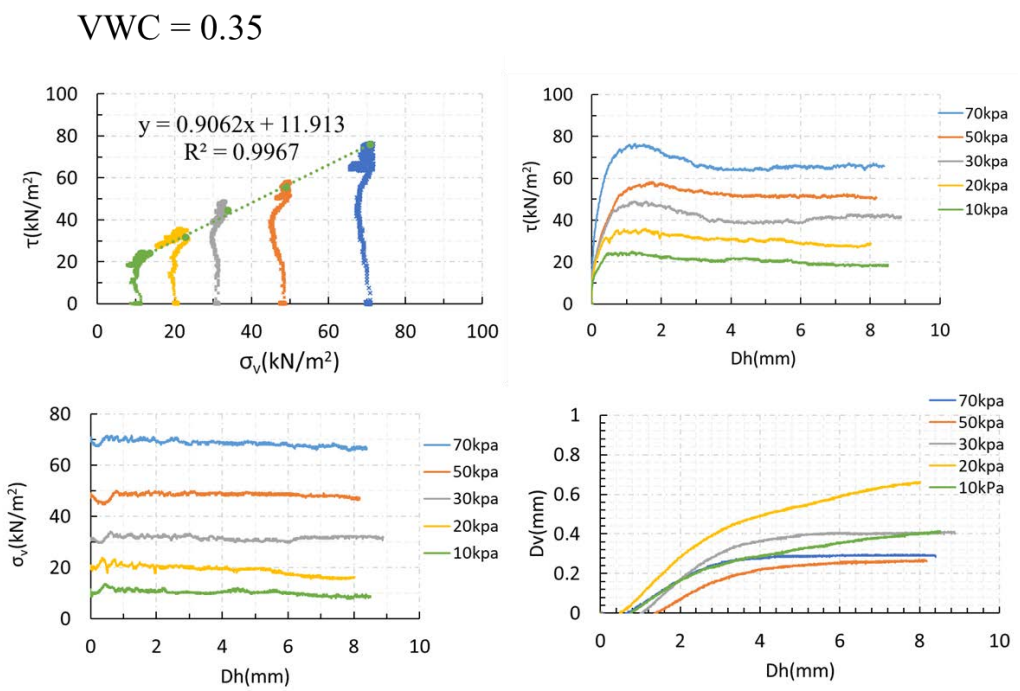

Figure 4.13 The relationship between shear stress, vertical stress, and displacement when VWC = 0.35.

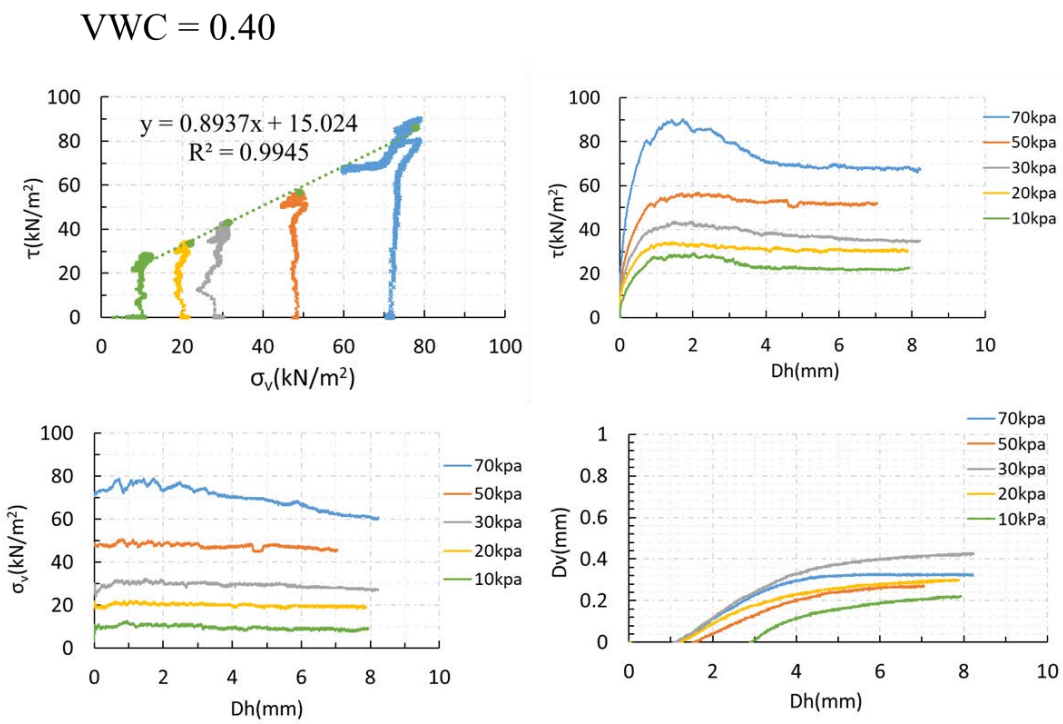

Figure 4.14 The relationship between shear stress, vertical stress, and displacement when VWC = 0.40.

4.2 EXPERIMENTAL PROCEDURES

Although both laboratory experiments and on-site monitoring were used in this study, the majority of tests conducted as part of this study were performed in the laboratory experiment. Therefore, detailed descriptions of the experimental procedures are focused on the laboratory testing system. An introduction of testing procedures on-site monitoring is presented in the subsequent section as well. To simulate the process of rainfall-induced slope failure, a series of test cases were conducted as part of this research are summarized below.

Figure 4.15 shows the layout of sensors in the soil and the layout displacement meters in the laboratory experiment, E1~E10 are the exciters; CH01~CH30 are the receivers; VWC1~VWC10 are the soil moisture sensors, Dis1~Dis19 are the displacement meters.

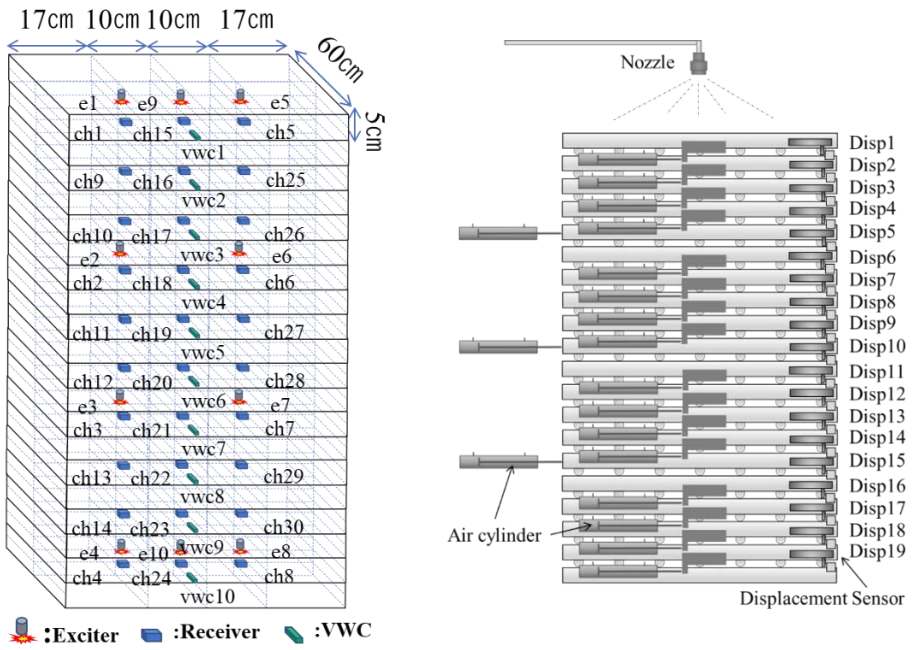

(a) (b)

Figure 4.15 The layout of sensors. a) E1~E10 are the exciters; CH01~CH30 are the receivers; VWC1~VWC10 are the soil moisture sensors. b) Dis1~Dis19 are the displacement meters.

Test Procedure of multi-layers shear test contains the following steps:

1) Prepare the soil specimen. Compose the silica sand No. 4, No. 5, No. 7 and No. 8 mixed at a ratio of 1:1:3:1. Weight the dry mixed sand (Dr = 50%), add water (VWC = 7.4%) and make the wet mixed sand uniform. Construct the soil model by tamping at every 25 mm in the frame(600mm*540mm*50mm).
2) Layout the sensors in soil. The position of the sensors is based on test design (Figure 4.16~Figure 4.19). Check the signal of sensors and confirm they work correctly.
3) Redo steps 1 and 2 until Construct 20 layers (Figure 4.20~Figure 4.21).
4) Set up the load cells and displacement sensors at every layer, and confirm they work correctly.
5) Start to record all data includes elastic wave, soil moisture, shear force, and shear displacement.
6) Set the shear force by tuning the air cylinder to the corresponding slope angle. wait and check the shear displacement until not change.
7) Start the rainfall. Check the VWC and shear displacement during the rainfall. If the VWC at the bottom becomes stable and there is no shear displacement at any layer, go to step 8.
8) Stop the rainfall. Drain the water out more than 20hours.
9) Redo step 6 to step 8 until the model failure.

Shear stress corresponding to the slope angle was different at every layer because the soil weight increased with the depth. The greater the depth, the stronger the shear stress that was applied, shown in Figure 4.22.

High soil moisture was observed at the bottom of the model in both rainfall and drain events. High soil moisture decreases the soil strength when high shear stress is applied. Therefore, the layers near the bottom failed more easily than the other layers. Figure 4.23 shows the model failed after the shear force was set corresponding to the slope angle of 33-degrees.

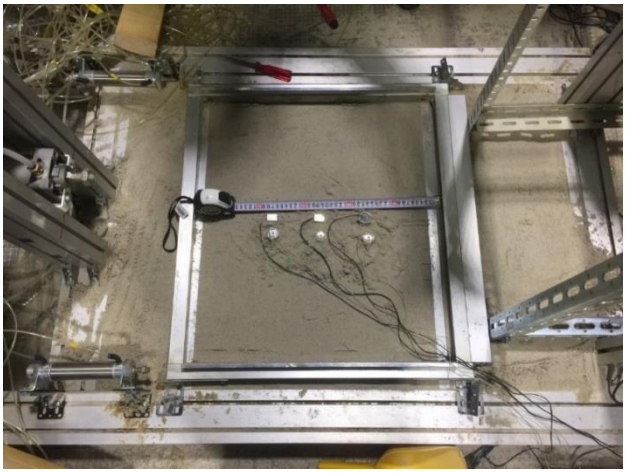

Figure 4.16 The layout of exciters and receivers in the bottom layer

Figure 4.17 The layout of the receivers.

Figure 4.18 The layout of the exciters.

Figure 4.19 The layout of the soil moisture sensor and receivers.

Figure 4.20 Prepared five layers.

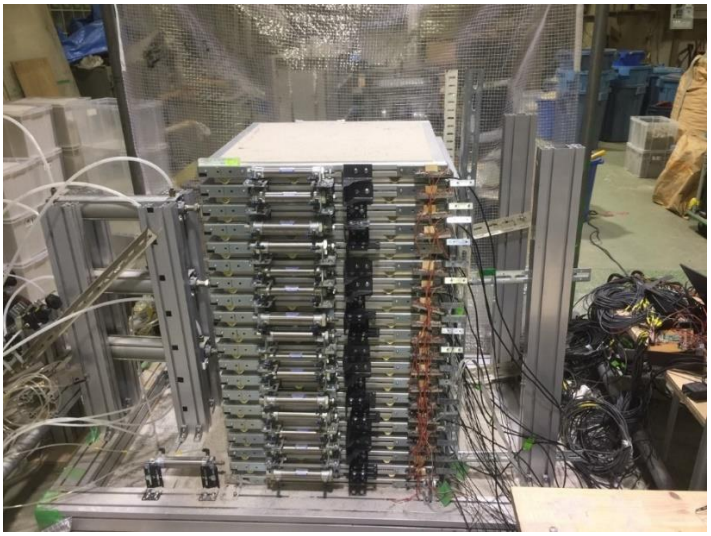

Figure 4.21 Finished the setup of the model.

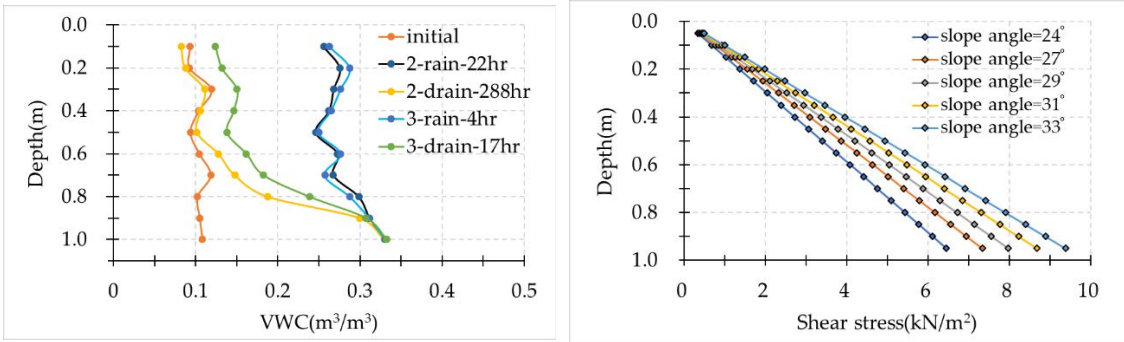

(**a**) (**b**)

Figure 4.22 (a) Soil moisture distribution with depth after the rainfall and drain events; (b) shear stress with a depth corresponding to the slope angle.

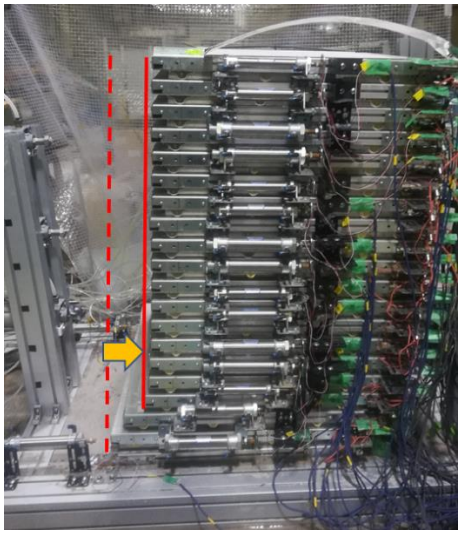

Figure 4.23 The model failed after the shear force was set corresponding to the slope angle of 33-degrees.

4.3 CONFIRM THE ELASTIC WAVE SIGNALS

The elastic wave is generated by exciter and detected by receivers. The vertical survey line and the vertical axis of the receivers were analyzed. The wave can be considered a compression wave because the survey line is in the compression direction. The wave signals of receivers on vertical survey lines are shown in Figure 4.24, Figure 4.25, Figure 4.26, note the different scales on the y-axes. The travel time of on these vertical survey lines are almost the same, it shows than the wave signals are correct (Figure 4.27). The concentric propagation of wave in soil is shown in Figure 4.28.

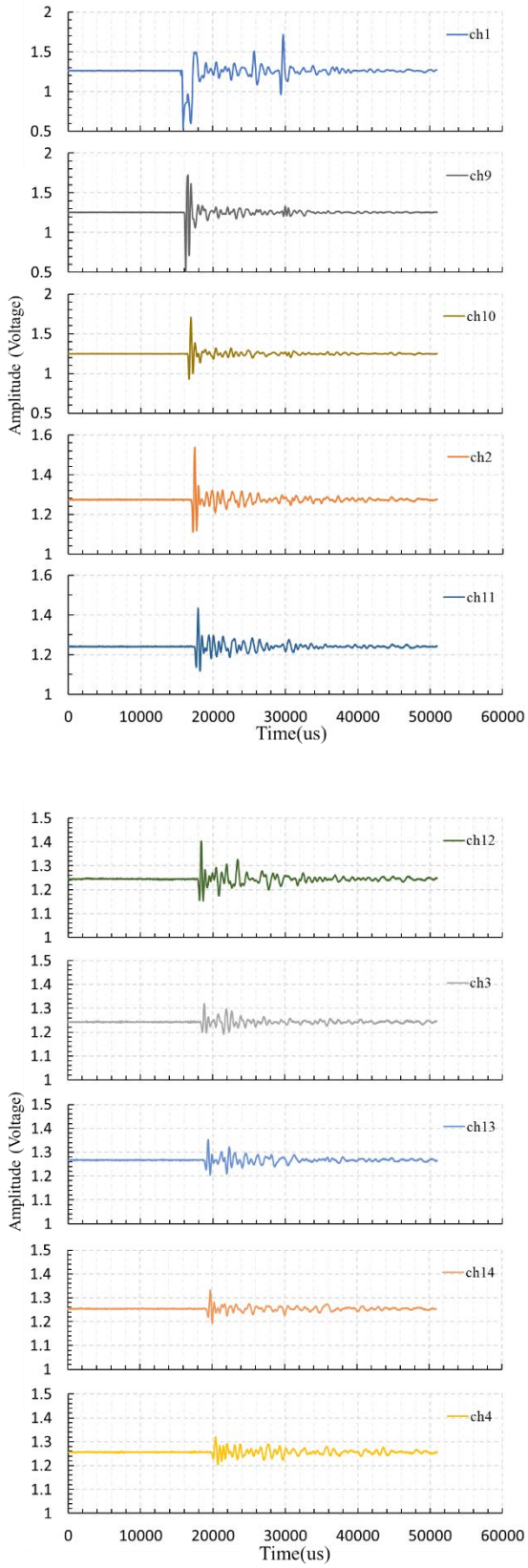

Figure 4.24 The wave signal of receivers on the vertical survey line under exciter(e1).

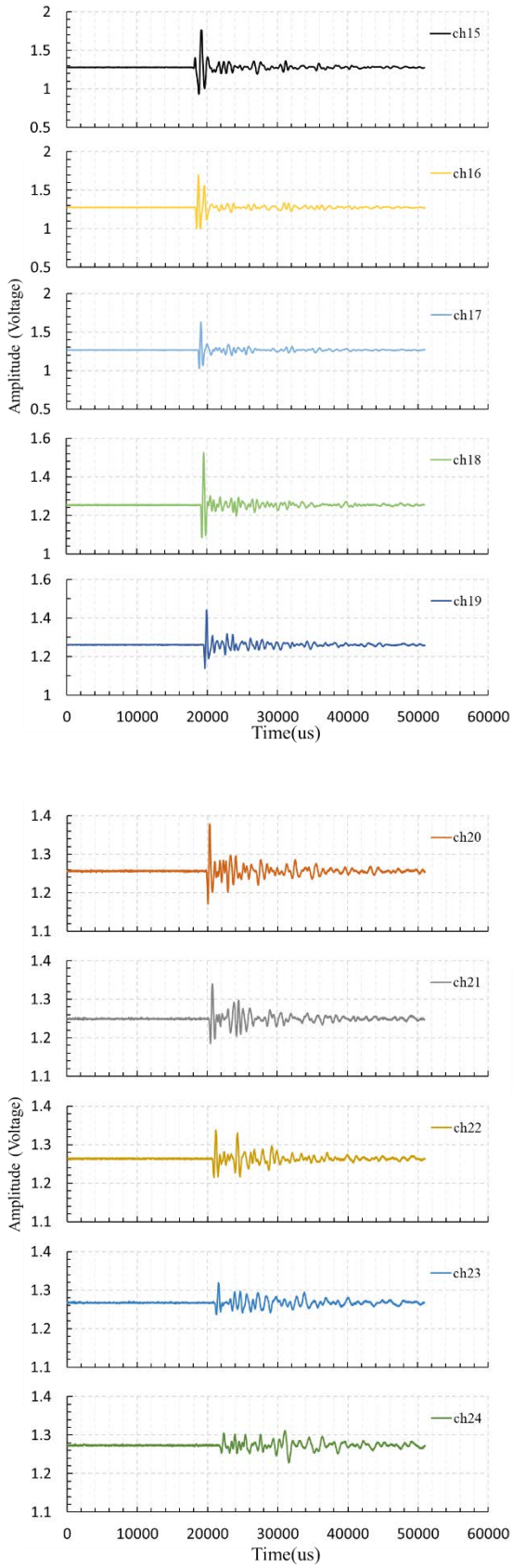

Figure 4.25 The wave signal of receivers on the vertical survey line under exciter(e9)

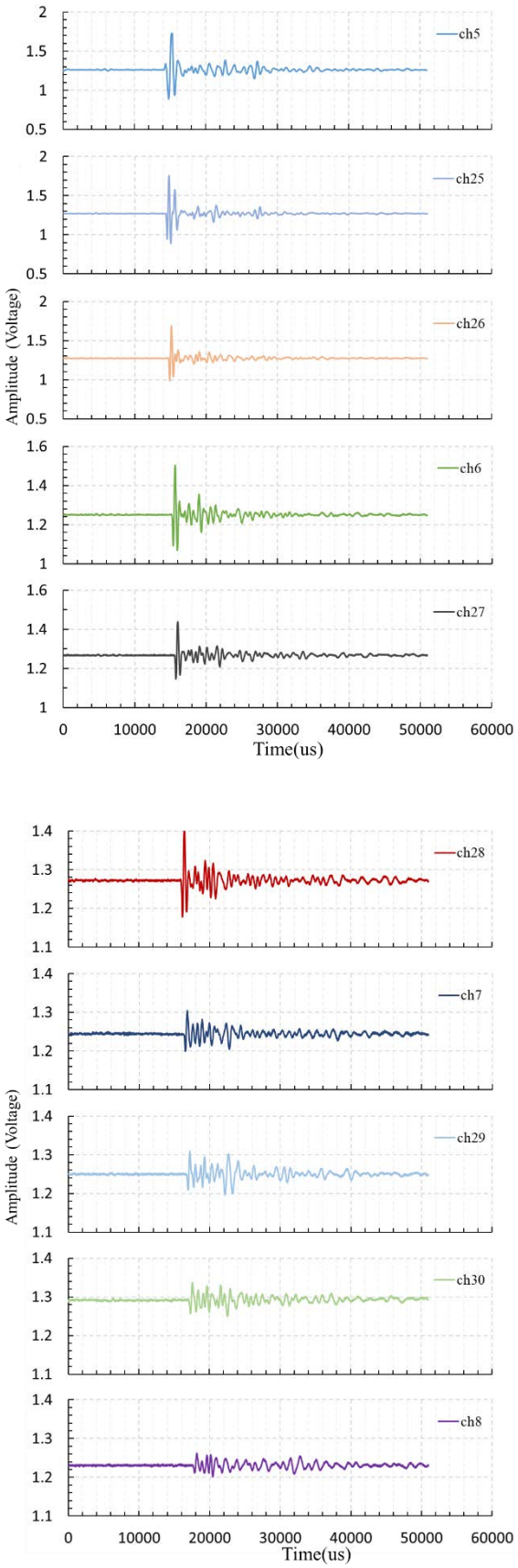

Figure 4.26 The wave signal of receivers on the vertical survey line under exciter(e5)

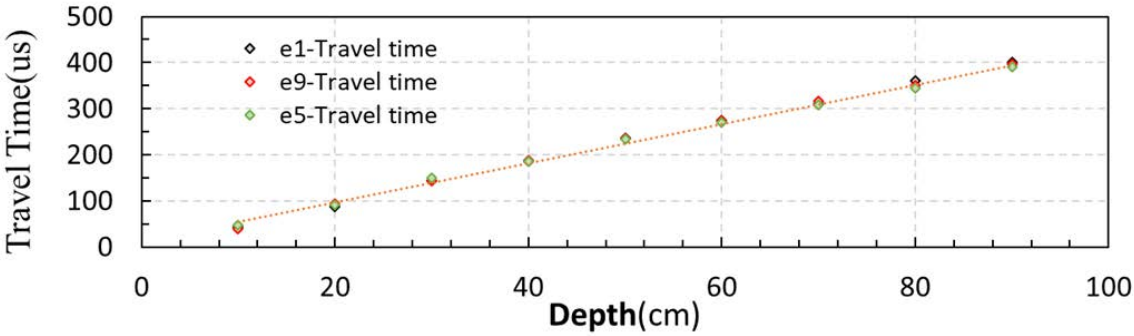

Figure 4.27 The travel time on 3 vertical survey lines.

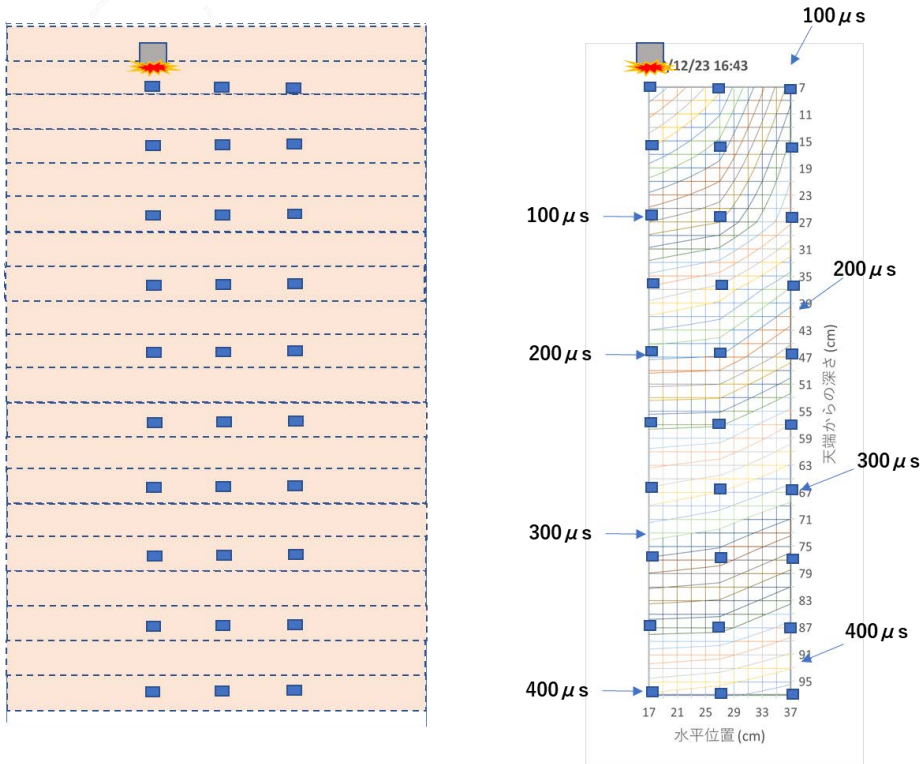

Figure 4.28 The travel times of all the sensors show the concentric propagation of elastic wave in soil

4.4 SUMMARY

This chapter described the physical properties and soil strength of tested materials used in this study. The detailed experimental program designed to achieve the objectives of this study was presented. Details of experimental procedures, including preparation specimen, set up and arrangement of sensors were discussed. The elastic wave signal of every receiver was discussed as well.

4.5 REFERENCES

Coop, M. R., Sorensen, K. K., Freitas, T. B., & Georgoutsos, G. (2004). Particle breakage during shearing of a carbonate sand. Géotechnique, 54(3), 157-163.

Kuwajima, K., Hyodo, M., & Hyde, A. F. (2009). Pile bearing capacity factors and soil crushabiity. Journal of geotechnical and geoenvironmental engineering, 135(7), 901-913.

Yu, F., (2014). Experimental study on particle breakage under high pressure (Doctoral dissertation). The University of Tokyo.

CHAPTER 5

FACTORS AFFECT ON ELASTIC WAVE VELOCITIES IN SLOPE SURFACE LAYER

5.1. INTRODUCTION

Elastic wave propagation in soil as a non-destructive monitoring technique has received considerable attention in recent years. The application of elastic wave propagation in soil has been developed by many researchers, for example, shear waves were measured in laboratory specimens by means of piezoelectric transducers (Brignoli et al., 1996), and recently, both shear wave (S-wave) and compression wave (P-wave) velocities were designed to measure the unsaturated soil (Irfan and Uchimura, 2016). It was found that both P-wave and S-wave velocities decreased by nearly half when soil saturation was increased from 20% to 80% in laboratory triaxial experiments (Irfan et al., 2017). A series of model experiments found that elastic wave velocities continuously decreased in response to moisture content and deformation (Chen et al., 2017).

In this study, a full-scale multi-layer shear model was used to simulate the process of slope failure and observe the wave propagation, to investigate the changes of elastic wave velocities are affected by normal stress, soil moisture, shear stress and shear displacement in the process of shallow slope failure. The relationship of the elastic wave velocities and normal stress, soil moisture, shear displacement was driven as a multiplication formula, the coefficient of normal stress, soil moisture content, the shear stress, and the displacement was determined from a series of experiments were conducted. Finally, the elastic wave velocities calculated by the coefficient and the input soil moisture and shear stress were compared to the measured velocities.

5.2. METHOD TO CALCULATE THE WAVE VELOCITIES

➢ ***Elastic Wave Velocities***

Figure 5.1 shows the method to calculate the elastic wave velocity. The wave signal is generated by an exciter installed at the top layer. The wave signal travels through the soil and is detected by receivers. Figure 5.1 shows that the ch4, the farthest from the exciter, can detect a clear wave signal. The vertical survey line and the vertical axis of the receivers were analyzed. The wave can be considered a compression wave (P-wave) because the survey line is in the compression direction (Steven L, 1996). Several compression wave velocities on the vertical survey line were investigated, and, due to soil moisture, shear stress and shear displacement, are different in these block areas. The wave velocity is expressed by

$$V_i = \frac{D_i}{T_i} = \frac{D_i}{t_{i+1} - t_i} \; (i = 1,2,3,4) \tag{5-1}$$

where Vi is the wave velocity, Di is the distance, t is the first travel time of the wave signal, i is the number of the receiver.

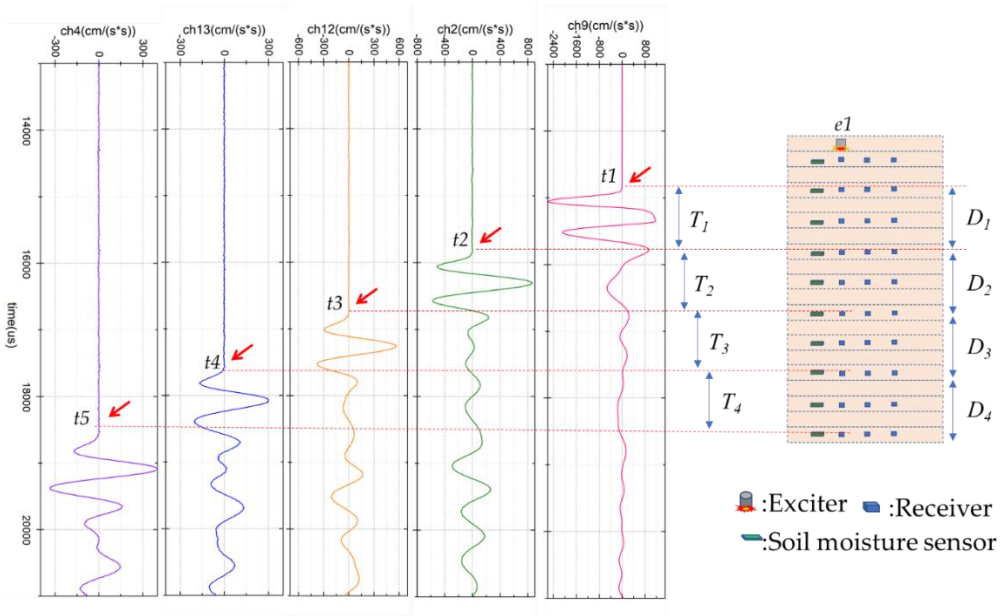

Figure 5.1 Waveforms and the method to calculate the elastic wave velocity. The wave signal is generated by exciter e1 and detected by receivers in the vertical survey line. The wave velocity is defined by the travel distance divided by the travel time between two receivers. t1~t5 are the first travel times of the wave signals.

- ***Automatic Travel Time Picking***

In this study, 30 waveforms can be measured by 30 channels with a sampling rate of 100 kHz. A total of 2,592,000 waveforms can be collected in a day's wave monitoring test. Picking the first travel time manually is very time consuming, and it is impossible to adopt this method to analyze the huge amount of data. Automatically picking the travel time by computer is necessary for analyzing the data.

Many researchers have developed techniques and methods for automatically measuring the first travel time of a wave. For example, a computer-based system dedicated full time to automatic detection and location of local seismic events (Stewart, 1977) and automatic detection of P-wave and S-wave travel times of small earthquakes (Morita, 1984) has been developed. Reliable automatic picking of the first travel time of acoustic emissions and ultrasound signals in concrete has also presented (Kurz et al., 2005). It showed that different versions of automatic picking methods appeared due to the different characteristics of the wave signal.

Depending on the wave signal generated by the newly designed exciter in this study, the algorithm for automatic picking of the travel time is based on the Akaike information criterion (AIC) (Maeda, 1985; Takanami and Kitagawa, 1991), which can provide accurate and reliable travel time determination of elastic wave signals.

A waveform with a length of N samples can be divided into two parts at a point k, shown in Figure 5.2. The first part includes k samples and its normal distribution is σ_1; the second part includes (N − k) samples and its normal distribution is σ_2. The AIC value at k is defined by the following formula

$$AIC(k) = k * log({\sigma_1}^2) + (N - k) * \log({\sigma_2}^2). \tag{5-2}$$

The normal distribution σ is defined as

$$\sigma^2 = \frac{1}{n-1}\sum_{i=1}^{n}(x_i - \mu)^2 \tag{5-3}$$

where n denotes the length of the signal, x_i is sample i of the time series, and μ is the mean value of the whole time series x, defined as

$$\mu = \frac{1}{n}\sum_{i=1}^{n} x_i. \tag{5-4}$$

The AIC value can be calculated by Equation (5-2) when setting the index k from 1 to N. The minimum is the first travel time of the elastic wave, shown in Equation (5-5). In Figure 5.3, the AIC value is represented by the dashed line, the minimum AIC value denotes the first travel time of the signal.

$$\text{Travel time } = \text{Min}\{AIC(1), AIC(2), \ldots, AIC(N-1), AIC(N)\} \tag{5-5}$$

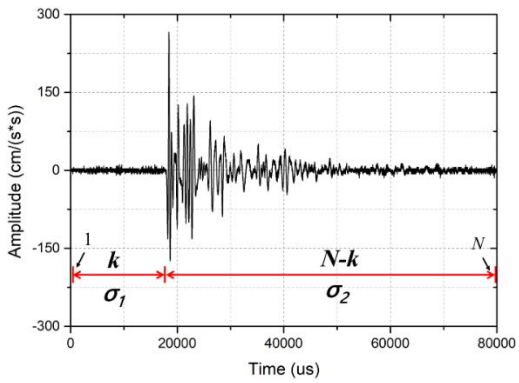

Figure 5.2 A time series of a wave signal is divided into two parts; the first part includes k samples and its normal distribution is σ_1; the second part includes (N– k) samples and its normal distribution is σ_2.

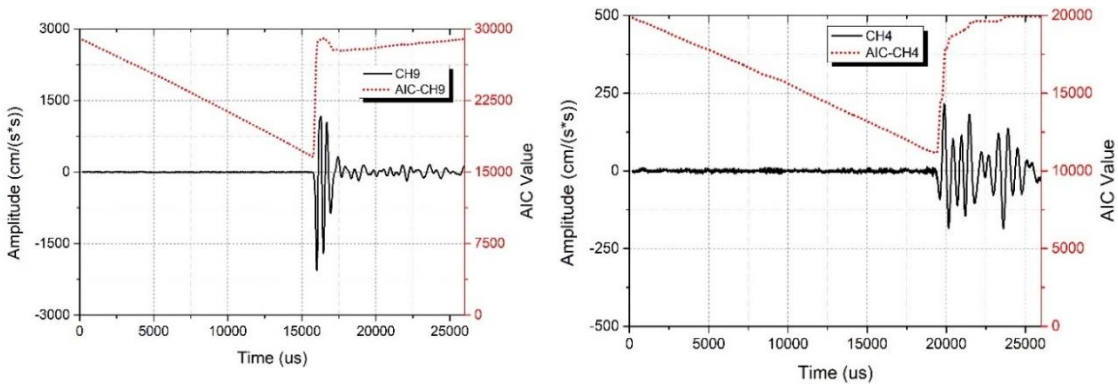

(**a**) (**b**)

Figure 5.3 The waveform and AIC value. The AIC value is represented by the dashed line, the minimum AIC value denotes the first travel time. (a) Strong signal near the exciter, (b) weak signal far away from the exciter. Note the different scale on the y-axes in (a) and (b).

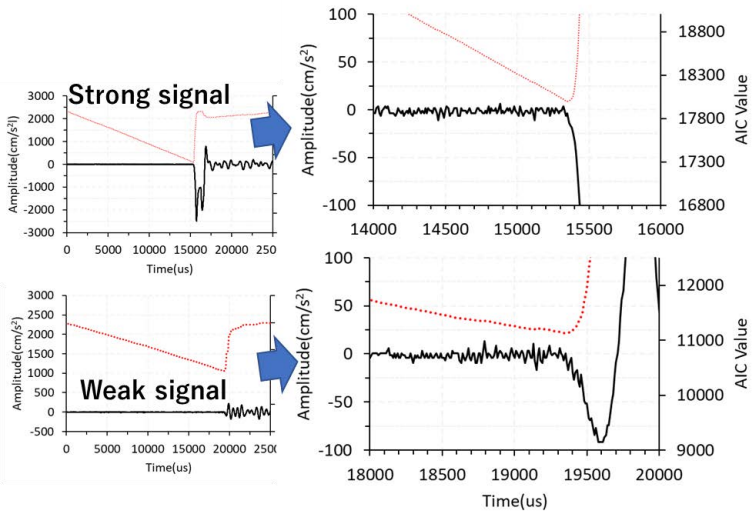

Figure 5.4 Enlarge the AIC value and the wave signal.

The reliability and accuracy of the determination of the travel time of the elastic wave propagation in soil are important because the travel time is the premise for the interpretation of the corresponding results, and therefore of evaluating the instability of the slope surface layer. In order to examine the reliability of Equation (5-5), 100 waveforms were randomly extracted from the experiment, and the travel times were calculated by both the AIC algorithm and manually. The result is shown in Figure 5.5. The arrival times picked by the AIC algorithm and those picked manually were almost the same. This shows that the AIC algorithm can provide a highly accurate and reliable determination of the travel time of elastic wave signals.

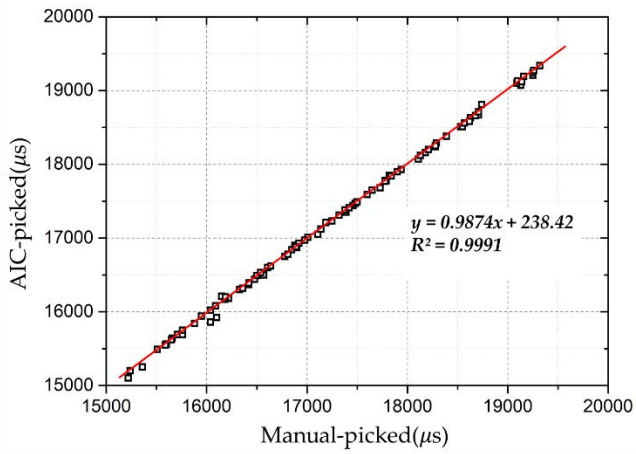

Figure 5.5 Travel times picked by the AIC have almost the same results as those picked manually.

5.3. TEST CONDITIONS

The layout of sensors in the soil is shown in Figure 5.6. E1~E10 are the exciters; CH01~CH30 are the receivers; VWC1~VWC10 are the soil moisture sensors.

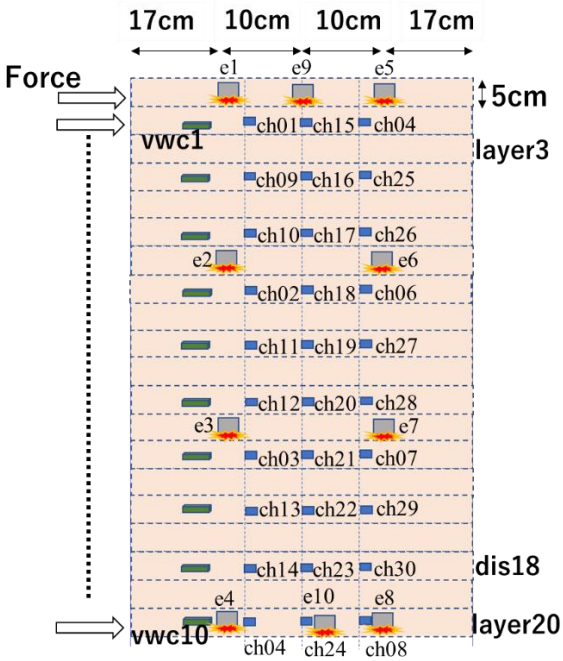

Figure 5.6 The layout of sensors in the soil.

The overall test program was divided into seven series of test cases, and the conditions of every test case are summarized in Table 5.1 and Figure 5.7. In these experiments, elastic wave velocities were investigated to be affected by the soil moisture, shear stress, and shear displacement.

Test case 1 contained the initial amount of soil moisture, and there was no shear force applied to any layer of the model. After 21 h of rainfall, the soil moisture in the model became stable. Then the rainfall was stopped, and the water was drained out for 46 h. The maximum wave velocities observed in several different survey lines, defined in Figure 5.1, are named with Vp(initial), which was used as a comparison standard value to express the change ratio of velocities by the following test. Test case 2 was used to confirm the effect of the loading and unloading shear force on the wave velocities. Test case 3 was used to analyze the effect of soil moisture on the wave velocities during the rainfall and drain events without a loading shear force. Test cases

4, 5, and 6 were used to study the effect of shear stress on the wave velocities during the rainfall and drain events, without shear displacement. Test case 7 was used to find out the relationship between shear displacement and wave velocities under constant shear stress before slope failure. Soil moisture was constant during this test. Figure 5.7 shows the test procedure over time. The rainfall or drain condition, the shear stress corresponding to the slope angle and the VWC on the top slope is shown.

Table 5.1 Test conditions

Test Case	Soil moisture Control	Shear Force (Slope Angle)
1-1	Rainfall (21 h)	0°
1-2	Drain (46 h)	0°
2-1	Rainfall (24 h)	24°
2-2	Drain (288 h)	0°
3-1	Rainfall (4 h)	0°
3-2	Drain (19 h)	0°
4-1	Rainfall (24 h)	27°
4-2	Drain (28 h)	27°
5-1	Rainfall (22 h)	29°
5-2	Drain (70 h)	29°
6-1	Rainfall (23 h)	31°
6-2	Drain (41 h)	31°
7	Constant	32°, 33°

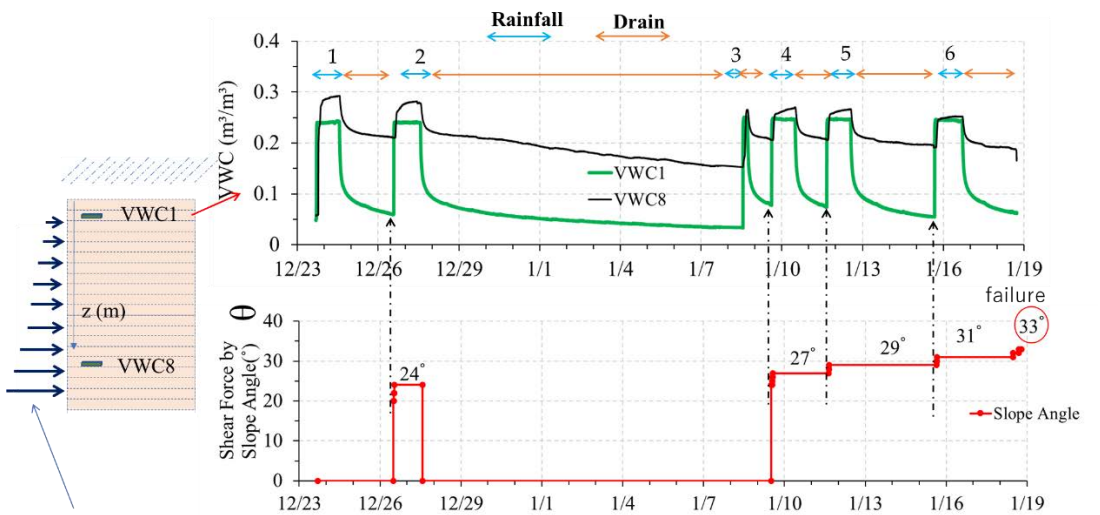

$\tau = \sigma_v * \tan(\theta) = z\,\gamma_t * \tan(\theta)$

Figure 5.7 Rainfall events and loading the shear stress in the test procedure.

5.4. TEST RESULTS

5.4.1 Normal Stress Effects on Elastic Wave Velocities

Wave velocity propagation in soil depends on the state and history of the effective stresses, void ratio, degree of saturation, and type of particles. Based on early studies, the relationship of wave velocity and effective stress for granular geomaterials is expressed as a power function having two parameters: a coefficient and an exponent. The velocity-stress power relationship for granular media under isotropic loading is expressed as (B. O. Hardin & Richart, 1963; B. O. Hardin, 1978);

$$Vp = a(\sigma)^{m/2} \tag{5-6}$$

Where Vp is compression wave velocity, σ represents effective isotropic stress (the unit is 1kPa), a and m are material constants associated with the type of grains, void ratio, the nature of contacts and the stability of soil skeleton. Parameters a and m are determined by experiment.

- ***In initial status***

In the initial status, the soil moisture in the model was constant, no shear strength was applied at any layer. Thus, the effect of soil moisture, shear stress and displacement can be ignored. The wave velocity was found larger at the bottom than at the top. It was the effect of the weight of the specimen, in other words, the normal stress was different from the depth. The more depth the higher stress. The relationship of elastic wave velocities and normal stress can be determined from Figure 5.8.

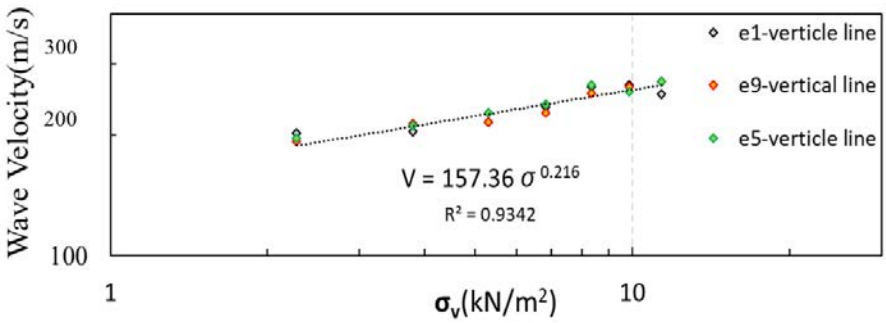

Figure 5.8 The effects of normal stress on elastic wave velocities.

The relationship between normal stress and elastic wave velocities is expressed as

$$Vp = 157.36(\sigma)^{0.432/2} \tag{5-7}$$

In the formula (5-6), the coefficient a is 157.36, the exponent m is 0.432.

- ***In rainfall events***

In this section, the situation of the rainwater infiltrates into the upper layer but still not reach the elastic wave survey line is analyzed. The purpose of this analysis is to confirm the elastic wave velocities affected by normal stress. The soil moisture content of the upper layer increased and made normal stress increase. The elastic wave survey line between receivers ch12 and ch13 is analyzed, shown in Figure 5.9.

Several rainfall events under a different shear force such as no shear force shown in Figure 5.10, slope angle 24 in Figure 5.11, slope angle 27 in Figure 5.12, slope angle 29 in Figure 5.13 and slope angle 31 in Figure 5.14. The summary of the elastic wave velocities response with normal stress due to rainwater infiltrates into the upper layer in different shear stress is shown in Figure 5.15. After calibration with shear stress, the elastic wave velocities response with normal stress is the same relationship as the initial state.

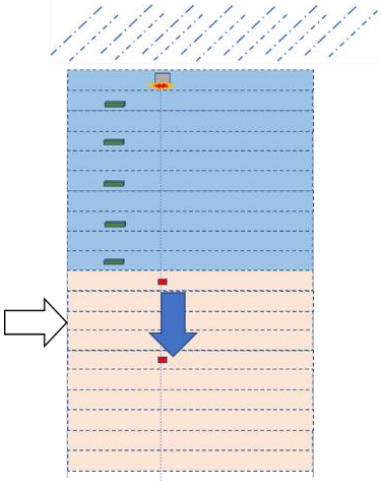

Figure 5.9 The soil moisture content increased at the upper layer but still not reached the elastic wave survey line between receivers ch12-ch13.

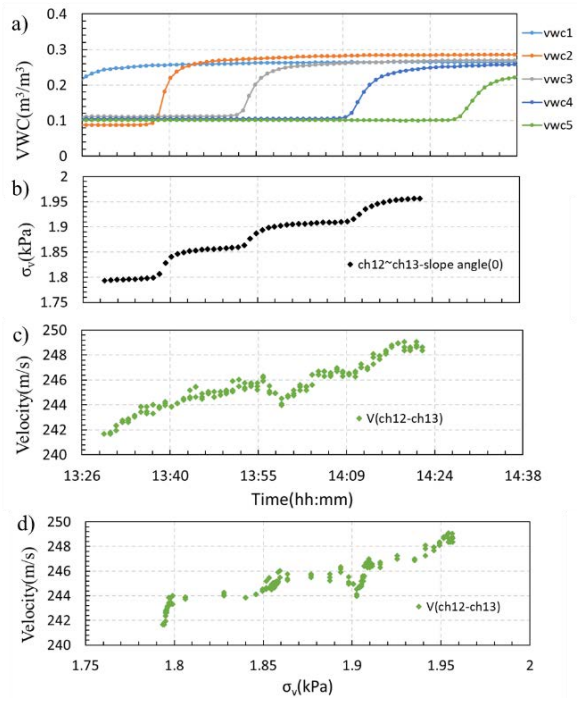

Figure 5.10 Test case 3-1(slope angle 0). a) VWC. b) Normal stress. c) Elastic wave velocities. d) Elastic wave velocities response with normal stress.

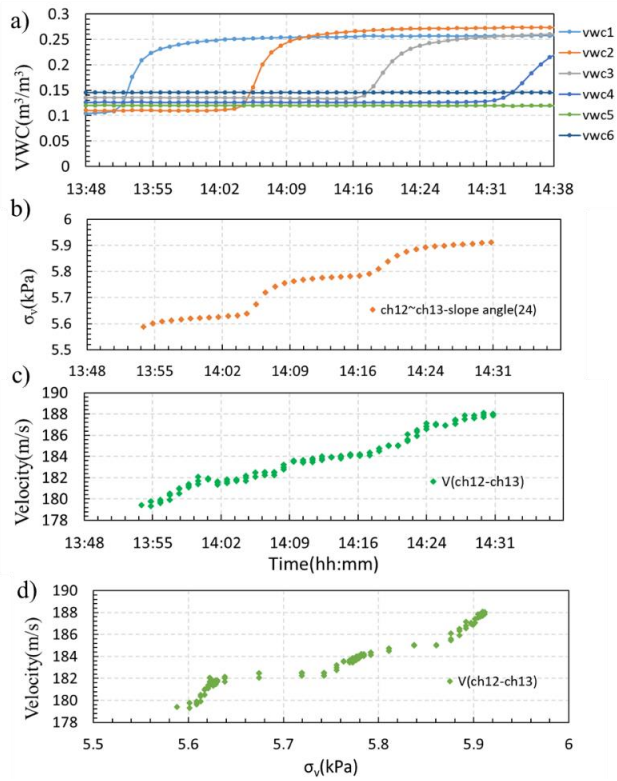

Figure 5.11 Test case 2-1(slope angle 24). a) VWC. b) Normal stress. c) Elastic wave velocities. d) Elastic wave velocities response with normal stress.

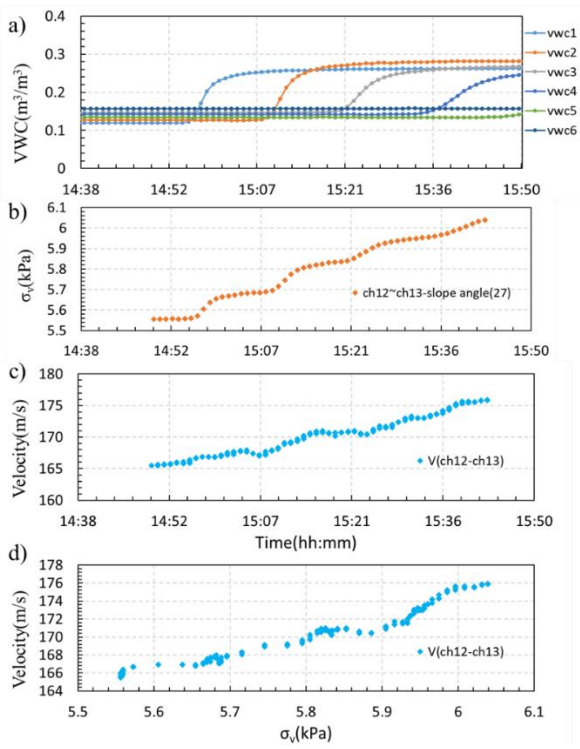

Figure 5.12 Test case 4-1(slope angle 27). a) VWC. b) Normal stress. c) Elastic wave velocities. d) Elastic wave velocities response with normal stress.

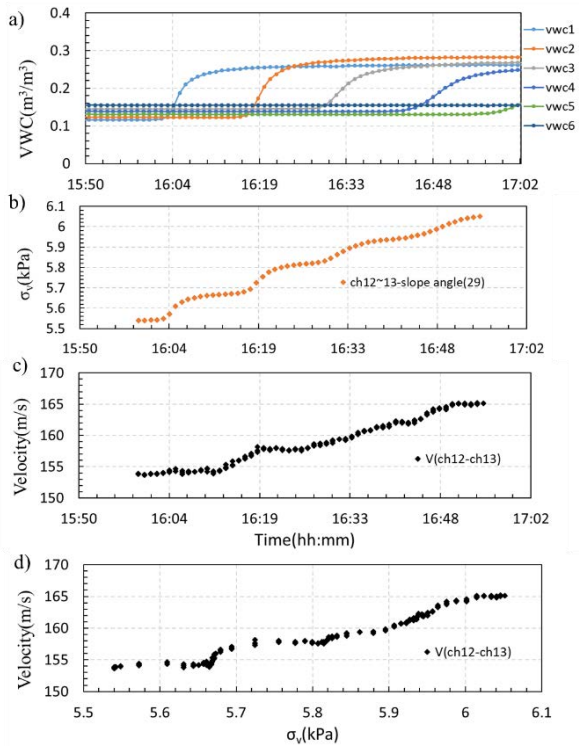

Figure 5.13 Test case 5-1(slope angle 29). a) VWC. b) Normal stress. c) Elastic wave velocities. d) Elastic wave velocities response with normal stress.

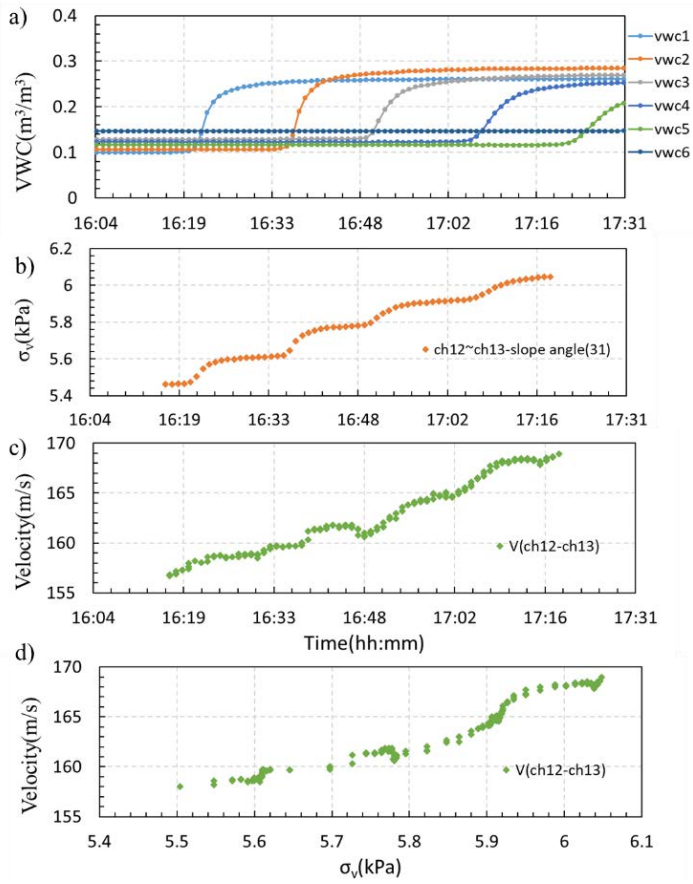

Figure 5.14 Test case 6-1(slope angle 31). a) VWC. b) Normal stress. c) Elastic wave velocities. d) Elastic wave velocities response with normal stress.

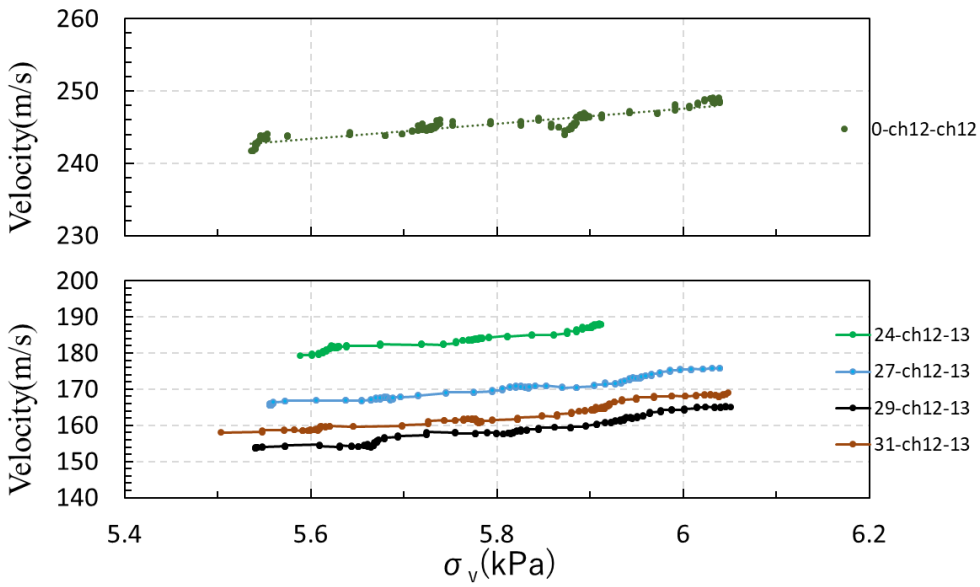

Figure 5.15 Summery the elastic wave velocities response with normal stress due to rainwater infiltrate into the upper layer in different shear stress.

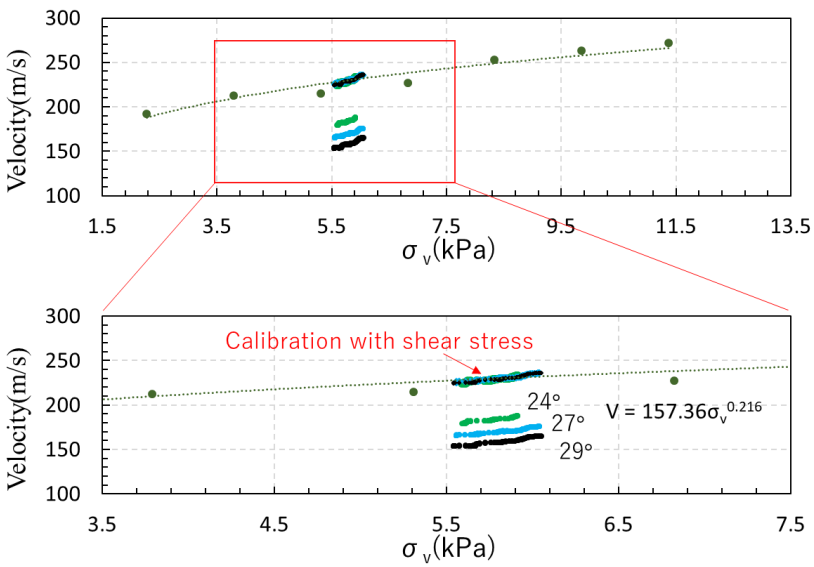

Figure 5.16 Calibration the elastic wave velocity with shear stress

5.4.2 The Effects of Soil Moisture on Elastic Wave Velocities

➢ ***Rainfall event without shear force***

In test case 3, no shear strength was applied to any layer. Soil moisture in the model changed by the rainfall event. The effect of shear stress and displacement can be ignored. The wave velocity between ch9 and ch2 is investigated because it is near the top, small effect of the normal stress. Figure 5.17 shows the VWC data of rainfall event in test case 3-1. Figure 5.18 shows the effects of soil moisture on elastic wave velocities at the ch9-ch2. The wave velocity increased at the beginning of the rainfall; this is the effect of the increase of normal stress at the upper layer.

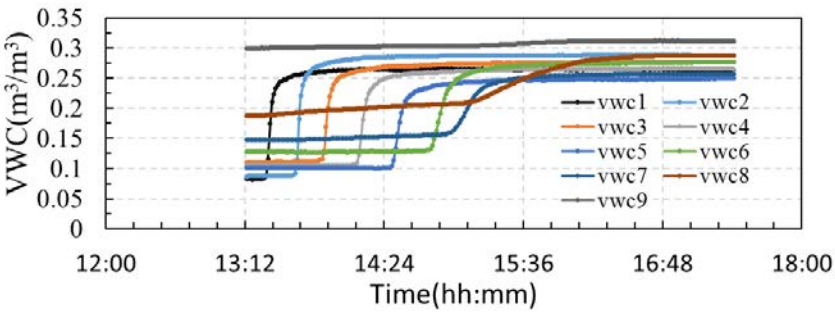

Figure 5.17 VWC data of rainfall event in test case 3-1.

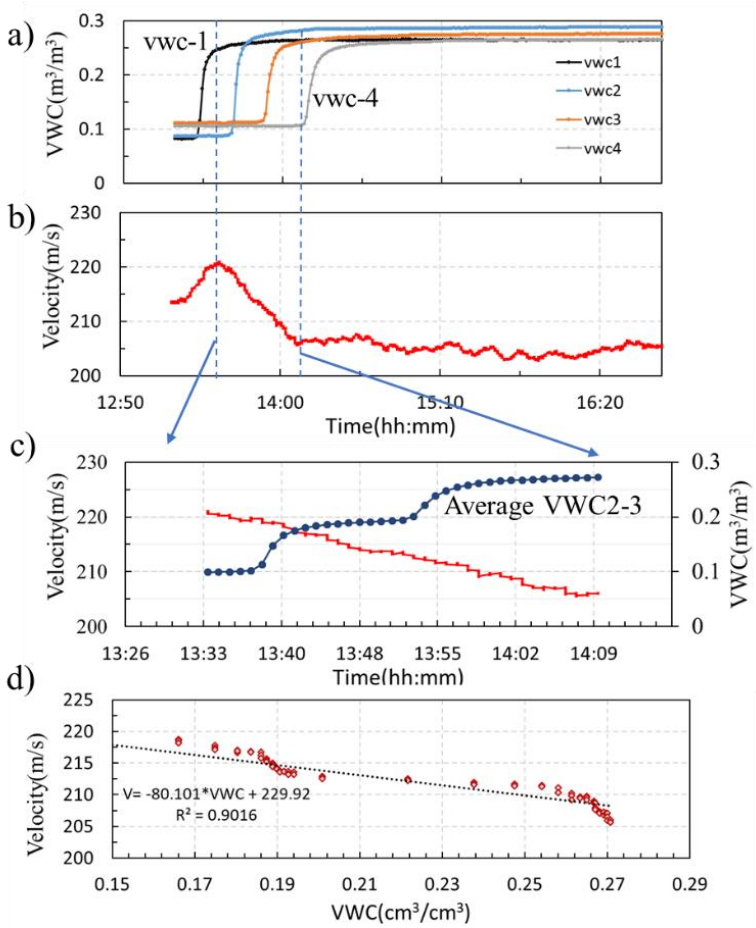

Figure 5.18 The effects of soil moisture on elastic wave velocities at the ch9-ch2.

The main purpose of test case 3 was to find out the relationship between the wave velocities and soil moisture without shear force applied at any layer. Before test case 3, water in the soil was drained for 288 h. There was subsequently very low soil moisture in the layer near the top of the model. Then test case 3 was conducted with 4 h of rainfall and 19 h of drain water. The response of elastic wave velocities at different VWC values is summarized in Figure 5.19.

Figure 5.19a shows the changes in VWC during the rainfall and drain events over time. During the rainfall event, the VWC near the top surface increased from 0.1 to 0.25 m^3/m^3, whereas the VWC near the bottom increased from 0.27 to 0.31 m^3/m^3. The response of the wave velocities to the rainfall and drain events over time is shown in

Figure 5.19b. The wave velocity ratio increased at the beginning of the rainfall, shown by number 1. That is, when the rainwater infiltrated into the area above the wave measure area, the soil moisture content of the upper layer increased and made the vertical compressive stress increase, resulting in an increase of the wave velocity ratio. This is similar to the behavior of Vp during the unloading of isotropic stress in the element test (Irfan et al., 2017).

When the rainwater started to infiltrate the wave measurement area, the wave velocity ratio decreased as the soil moisture increased, shown by the number 2. A gradual increase in softening of the soil specimen upon water infiltration may be responsible for the decreasing wave velocities. This decrease continued until the soil moisture of the specimens became stable. On the contrary, the wave velocity ratio increased with decreasing soil moisture during the drain stage, shown by the number 3. Figure 5.19c shows the wave velocities against the VWC using the same data as Figure 5.19a,b. A clear relationship between the VWC and the wave velocity ratio can be observed. The wave velocity ratio reduced by 0.1 ~ 0.2 when the VWC increased from 0.1 to 0.27 m3/m3. This is an approximately linear relationship between wave velocities and soil moisture. Compared to the results of the element test (Irfan et al., 2017) and the model test (Chen et al., 2018), a similar trend of the wave velocities and soil moisture was confirmed. The wave velocities change with soil moisture with a character of near linearity, which is a feature that can be used in the landslide early warning system.

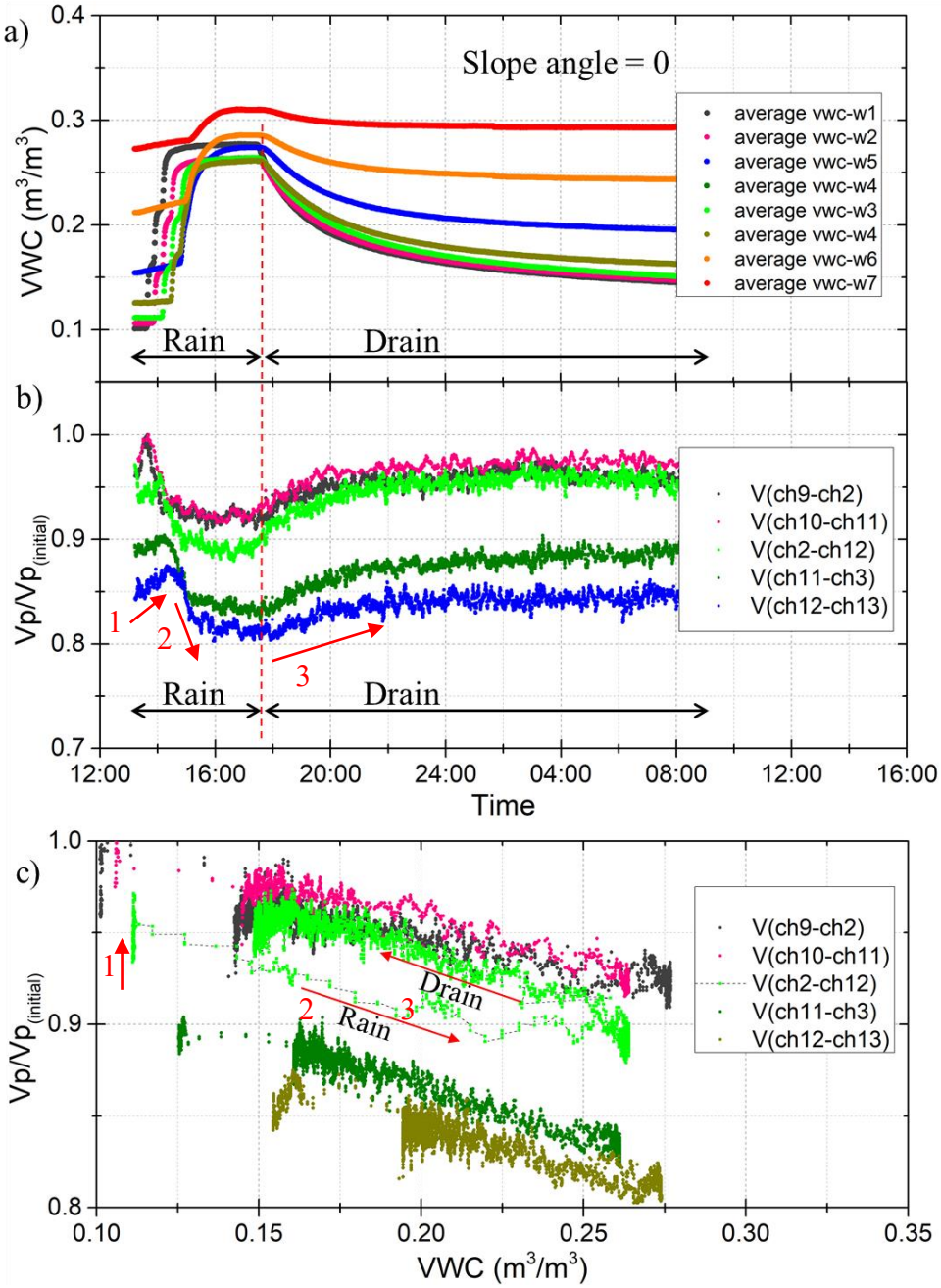

Figure 5.19 Response of elastic wave velocities at different VWC values during the rain and drain events (slope angle = 0); (**a**) average VWC versus time; (**b**) compression wave velocities (Vp/Vp (initial)) versus time; (**c**) compression wave velocities (Vp/Vp (initial)) versus the VWC.

Soil moisture is the key factor of a slope's stability in the context of rainfall-induced slope failure, which has been concluded by many researchers (Brand, 1981). When rainwater infiltrates unsaturated soil, the soil moisture will increase. This will lead to a decrease in soil matric suction, resulting in the soil losing its strength. Elastic wave propagation in soil is a geometric spreading; the wave velocities depend on the soil strength. The effects of soil moisture on the wave velocities can be explained by matric suction. The changes in soil moisture content can be expressed by the changes in matric suction; high soil moisture content means lower matric suction, and the weaker force between soil partials results in lower wave velocities. There is hysteresis in the path of wave velocities and the VWC between the rainfall and drain events (Figure 5.19c). This may be related to the hysteresis observed in the relationship between soil moisture and matric suction.

The other several vertical survey lines also had been analyzed. The survey line near the top model is shown in Figure 5.20, The survey line at the middle model is shown in Figure 5.21, The survey line at the middle model is shown in Figure 5.22.

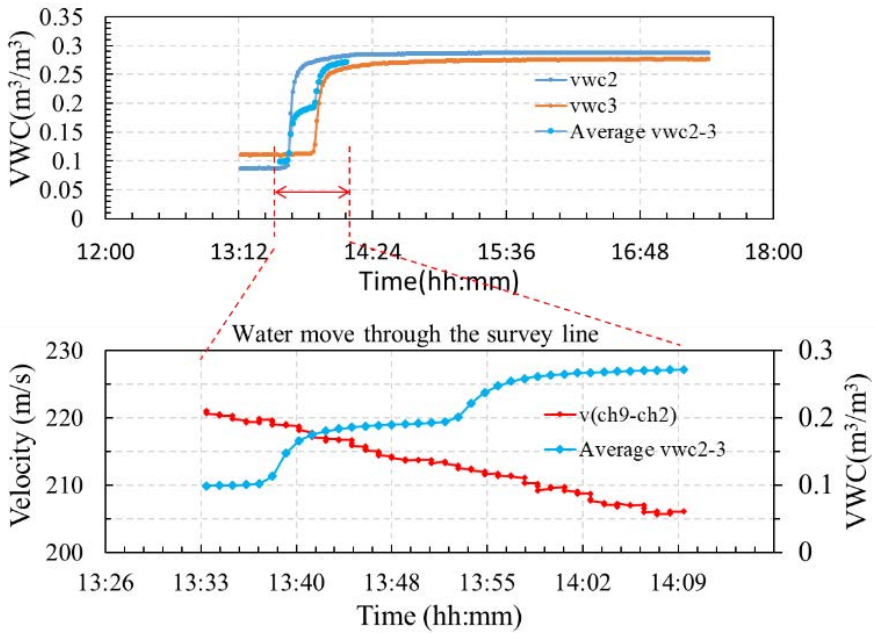

Figure 5.20 Elastic wave velocities changes with the VWC at the survey line between receivers ch9-ch2

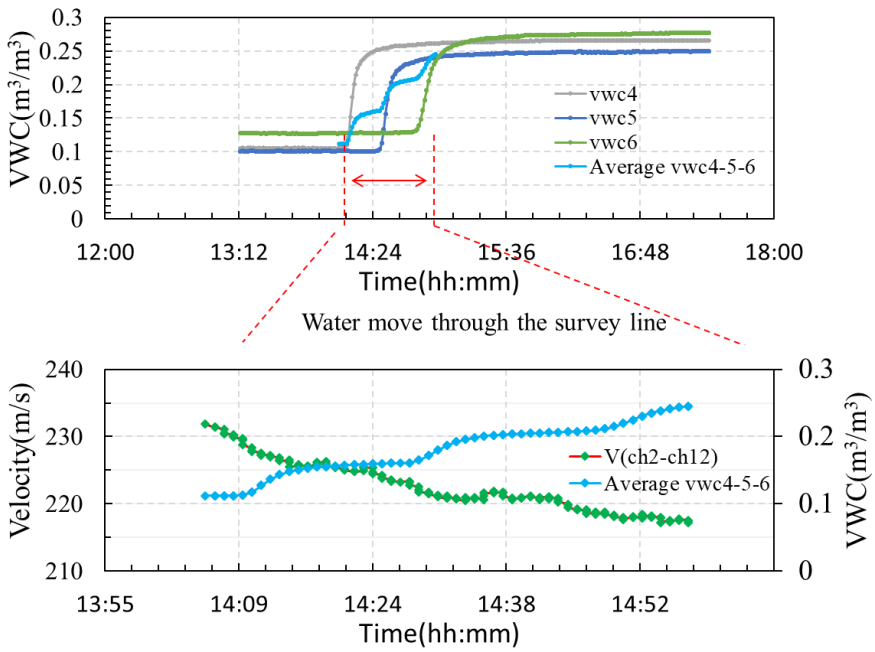

Figure 5.21 Elastic wave velocities changes with the VWC at the survey line between receivers ch2-ch12

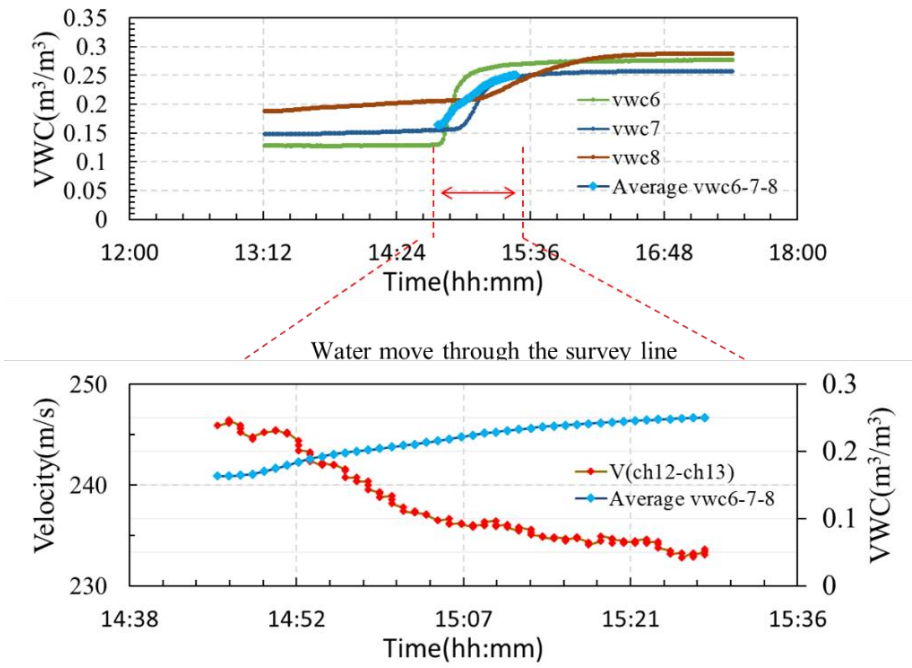

Figure 5.22 Elastic wave velocities changes with the VWC at the survey line between receivers ch12-ch13

➢ ***Rainfall event with different shear force***

In the test case 2-1, 3-1, 4-1, and 5-1, the shear force was set and kept in specified value (slope angle = 0, 24, 27, 29, 31) during the rainfall. The effect of VWC on elastic wave velocities was confirmed under different shear forces. Figure 5.23 shows Vp changes with VWC under different shear force at survey line ch12-ch13 in the time domain. The relationship between Vp and VWC is summarized in Figure 5.24 and Figure 5.25.

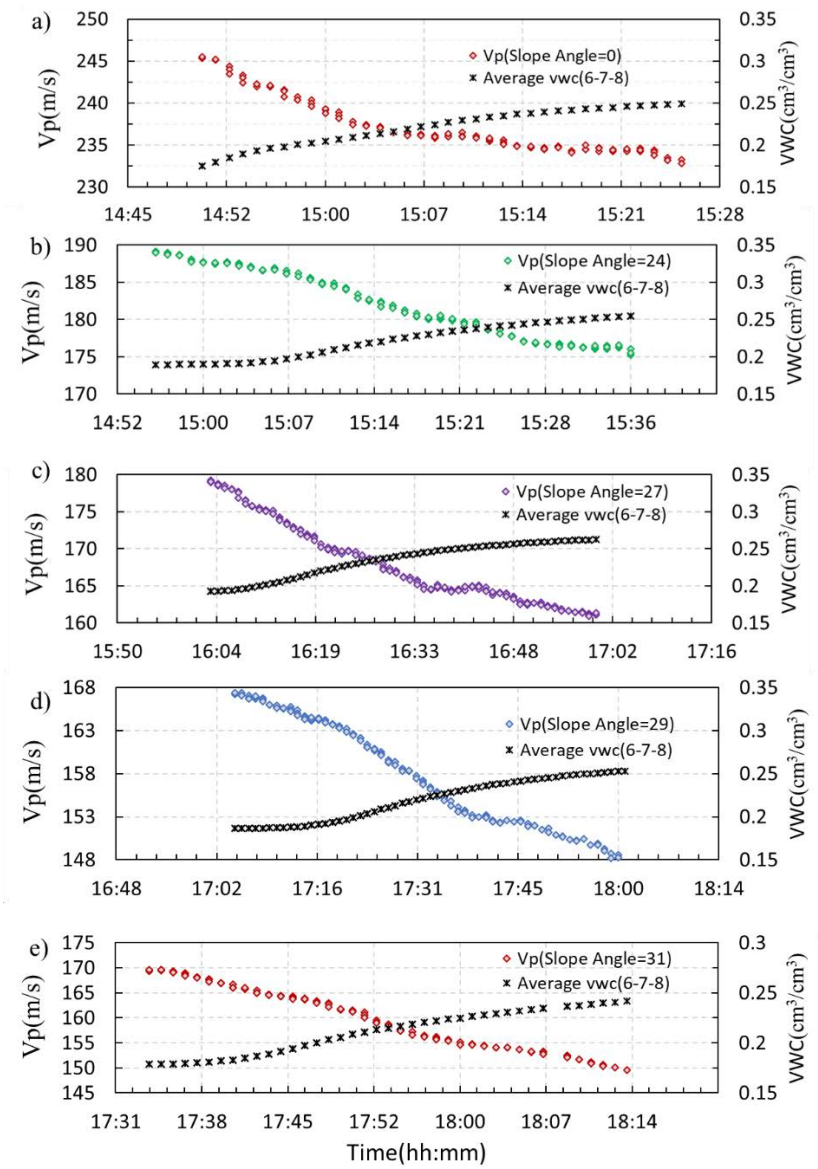

Figure 5.23 Vp change with VWC under different shear force(slope angle = 0, 24, 27, 29, 31) at survey line ch12-ch13 in time domain.

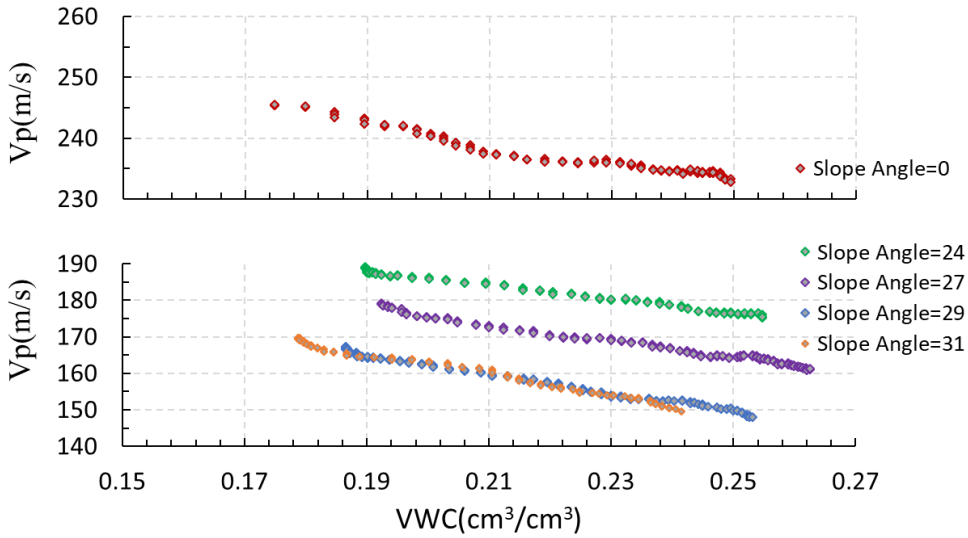

Figure 5.24 Vp change with VWC under different shear force(slope angle = 0, 24, 27, 29, 31) at survey line ch12-ch13

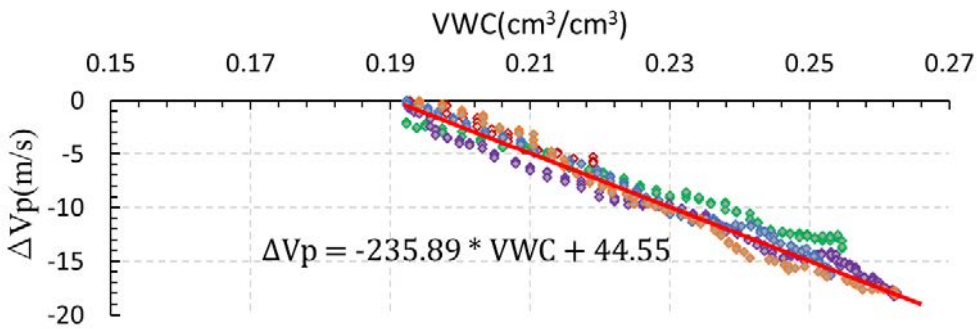

Figure 5.25 The relationship between Vp and VWC at the survey line ch12-ch13.

When the water went through the vertical survey line ch12-ch13, the wave velocity was found decreasing with the increase of the VWC. The relationship between VWC and elastic wave velocities is expressed as

$$\Delta Vp = b * VWC + V0 \tag{5-8}$$

where the coefficient b is -234.89.

5.4.3 The Effects of Shear Stress on Elastic Wave Velocities

If the loads on the slope change, the shear stresses within the soil will change. Shear stresses also change due to earth pressure changes with different levels of soil moisture or soil deformation, resulting in an unstable slope or slope failure. To understand the effect of loading and unloading shear force on elastic wave velocities, the survey line between ch12 and ch13 was analyzed (Figure 5.6). The test cases of 2, 4, 5, and 6 in Table 5.1 were included. The results are shown in Figure 5.26. This shows that when loading the shear stress corresponds to a 24-degrees slope angle, the Vp/Vp(initial) ratio dropped from 0.85 to 0.65, where the VWC = 0.19. On the contrary, when unloading the shear stress from 24-degrees to 0-degree, the wave velocities ratio increased from 0.6 to 0.8, where the VWC = 0.28. Furthermore, when loading the shear stress so it corresponds to a 27-degrees slope angle or higher, the Vp/Vp(initial) ratio reduced to 0.62, or below 0.6. This shows that the stronger the shear stress, the lower the wave velocities ratio. It can be considered that this is because the resistance force against the shear in the specimens changes the direction of wave propagation, resulting in a reduction of the vertical wave velocity. We attempted to find related research, but most of it focused on how the vertical compressive stress affects the wave velocity in the element test. No previous research directly focused on the effect of shear stress on wave velocity.

The changes in wave velocity ratio with the VWC in loading shear stress is parallel with the unloading shear stress. That is, the relationship between wave velocities and shear stress is independent. This shows the advantage of wave velocities in reflecting VWC and shear stress, meaning they are suitable for predicting the stability of the slope.

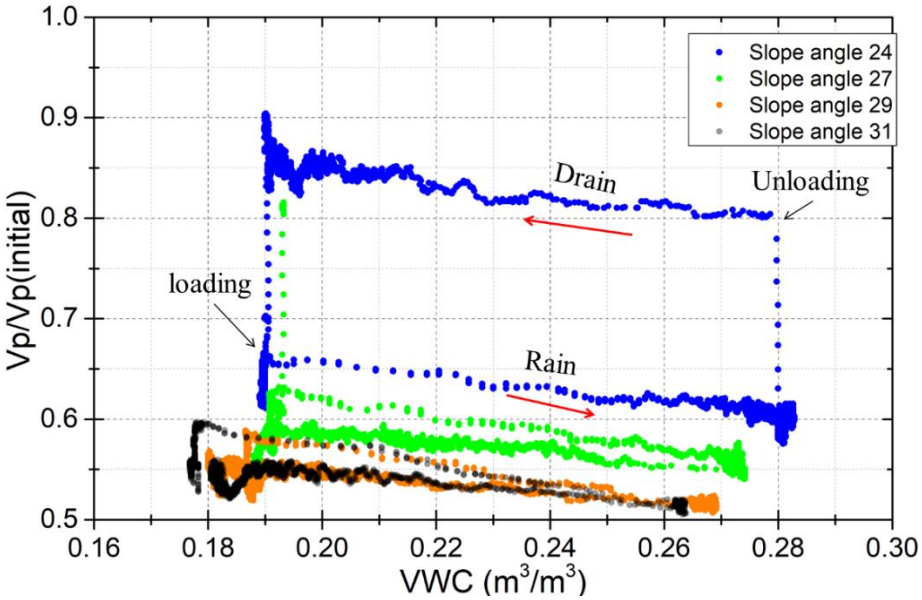

Figure 5.26 Wave velocities ratio changes with slope angle at the survey line between receivers ch12 and ch13.

The effects of shear stress on elastic wave velocities in several areas were investigated. These areas were at different depths in the model, located in the vertical survey line under the exciter (E1). The results are shown in Figure 5.27 and Figure 5.28. Figure 5.27a shows the response of wave velocities at different shear stress levels during rainfall events. Figure 5.28a shows the response of wave velocities at different shear stress levels during drain events. Figure 5.27b and Figure 5.28b show the wave velocity ratio against the shear stress at every layer with the same soil moisture content. The relationship between the wave velocity ratio and the shear stress is near linear. This shows that the closer to the bottom, the lower the wave velocities. The wave velocity ratio reduced by 0.2~0.3 at the middle layer and about 0.5 near the bottom where the shear stress is highest.

In the natural slope, shear stresses increase by many factors like water pressure in cracks at the top of the slope, increase in soil weight due to increased soil moisture content, and earthquake shaking. Wave velocities are very sensitive to shear stress. This feature is helpful for monitoring the stability of the slope. Monitoring the wave velocities in a natural slope may detect the changes in shear stress and easily enable one to find the stability of the slope at an early stage.

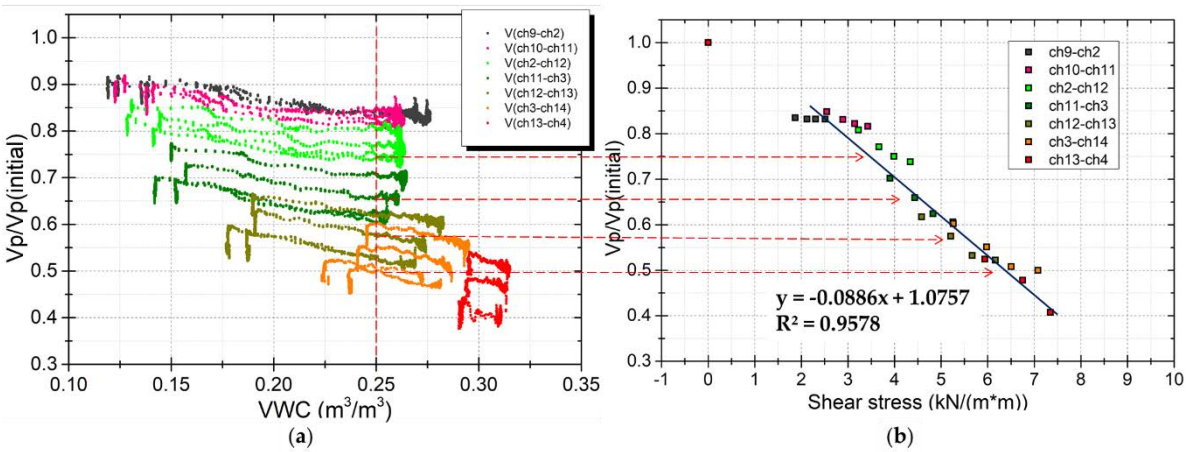

Figure 5.27 Response of wave velocities at different levels of shear stress during rainfall events. (a) Wave velocities ratio against shear stress during the rainfall event. (b) Wave velocities ratio response with shear stress at the same 0.25 m3/m3 of VWC.

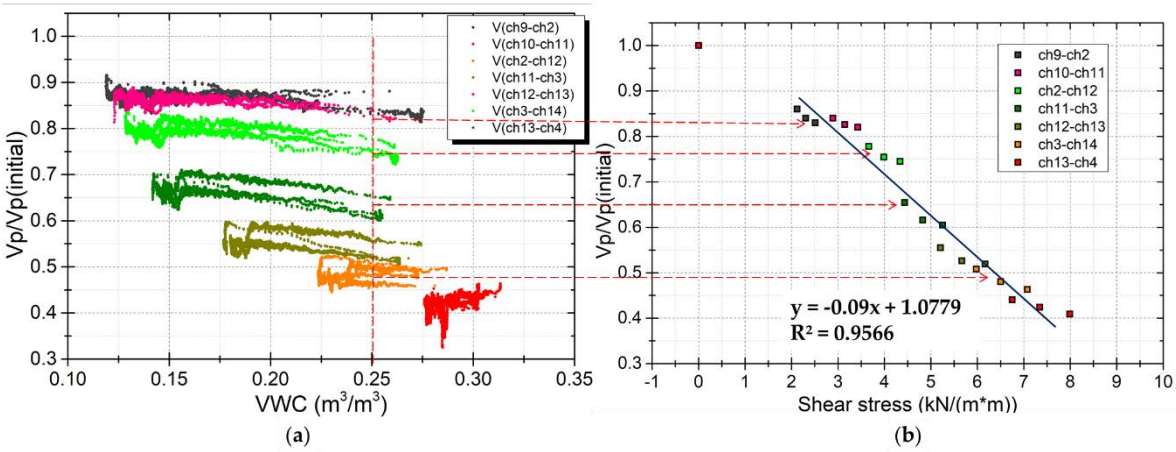

Figure 5.28 Response of wave velocities at different levels of shear stress during drain events. (a) Wave velocity ratio against shear stress during the drain event. (b) Wave velocity ratio response with shear stress at the same 0.25 m3/m3 of VWC.

The relationship between the wave velocity ratio and the shear stress is near-linear, in the rainfall event, it is expressed as

$$Vp/V0 = c * \tau + 1.0757 \tag{5-9}$$

where the coefficient c is –0.0886.

5.4.4 Elastic Wave Velocities and Shear Displacement

Test case 7 was used to investigate the effect of shear displacement on elastic wave velocities before slope failure. Soil moisture content did not change during this test. High shear stress and high soil moisture content were observed near the bottom, and maximum displacement was observed near the bottom after a shear force corresponding to a slope angle of 33-degrees was applied. Therefore, the displacement of the sensor Dis18 and the velocities at the vertical survey line between receivers ch13 and ch4, which are near the bottom of the model, were analyzed. Figure 5.29 shows the wave velocities and displacement plotted over time. When the shear force corresponding to a slope angle of 32-degrees was set, a very small displacement appeared but stopped moving after 2 h. When the shear force corresponding to a slope angle of 33-degrees was set, the slope started moving with an average speed of 3 mm/h, then accelerated and finally failed. The model showed that with increased displacement, the wave velocities decreased rapidly. The displacement–time relationship before the failure of the soil, defined as the creep of the soil (Sasahara and Sakai, 2014), could be observed in this test. Therefore, wave velocities can be used to detect the creep of the soil.

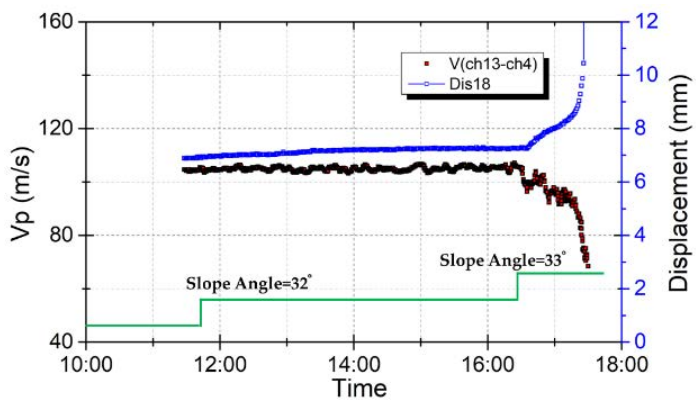

Figure 5.29 Effect of wave velocities on displacement during an applied shear force.

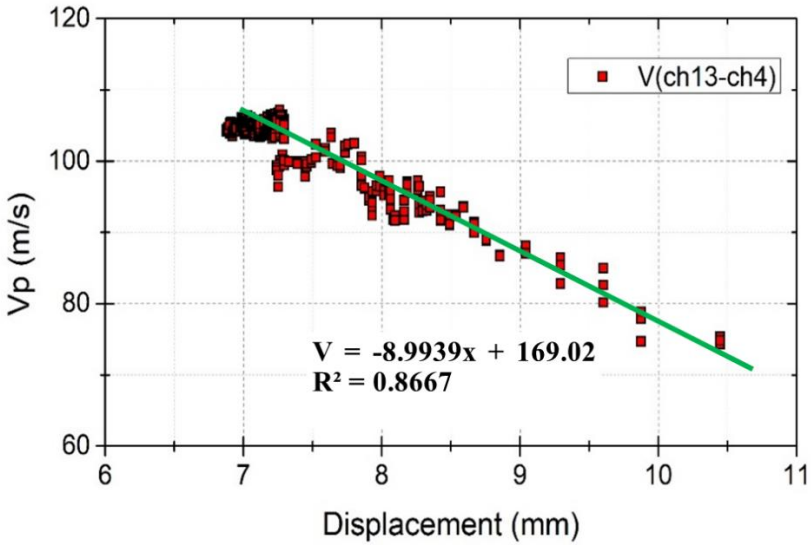

Figure 5.30 Wave velocity changes with displacement.

The same wave velocities and displacement data in Figure 5.29 were plotted in Figure 5.30. This figure shows that there is a linear relationship between wave velocities and displacement. The wave velocities changed from 105 m/s to 75 m/s when the displacement developed from 7 mm to 10 mm. That is, the wave velocity ratio dropped by 0.2 after a displacement of 3 mm. This shows that elastic wave velocities are also sensitive to shear displacement. Therefore, elastic wave velocities can be used to detect the slope when it starts to move and send out an alarm to warn of the dangerous situation of the slope before it fails.

The model showed that with increased displacement, the wave velocities decreased rapidly. The relationship of shear displacement and elastic wave velocities is expressed as

$$Vp = d * x + V0 \tag{5-10}$$

where the coefficient d is -8.9939.

5.4.5 Elastic Wave Velocities and Shear Strain

The effects of shear stress and shear deformation on elastic wave velocities have been discussed at 5.4.2 and 5.4.3. Consider a deformation field results from a stress field induced by applied shear forces in a continuous soil specimen body, the effects of shear stress and shear deformation on elastic wave velocities can be merged to one parameter as shear strain. In the multi-layer shear model, the small displacement at most layers was not well measured at the initial shear force applied, shown in Figure 5.31. To investigate the relationship of shear stress and displacement, a series of direct shear tests were performed on unsaturated mixed silica sand (VWC = 0.1 m^3/m^3). Direct shear tests were carried out following JGS 0561-2009. The detail of the direct shear test is introduced in Chapter 4.1.2.

The direct shearing process was including 6 different vertical loadings which start from 10kPa, 20kPa, 30kPa,50kPa, and 70kPa. Each shearing stage took 7 minutes with a shear rate of 1.4mm/min to reach a shear displacement of 10mm. Experimental results obtained from direct box-shear test are shown in Figure 5.32, the dot lines are shear stress τ plotted against horizontal displacement.

The normal stress observed in the multi-layer model is less than 10kPa, but the normal stress of the direct shear test is started from 10kPa. In order to obtain the relationship of horizontal displacement and shear stress under 10kPa, a fitting formula expressed by the following,

$$\tau = \tau_{max} - A/(x - x_0) \tag{5-11}$$

where τ is the shear stress, τ_{max} is the maximum shear stress, x is the horizontal displacement, x_0 is the initial horizontal displacement, A is the coefficient.

The linear relationship between vertical stress and coefficient A is shown in Figure 5.33. An extrapolation range in lower vertical stress can be used to predict the corresponding coefficient A, so the relationship of the normal stress and horizontal displacement in the multi-layer model with accuracy, shown in Figure 5.34.

The small horizontal displacement (Figure 5.35) and larger horizontal displacement (Figure 5.30) effect on elastic wave velocities can be summarized in Figure 5.36.

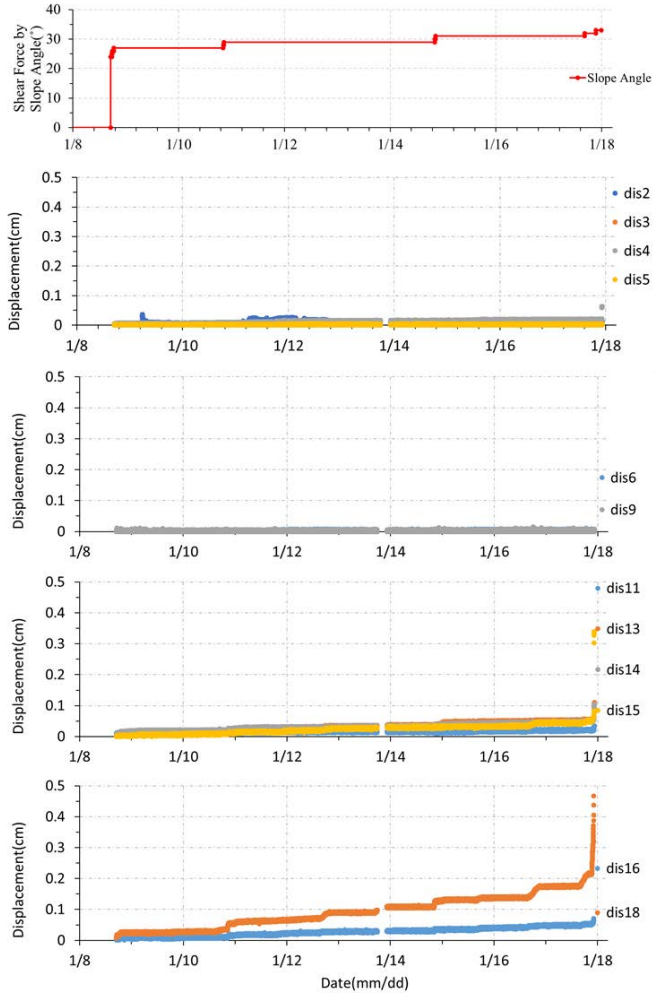

Figure 5.31 displacement data of multi-layer model

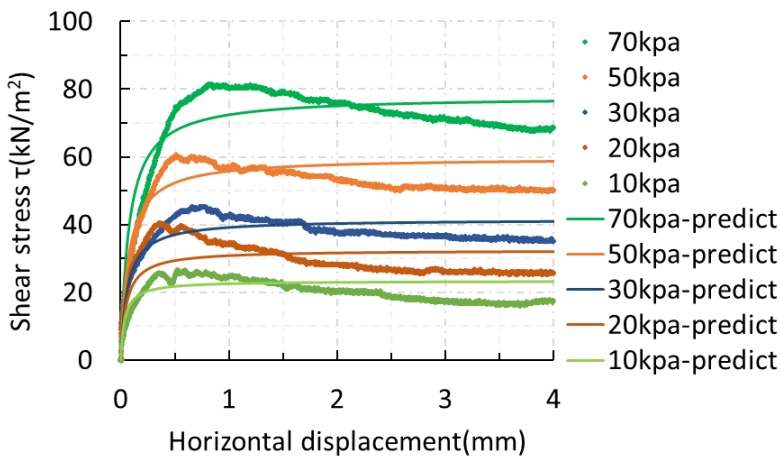

Figure 5.32 Shear stress versus horizontal displacement at several different vertical loading.

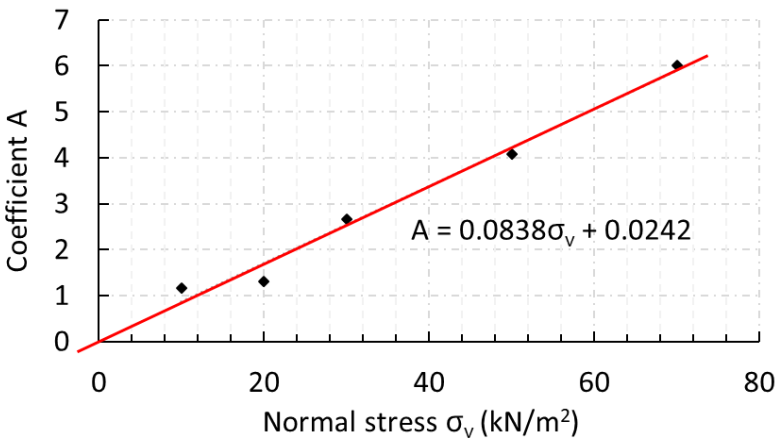

Figure 5.33 The linear relationship of vertical stress and coefficient A.

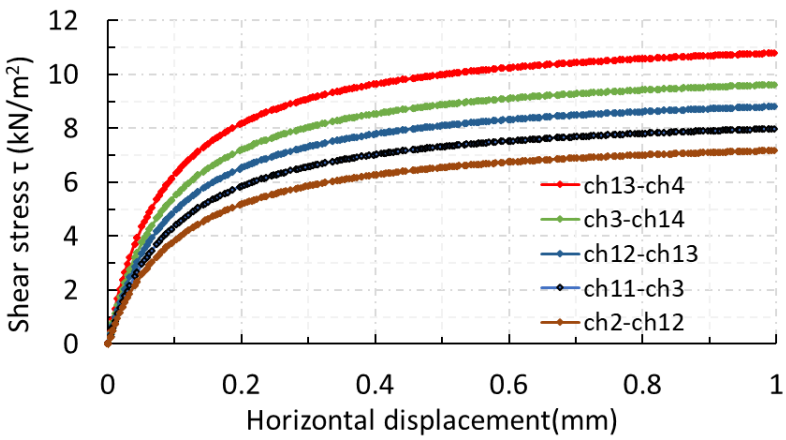

Figure 5.34 Predict the relationship of the normal stress and horizontal displacement in the multi-layer model with the corresponding coefficient A.

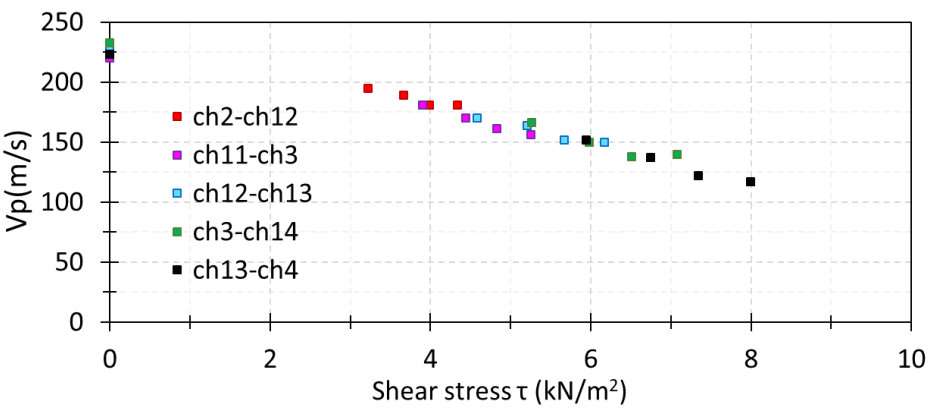

Figure 5.35 Response of elastic wave velocities at different shear stress with small displacement.

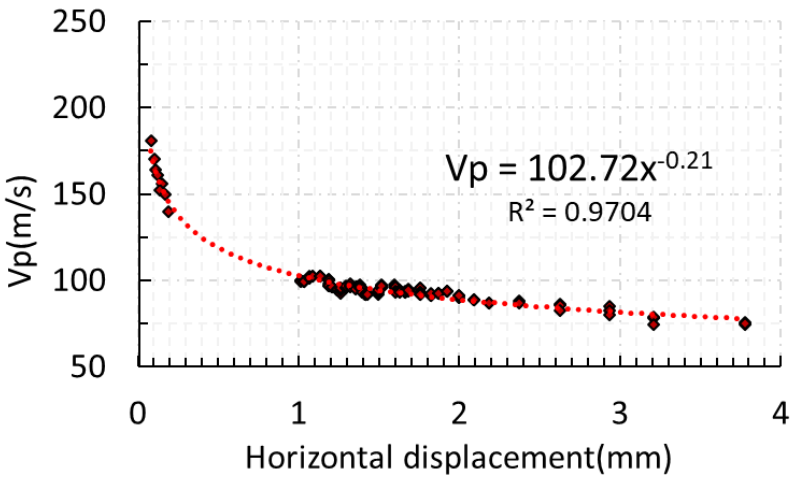

Figure 5.36 Response of elastic wave velocities at small displacement and large displacement.

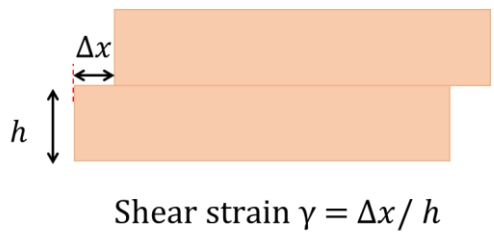

Figure 5.37 The define of shear strain.

Shear strain is defined as the ratio of displacement x to the transfer dimension h. The displacement can be expressed shear strain

$$Vp = c * (\gamma)^{d} \tag{5-11}$$

From the relationship of elastic wave velocities and displacement shown in Figure 5.36, the coefficient c and d can be obtained.

$$Vp = 45.17 * (\gamma)^{-0.21} \tag{5-12}$$

5.4.6 Elastic Wave Velocities in 10-Layer Model (Capillary Barriers)

The aim of this experiment is to understand the retention mechanisms of infiltrating water due to the capillary barriers. Capillary barriers can occur at the interface between unsaturated fine and coarser soil layers. The phenomena of capillary barriers are related to capillary tension that prevents the downward movement of water from a finer soil into an underlying coarser soil (Shackelford et al. 1994). The high soil moisture content at the interface between unsaturated fine and coarser soil layers has weakened the strength of the soil results easy failure.

The experimental apparatus is using 10 layers multi-layer shear model, shown in Figure 5.38. The layout of sensors in the soil is shown in Figure 5.39. E1 ~ e6 is the exciter, A1 ~ A8 is the accelerometer(receiver), W1 ~ W10 is the volumetric water content sensor. Figure 5.40 shows the layout of the load cell and displacement sensors. Load cells are using to measure the shear force, Table 5.2 shows the location of the load cell and displacement sensors.

Figure 5.41 and Figure 5.42 show the test material in the model. Mixed Silica sand is used as the fine-grained soil layer. Silica sand No1 is used as the coarse-grained soil layer.

The overall test program was divided into seven series of test cases, and the conditions of every test case are summarized in Figure 5.44 and Figure 5.45. In these experiments, elastic wave velocities were investigated to be affected by the soil moisture, shear stress, and shear displacement.

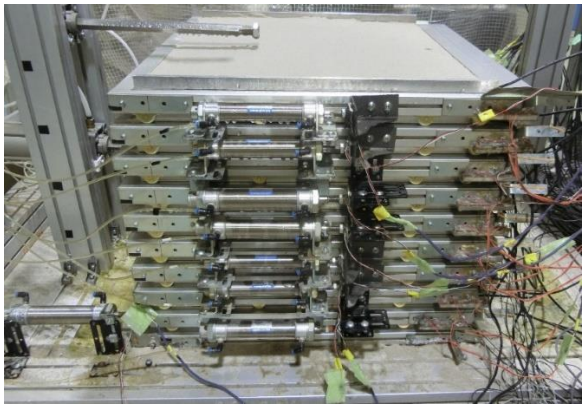

Figure 5.38 A photo of 10 layers multi-layer shear model.

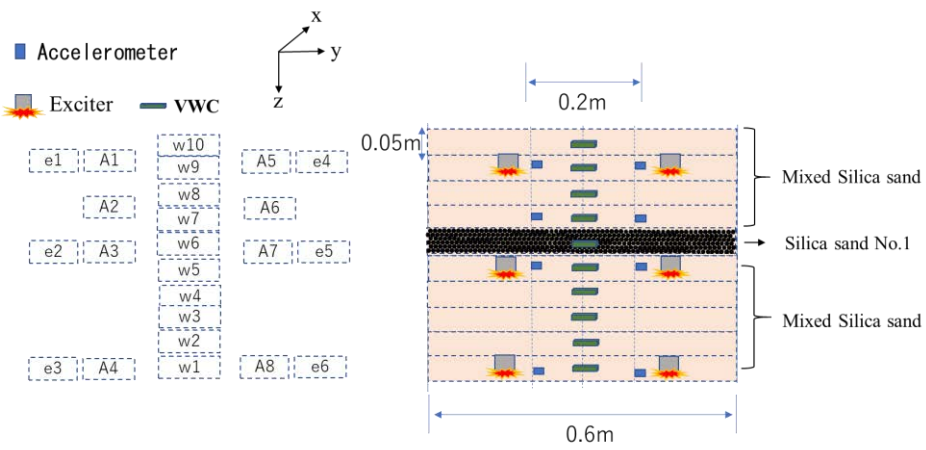

Figure 5.39 Sensors set up in the soil. E1~e6 is the excitor, A1~A8 is the accelerometer(receiver), W1~W10 is the volumetric water content sensor.

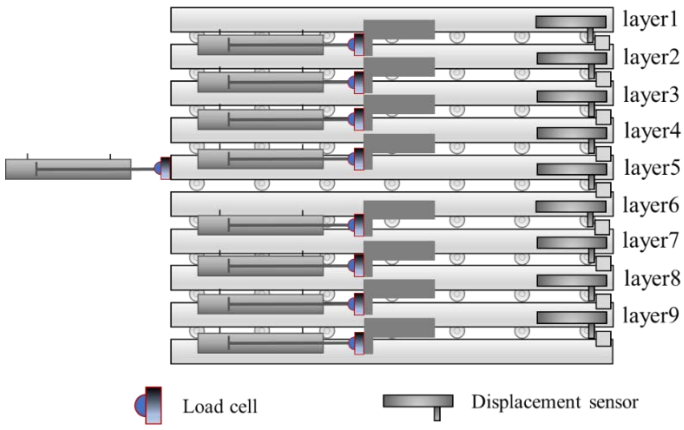

Figure 5.40 The layout of the load cell and displacement sensors.

Table 5.2 the location of the loadcell and displacement sensors.

	Load Cell		Displacement Sensor	
layer	Left side	Right side	Left side	Right side
1	1-No.25	2-No.33	1	2
2	3-No.21	4-No.28	3	4
3	5-No.22	6-No.31	5	6
4	7-No.9	8-No.20	7	8
5	17-No.12		19	20
6	9-No.30	10-No.34	11	21
7	11-No.15	12-No.18	13	14
8	13-No.10	14-No.26	15	16
9	15-No.2	16-No.1	17	18
10				

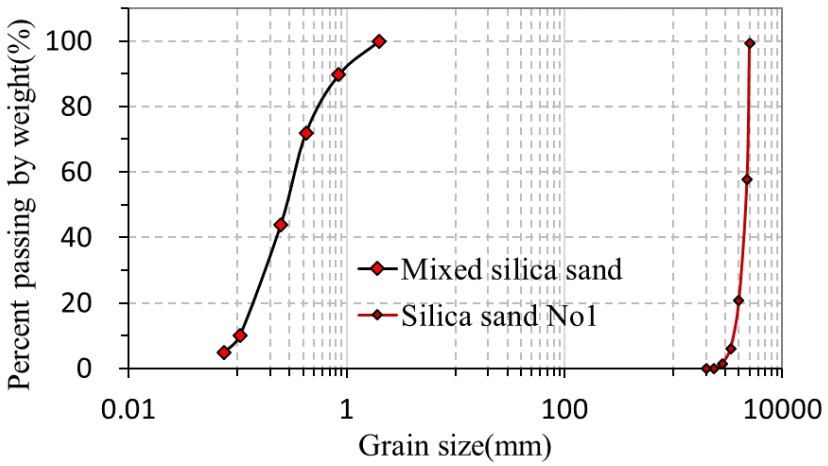

Figure 5.41 Grain size accumulation curve of the test material.

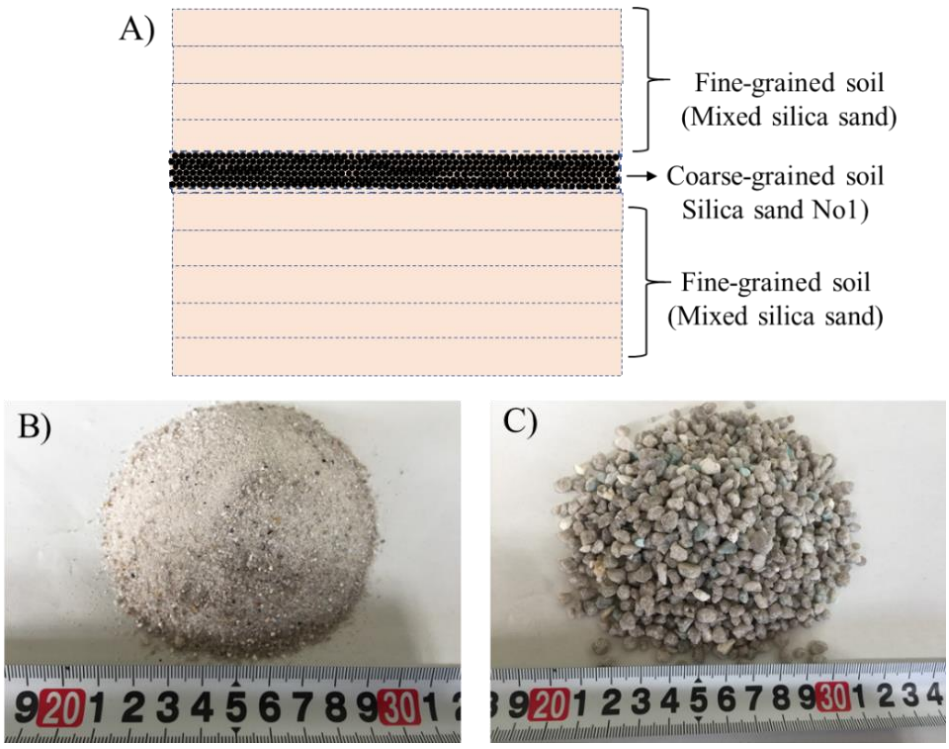

Figure 5.42 A) Test material in the model. B) Mixed Silica sand is used as the fine-grained soil layer. C) Silica sand No1 is used as the coarse-grained soil layer.

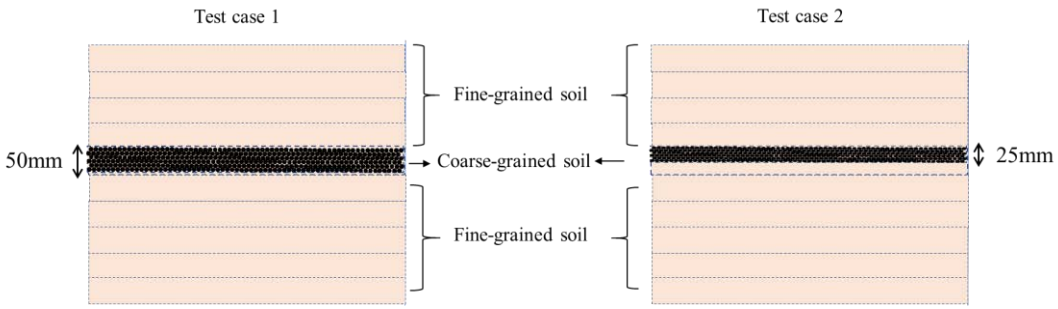

Figure 5.43 Two test cases had been conducted. The thickness of the coarse-grained soil layer is different, 50mm in test case 1 whereas 25mm in test case 2.

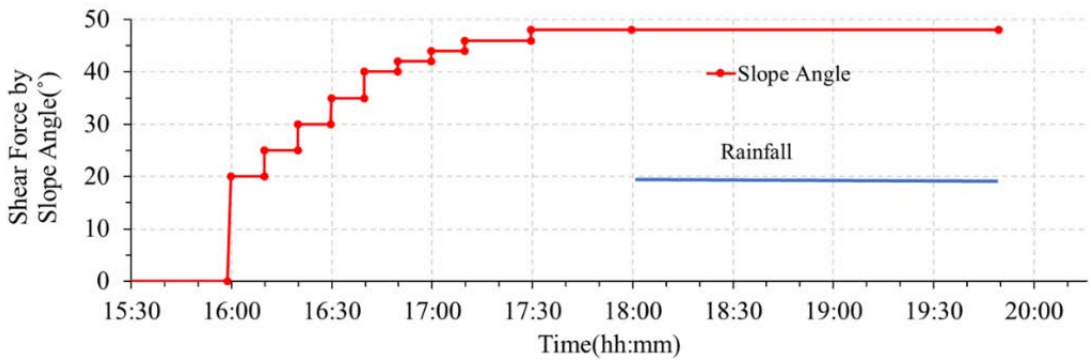

Figure 5.44 Test procedure shown in a time serial.

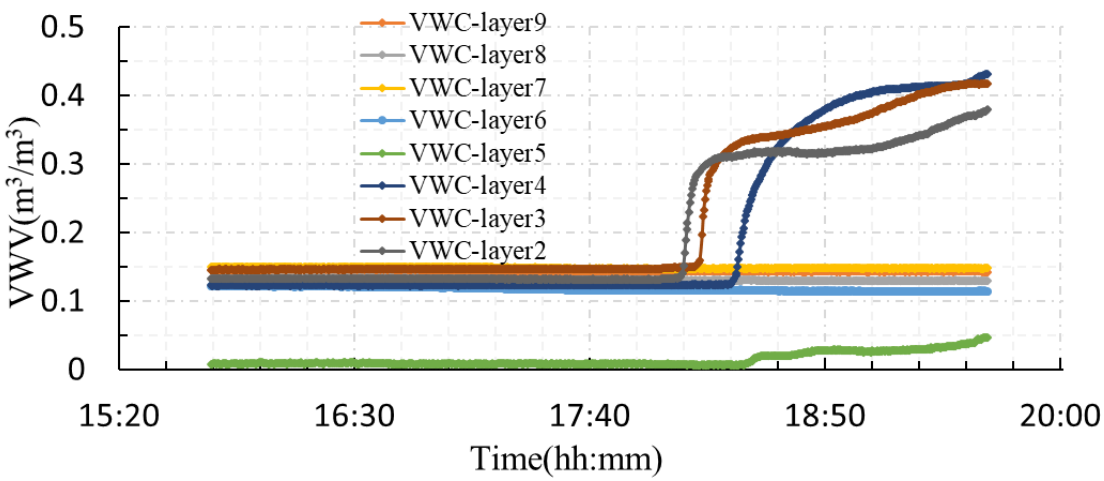

Figure 5.45 VWC in time domain

The test results are shown in Figure 5.46 ~ Figure 5.50. The relationship of shear stress and the correspond of horizontal displacement are summarized in Figure 5.47, The high soil moisture content at layer 4 weakened the strength of the soil results largest displacement and finally failure.

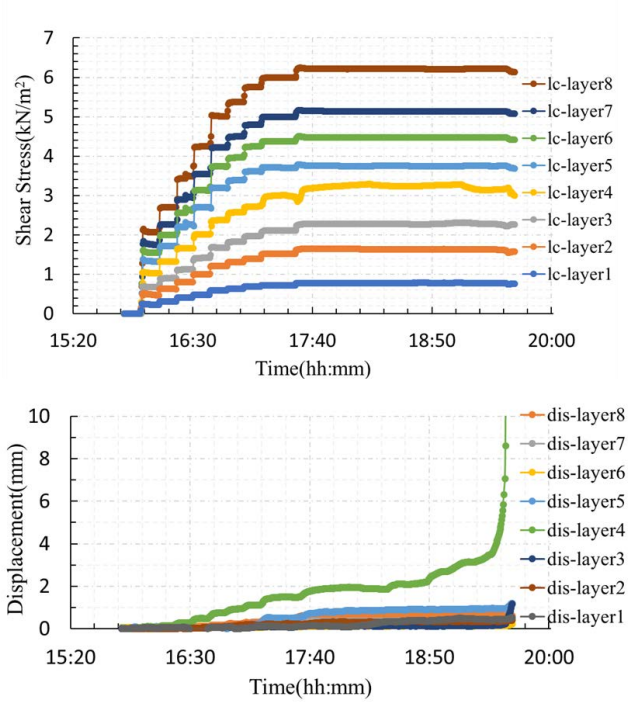

Figure 5.46 Shear stress and the correspond of horizontal displacement in time domain.

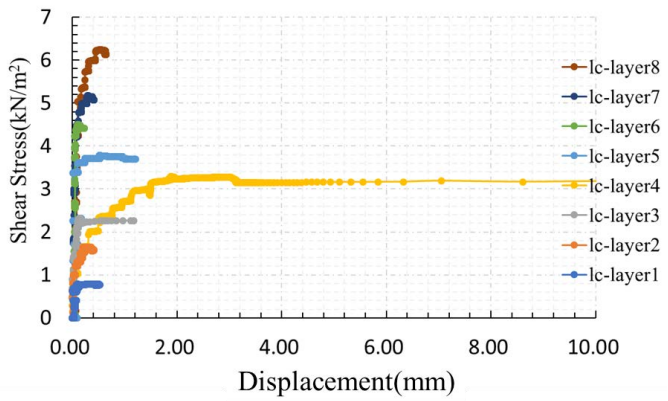

Figure 5.47 Shear stress versus horizontal displacement in different layer.

Vp at the vertical survey line of layer 2~3 in the time domain is shown in Figure 5.48, the Vp decrease with the increase of the shear stress, and decrease with the increase of the VWC.

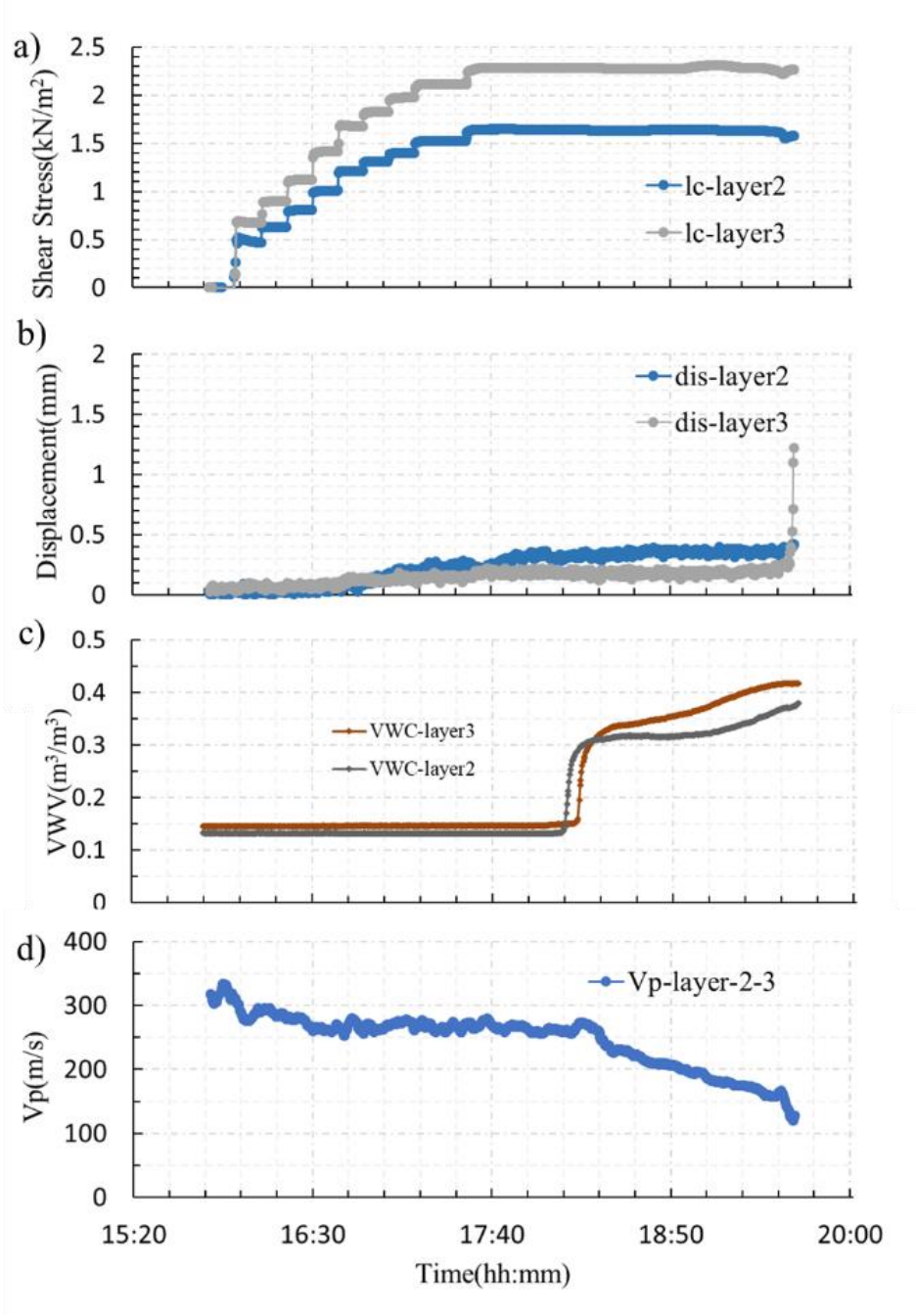

Figure 5.48 Vp at the survey line of layer 2~3 in time domain. a) Shear stress, b) Displacement, c) VWC, d) Vp at the survey line of layer 2~3.

Figure 5.49 shows the Vp at the vertical survey line of layer 4~5 in the time domain. The very high soil moisture content at layer 4, the Vp had also been observed that it decrease with the increase of the shear stress, VWC, and shear displacement.

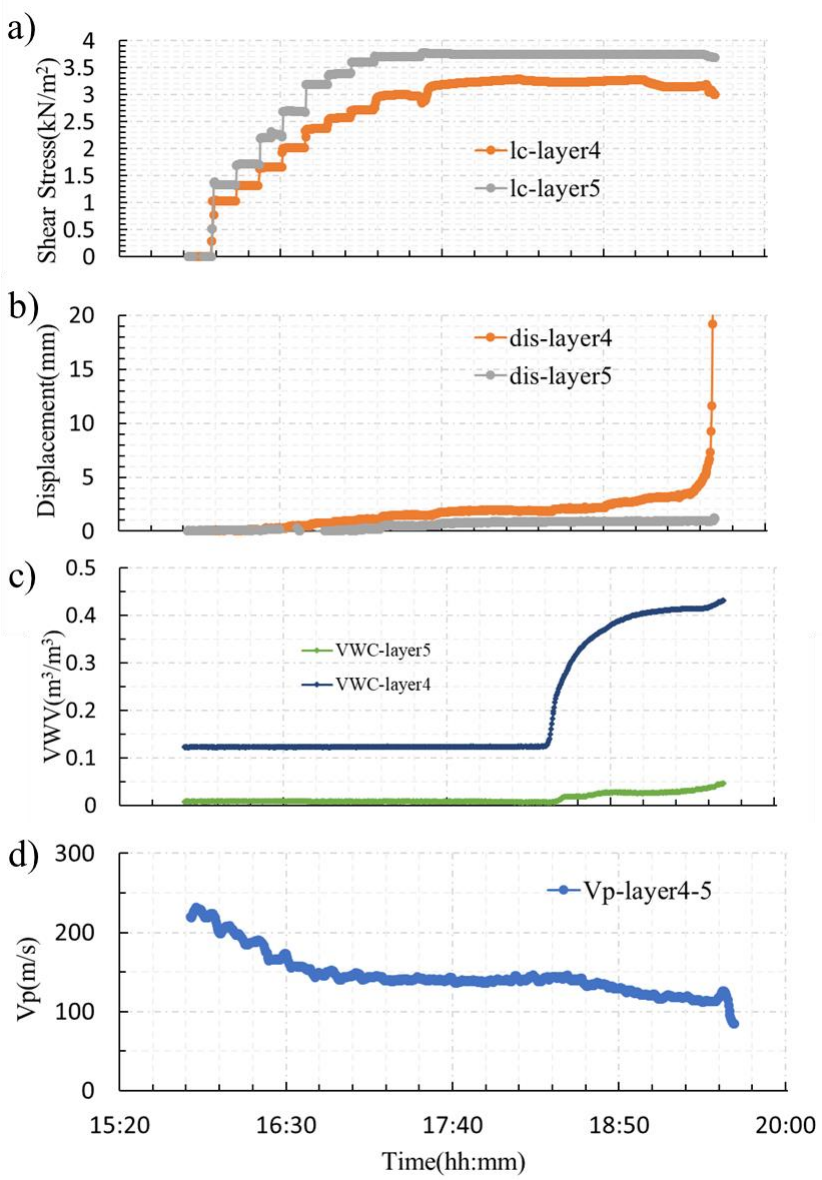

Figure 5.49 Vp at the survey line of layer 4~5 in time domain. a) Shear stress, b) Displacement, c) VWC, d) Vp at the survey line of layer 4~5.

Figure 5.50 shows the Vp at the vertical survey line of layer 6~9 in the time domain. No soil moisture content changes at the layer 6~9, because underlying coarser soil prevents the downward movement of water from a finer soil into it. The Vp had been observed that it decreases with the increase of the shear stress.

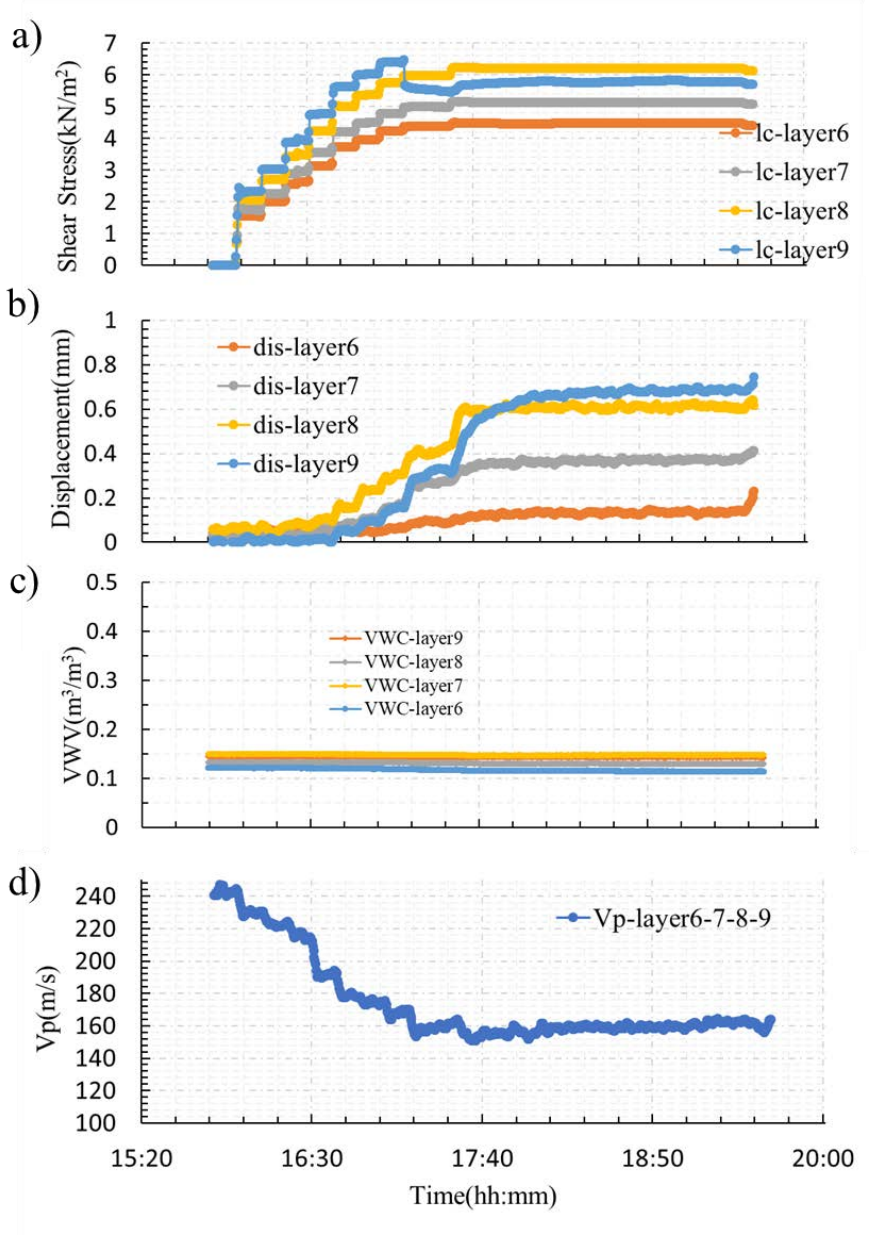

Figure 5.50 Vp at the survey line of layer 6~9 in time domain. a) Shear stress, b) Displacement, c) VWC, d) Vp at the survey line of layer 6~9.

5.4.7 Summarize the Factors Effect on Elastic Wave Velocities

The soil moisture, normal stress, shear stress, shear deformation are the main parameter of the status of an unstable slope or slope failure. These parameters can be evaluated by elastic wave velocities. The change of velocity is presented as the following formula

$$V = F(\sigma, VWC, \Upsilon) \quad (5\text{-}11)$$

$$= g(\sigma) * f(VWC) * k(\Upsilon) \quad (5\text{-}12)$$

$$= \left(a * (\sigma)^{m/2}\right) * (b * VWC) * (c * (\Upsilon)^{d}) \quad (5\text{-}13)$$

Where σ is normal stress, VWC is volumetric water content, Υ is the shear strain, coefficient a, m, b, c, and d are constants, and they are determined from experiments.

Based on the results of experiments, the coefficient a, m, b, c and d in the formula (5-13) are determined (a = 157.36, m = 0.43; b = - 235.89; c = 45.17; d = - 0.21).

5.4.8 Verification of the Factors Effect on Elastic Wave Velocities

The coefficient a, m, b, c and d in the formula (5-13) are determined by experiments. So, the elastic wave velocities can be calculated by the coefficient and the input soil moisture and shear stresses. Figure 5.51 shows the comparison of measured velocities and calculated velocities by the coefficient, soil moisture and shear stress in the test case 3-1. Figure 5.52 shows the measured velocities and calculated velocities by the coefficient, soil moisture and shear stress in the test case 4-1. Figure 5.53 shows the comparison of measured velocities and the velocities calculated by the coefficient and the input soil moisture and shear stresses through the whole test procedure. The results show they are a similar trend. The most effective of wave velocities is the shear stress, about 50% decrease near the bottom where the shear stress is highest.

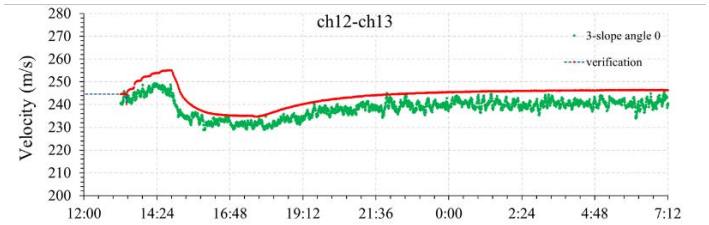

Figure 5.51 Measured velocities and calculated velocities by the coefficient, soil moisture and shear stress in the test case 3-1.

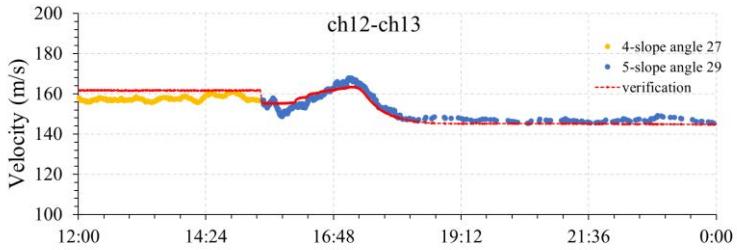

Figure 5.52 Measured velocities and calculated velocities by the coefficient, soil moisture and shear stress in the test case 4-1.

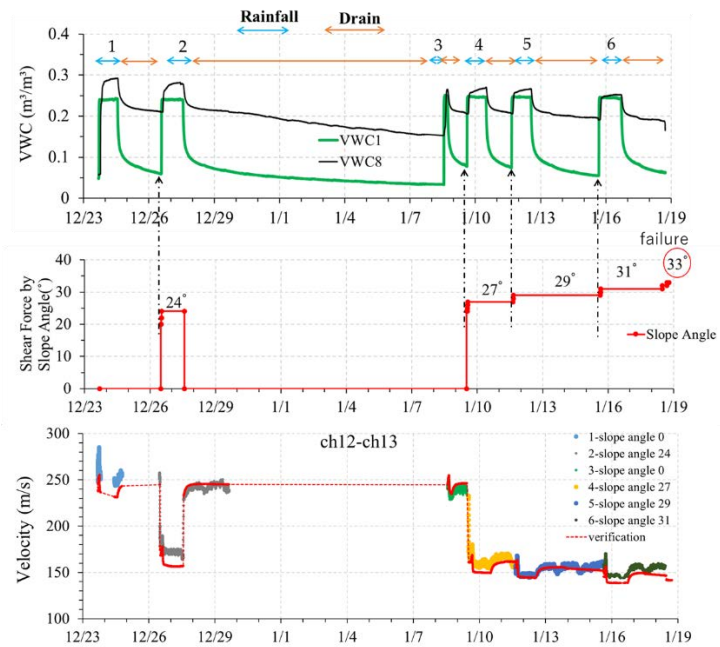

Figure 5.53 The comparison of measured velocities and the velocities calculated by the coefficient and the input soil moisture and shear stresses through the whole test procedure.

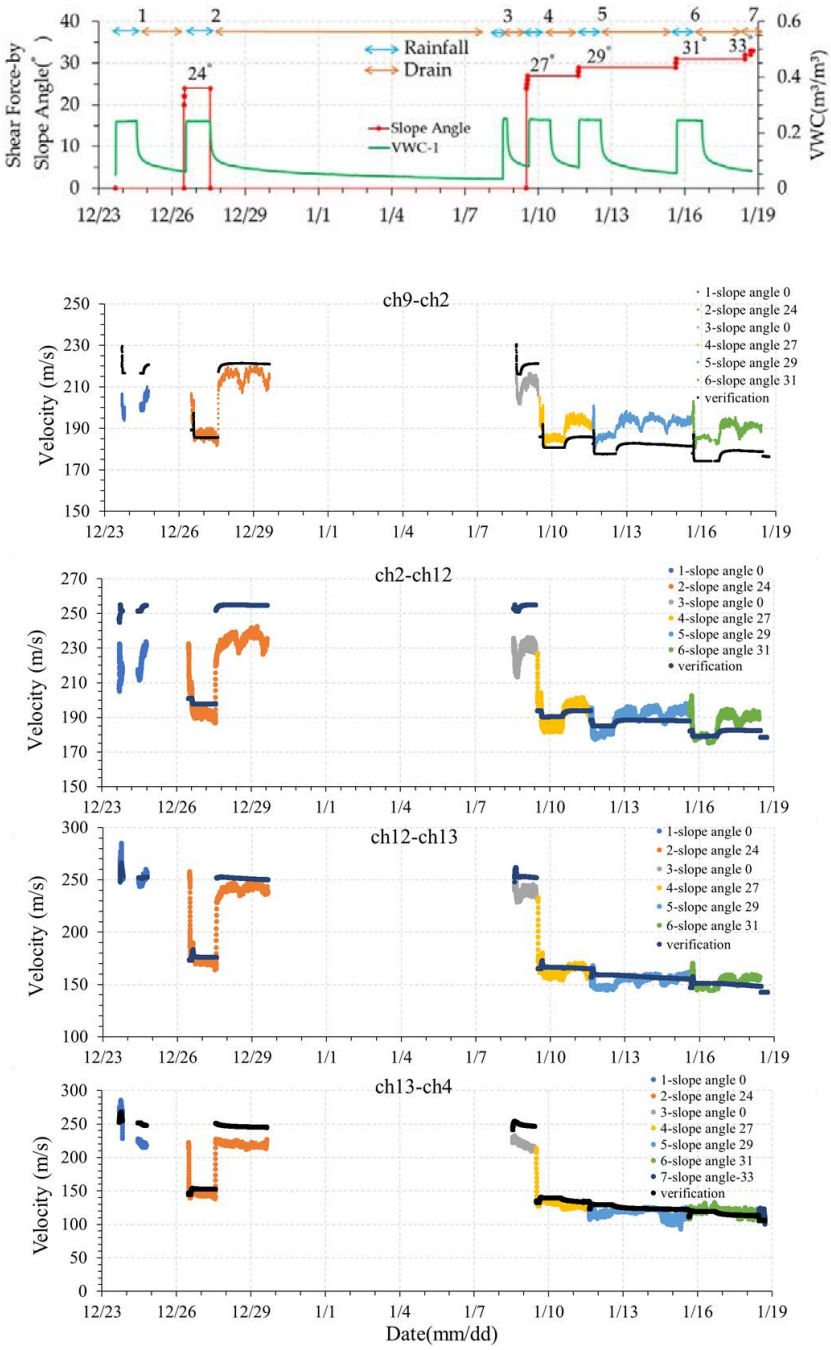

Figure 5.54 The comparison of measured velocities and the velocities calculated by the coefficient and the input soil moisture and shear stresses through the whole test procedure.

5.5. SUMMARY

Elastic wave is generated by a new type of exciter and received by MEMS accelerometers. The wave velocities are automatically processed by the AIC algorithm, which can calculate the elastic wave travel time with accuracy and reliability. Laboratory experiments using a multi-layer shear model simulating shallow slope failure were conducted to observe the changes in elastic wave propagation in a slope surface layer.

The changes of elastic wave velocities are a function of normal stress, soil moisture, shear stress, and shear displacement. Laboratory experiments using a multi-layer shear model simulating shallow slope failure were conducted and got the coefficient. The elastic wave velocities calculated by the coefficient and the input soil moisture and shear stresses, was compared to the measured velocities, it showed they were the similar trend. The results can be concluded as follows:

(1) The wave velocities increased with increasing normal stress.

(2) The wave velocities decreased with increasing soil moisture in the rain event and increased during the drain stage. The wave velocity ratio reduced by 0.1–0.2 when the volume of water content increased from 0.1 to 0.27 m^3/m^3.

(3) The stronger the shear force applied, the lower the velocities observed. A drop-in wave velocity of 0.2–0.3 was observed at the middle layer, and near 0.5 at the bottom layer.

(4) Increasing the displacement caused the wave velocities to also increase. The wave velocity ratio dropped by 0.2 after 3 mm of displacement.

5.6. REFERENCE

Brand, E.W., 1981. Some thoughts on rain-induced slope failures. Proc. Int. Conf. Soil Mech. Found. Eng. 3, 373–376.

Brignoli, E.G.M., Gotti, M., Stokoe, K.H., 1996. Measurement of shear waves in laboratory specimens by means of piezoelectric transducers. Geotech. Test. J.

Chen, Y., Irfan, M., Uchimura, T., Cheng, G., Nie, W., 2018. Elastic wave velocity monitoring as an emerging technique for rainfall-induced landslide prediction. Landslides 15, 1155–1172. https://doi.org/10.1007/s10346-017-0943-3

Chen, Y., Uchimura, T., Irfan, M., Huang, D., Xie, J., 2017. Detection of water infiltration and deformation of unsaturated soils by elastic wave velocity. Landslides 14, 1715–1730. https://doi.org/10.1007/s10346-017-0825-8

Irfan, M., Uchimura, T., 2016. Modified triaxial apparatus for determination of elastic wave velocities during infiltration tests on unsaturated soils. KSCE J. Civ. Eng. 20, 197–207. https://doi.org/10.1007/s12205-015-0404-2

Irfan, M., Uchimura, T., Chen, Y., 2017. Effects of soil deformation and saturation on elastic wave velocities in relation to prediction of rain-induced landslides. Eng. Geol. 230, 84–94. https://doi.org/10.1016/j.enggeo.2017.09.024

Kurz, J.H., Grosse, C.U., Reinhardt, H.W., 2005. Strategies for reliable automatic onset time picking of acoustic emissions and of ultrasound signals in concrete. Ultrasonics 43, 538–546. https://doi.org/10.1016/j.ultras.2004.12.005

Maeda, N., 1985. A Method for Reading and Checking Phase Time in Auto-Processing System of Seismic Wave Data. Zisin (Journal Seismol. Soc. Japan. 2nd ser.) 38, 365–379. https://doi.org/10.4294/zisin1948.38.3_365

Morita, Y.G., 1984. Automatic Detection of Onset Time of Seismic Waves and its Confidence Interval Using the Autoregressive Model Fitting. J-STAGE 2, 281–293. https://doi.org/https://doi.org/10.4294/zisin1948.37.2_281

Sasahara, K., Sakai, N., 2014. Development of shear deformation due to the increase of pore pressure in a sandy model slope during rainfall. Eng. Geol. 170, 43–51. https://doi.org/10.1016/j.enggeo.2013.12.005

Shackelford, C.D., 2014. The capillary barrier effect in unsaturated flow through soil barriers.

Steven L, K., 1996. Geotechnical earthquake engineering.

Stewart, S.W., 1977. Real-time detection and location of local seismic events in central California. Bull. Seismol. Soc. Am. 67, 433–452.

Takanami, T., Kitagawa, G., 1991. Estimation of the arrival times of seismic waves by multivariate time series model. Ann. Inst. Stat. Math. 43, 407–433. https://doi.org/10.1007/BF00053364

CHAPTER 6

ELASTIC WAVE ATTENUATION IN SHALLOW SLOPE

6.1. INTRODUCTION

Elastic wave propagation in soil as a non-destructive monitoring technique has received considerable attention in recent years. The application of elastic wave propagation in soil has been developed by many researchers, for example, Irfan and Uchimura found that the velocities of both of shear wave(S-wave) and compression wave(P-wave) velocities decreased with increasing degree of saturation by laboratory triaxial tests(Irfan and Uchimura, 2016), (Irfan et al., 2017), (Irfan and Uchimura, 2015). In a series model tests, elastic wave velocity has been observed that it responded sensitively to soil moisture content and deformation (Chen et al., 2017),(Chen et al., 2018),(Chen et al., 2019),(Tao et al., 2019). Thus, many studies were conducted focusing on the velocities of elastic wave, however, precise measurement of travel time is needed to measure the wave velocities.

In this study, a method using wave attenuation is presented to monitor slope deformations and soil moisture variations. It is an application of geometric spreading, which is as the wave moves away from the source, the area that the wave energy covers becomes larger and thus wave intensity decreases, and wave energy loss due to inelastic material behavior or internal friction during wave propagation (Bormann et al., 2012). Laboratory experiments using a Multi-layer shear model were conducted, wave attenuation affected by shear forces and corresponding with deformations on every layer, and the soil moistures in wet and dry processes have been investigated.

6.2. METHOD TO CALCULATE THE WAVE ATTENUATION

6.2.1 The Sensors Layout

The sensors layout in the soil is shown in Figure 6.1. Ten soil moisture sensors were set up in the soil, with a vertical interval of 100 mm, to measure the soil moisture distribution with depth. A total of 10 exciters and 30 receivers are set in the specified position in the soil. E1~E10 are the exciters used to generate elastic waves; CH01~CH30 are the receivers used to sense the elastic waves.

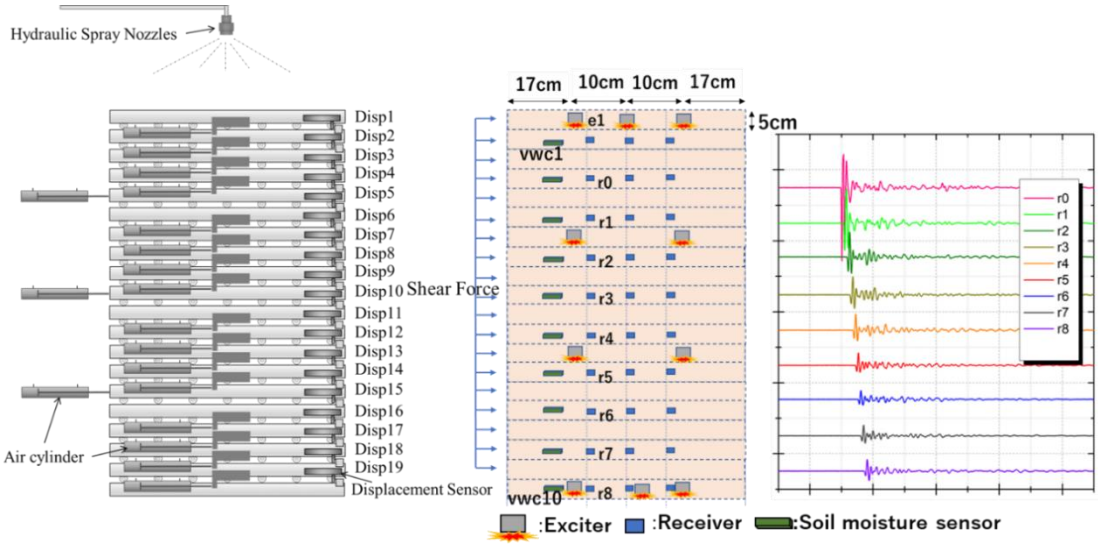

Figure 6.1 The layout of the air cylinder and the displacement sensors (left); Sensors layout in soil(middle); Waveform of One pulse wave which generated by exciter e1 and detected by receivers r0~r8(right)

6.2.2 Fast Fourier Transformation

The elastic wave signals can be converted from the time domain into the frequency domain, and the frequency component with maximum amplitude in the spectrum was defined as the dominant frequency, by applying the Fast Fourier Transformation (FFT). In wave signal processing, the spectrum of a signal is believed to have an intimate correlation with identical events such as rainfall event and deformation in the processes of slope failure. A signal in the time domain may difficult to find out the

significant features, whereas it may show obvious characteristics in the frequency domain. Figure 6.2 shows the pulse elastic signals in the time domain signal and the corresponding frequency spectrum. It is clear to see that the amplitude of high frequency decreases sharply after the rainfall.

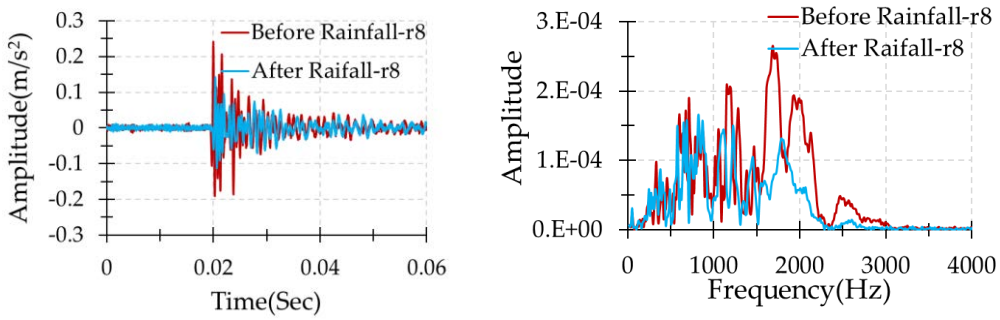

(**a**) (**b**)

Figure 6.2 The pulse elastic signals in the time domain signal and the corresponding frequency spectrum: (a) The pulse elastic wave signals shown in the time domain. (b). The corresponding frequency spectrum.

6.2.3 Elastic Wave Attenuation

Wave energy density E contained in elastic wave may be expressed as

$$E = \sum_{f=1}^{f=3000} \left(\frac{1}{2}\right) * 4\pi^2 \rho \left(f * A_f\right)^2, \tag{6-1}$$

where ρ is the density of material, f is frequency, A_f is the amplitude of wave. Frequency is resolved from 1~3000Hz.

The elastic wave attenuation is defined by the wave energy ratio, calculated by

$$\text{Energy ratio } = E_n/E_0 (\text{n=1,2, …,8}), \tag{6-2}$$

where E_0 is energy of the receiver near the exciter (r0), E_n is others receiver' energy which far away from exciter(r1~r8).

Figure 6.2 shows the pulse elastic signals in time domain signal and energy density.

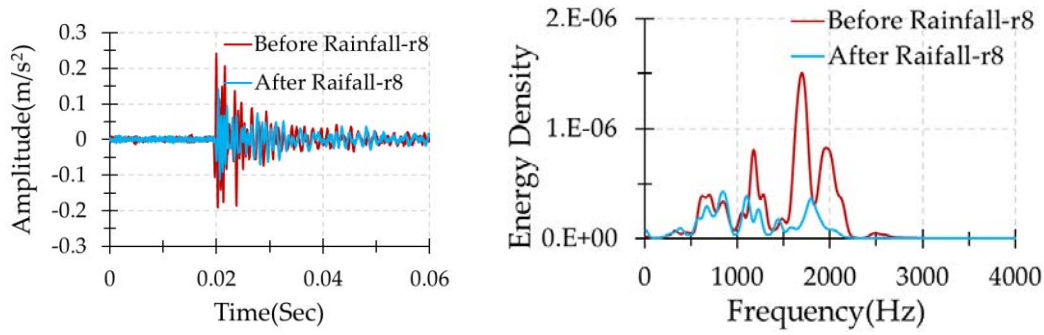

(**a**) (**b**)

Figure 6.3 The pulse elastic signals in time domain signal and energy density: (a) The pulse elastic wave signals shown in the time domain. (b). The corresponding energy density.

6.3. TEST CONDITIONS

Three test cases were conducted with the conditions in Table 1. In Test Case 1, the slope angle was zero, it means no shear force put on any layer of the model. Rainfall was applied for 4 hours until VWC (Volume Water Content) became stable, then rainfall was stopped, and water was drained out by gravity about 20hours. In Test Case 2, the slope angle was set to be 27, 29, and 31-degree. Displacement was not found changing during the artificial rainfall(24hours) and drain(24hours) events. In Test Case 3, the slope angle was set to 33-degree. No rain was applied but the displacement continuously increased until failure.

Table 6.1 Test cases

Test Case	Moisture Control	Slope Angle
1	Rain(4hours)/Drain(20hours)	0
2-1	Rain(24hours)/Drain(24hours)	27
2-2	Rain(24hours)/Drain(24hours)	29
2-3	Rain(24hours)/Drain(24hours)	31
3	Constant	33

6.4. TEST RESULT

6.4.1 Soil Moisture and Wave Energy Ratio

Figure 6.4 shows the changes of wave energy ratio with VWC during the rainfall and drain event in the time series observed in Test Case1. It took 4 hours rainfall to make the VWC be stable, and more than 20 hours to drain the water out. The deeper from the surface, the higher moisture was observed. Figure 6.4 b shows energy ratio changes in the time series. With soil moisture increased in the rainfall event, the energy ratio decreased. During the drain stage, the energy ratio increased. Figure 6.4 c and Figure 6.4 d show the energy ratio at every receiver against the VWC averaged between the nearer and farther receivers. The energy ratio reduced 20%~50% when the VWC grew up from 0.1 to 0.25 m^3/m^3.

The effects of soil moisture on the wave energy ratio could be explained by matric suction. When the soil moisture becomes higher, the matric suction decreases, and the weaker of force between soil partials results in lower of wave energy propagation. There is hysteresis in the path of energy ratio and VWC between rainfall and drain event. This may be related to the hysteresis observed in the relationship between soil moisture and matric suction.

6.4.1 Shear Stress Effect on Wave Energy Ratio

The response of energy ratio at different shear force corresponding to slope angle during rainfall and drain event is shown in Figure 6.5 and Figure 6.6, which are the results of the Test Case 2. The stronger shear force applied, the lower energy ratio is observed. Wave energy ratio reduced 20%~40% when shear force increases from 27 to 31degrees. For example, in Figure 6a, at the 0.1 m3/m3 of VWC, when shear force was set to 27-degrees, 29-degrees and 31-degrees, the energy ratio decreased from 0.18, 0.14, and 0.11, wave energy ratio reduced from 22% to 38%.

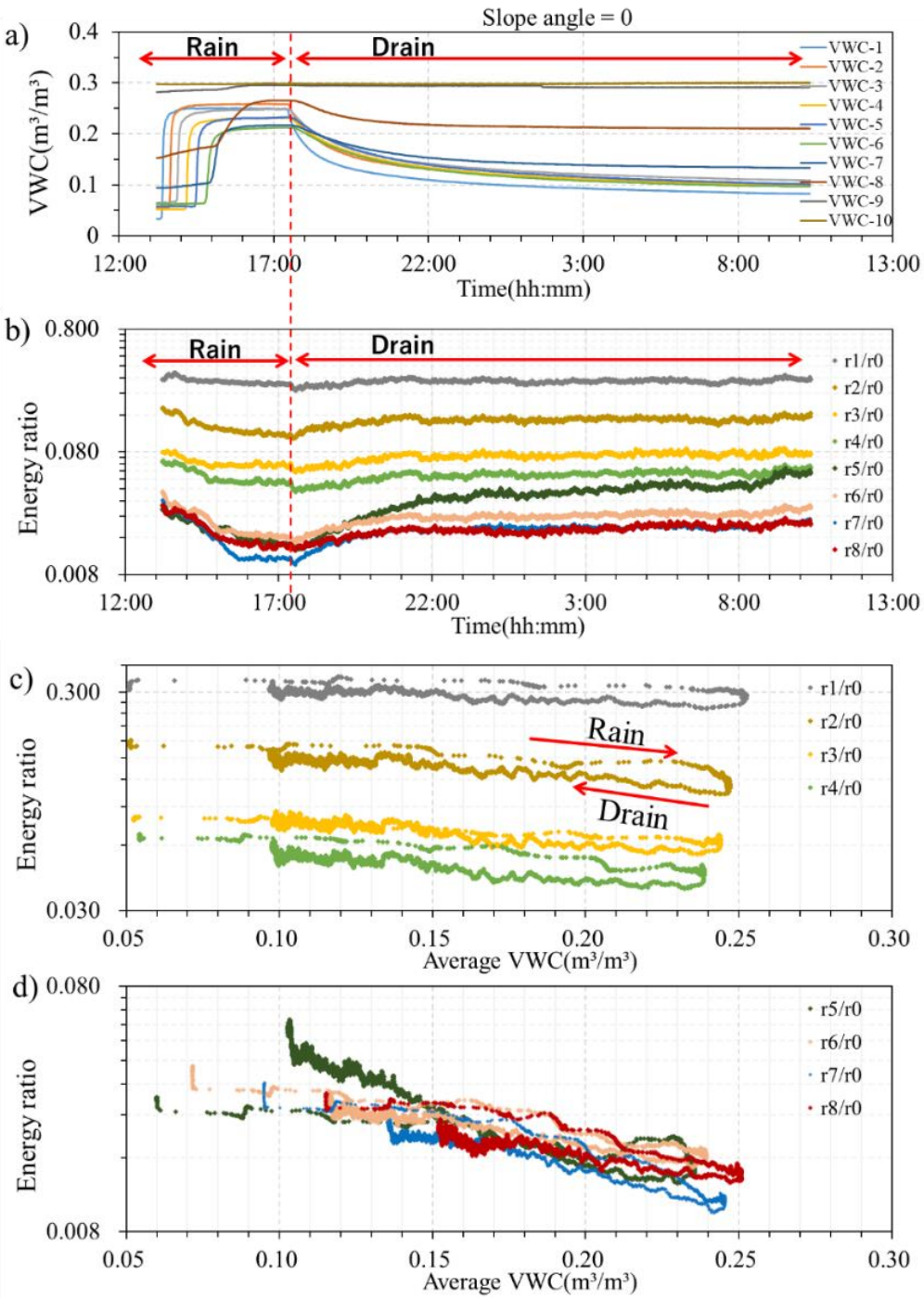

Figure 6.4 Energy ratio changes with VWC (slope angle = 0)

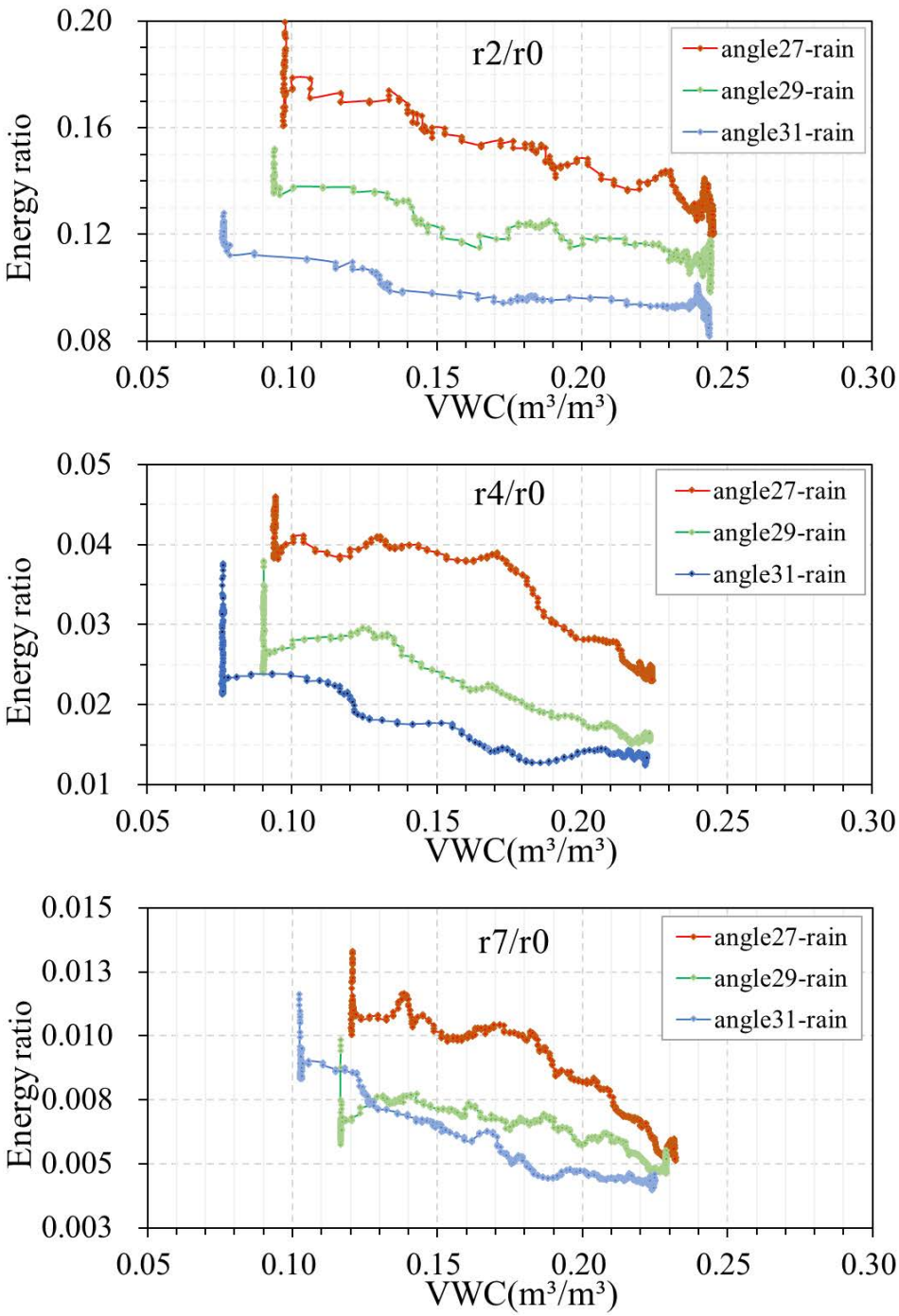

Figure 6.5 Energy ratio changes with VWC in the rain event (slope angle = 27, 29,31)

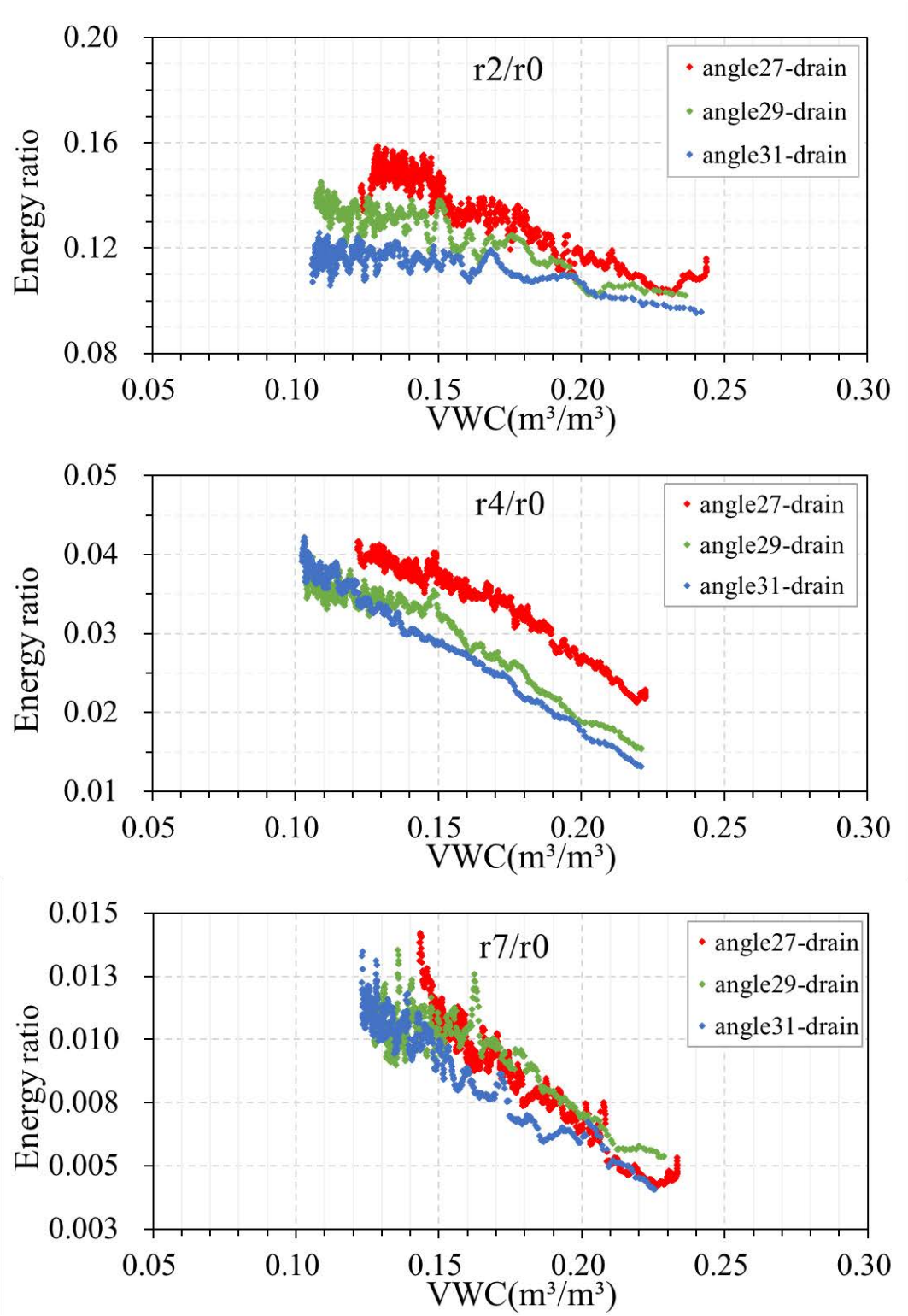

Figure 6.6 Energy ratio changes with VWC in the drain event (slope angle = 27, 29,31)

6.4.2 Shear Displacement Effect on Wave Energy RSatio

Figure 6.7 shows the response of wave energy ratio and displacement during shearing in the Test Case 3. VWC did not change in this test. After the shear force was set corresponding to the slope angle of 33-degree, the displacement started with an average 3mm/h of moving speed, then accelerated and finally failed, which observed at the displacement sensor No18, so energy ratio of r8/r5 was analyzed. With the increasing displacement, the wave energy ratio also decreased rapidly. Figure 6.7b shows the wave attenuation against the displacement. Wave energy ratio dropped by 50% during a 3 mm of displacement.

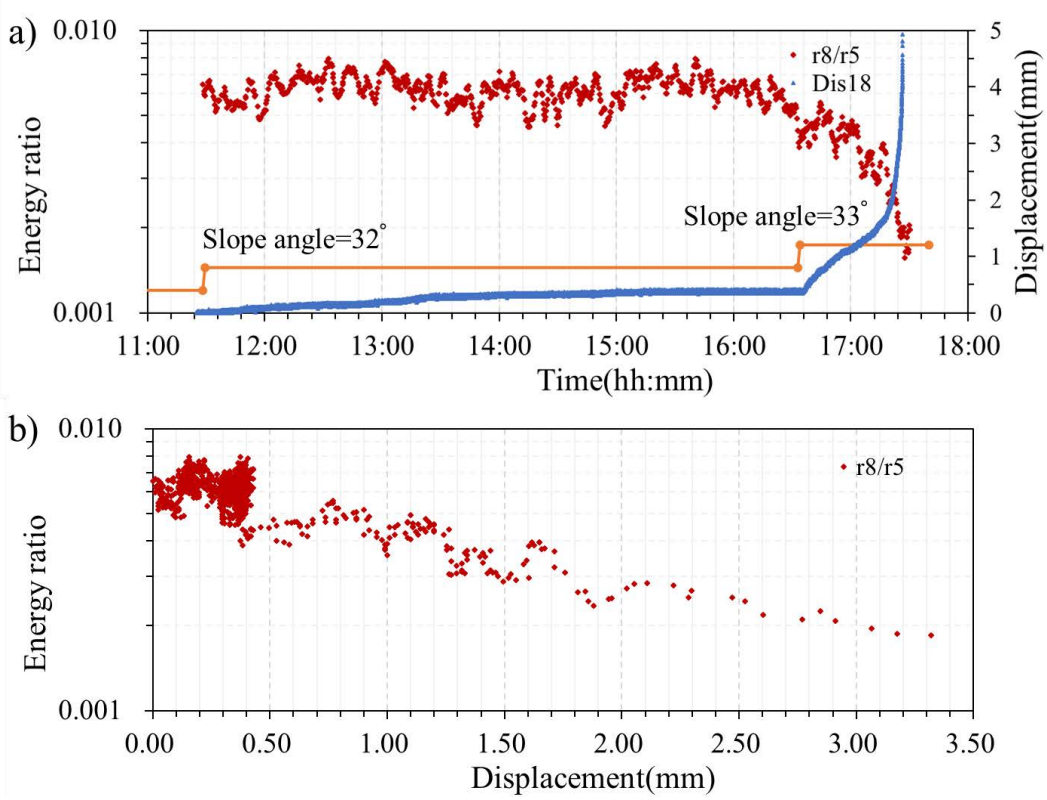

Figure 6.7 Elastic wave energy ratio changes with displacement

6.5. SUMMARY

Laboratory experiment using the multi-layer shear model was conducted to observe the changes of elastic wave propagation in slope surface layer. The results show that the wave attenuation increased with the increasing soil moisture, the wave energy reduced by 20%~50% when the VWC grew up from 0.1 to 0.25 m^3/m^3. The stronger shear force applied, the lower energy ratio observed. With increasing the displacement, the wave attenuation also increased.

6.6. REFERENCE

Bormann, P., Engdahl, E., Kind, R., 2012. Seismic Wave Propagation and Earth models. p. p36. https://doi.org/10.2312/GFZ.NMSOP-2_ch2

Chen, Y., Irfan, M., Uchimura, T., Cheng, G., Nie, W., 2018. Elastic wave velocity monitoring as an emerging technique for rainfall-induced landslide prediction. Landslides 15, 1155–1172. https://doi.org/10.1007/s10346-017-0943-3

Chen, Y., Irfan, M., Uchimura, T., Wu, Y., Yu, F., 2019. Development of elastic wave velocity threshold for rainfall-induced landslide prediction and early warning. Landslides 16, 955–968. https://doi.org/10.1007/s10346-019-01138-2

Chen, Y., Uchimura, T., Irfan, M., Huang, D., Xie, J., 2017. Detection of water infiltration and deformation of unsaturated soils by elastic wave velocity. Landslides 14, 1715–1730. https://doi.org/10.1007/s10346-017-0825-8

Irfan, M., Uchimura, T., 2016. Modified triaxial apparatus for determination of elastic wave velocities during infiltration tests on unsaturated soils. KSCE J. Civ. Eng. 20, 197–207. https://doi.org/10.1007/s12205-015-0404-2

Irfan, M., Uchimura, T., 2015. Helical filter paper technique for uniform distribution of injected moisture in unsaturated triaxial specimens. Soils Found. 55, 749–760. https://doi.org/10.1016/j.sandf.2015.06.008

Irfan, M., Uchimura, T., Chen, Y., 2017. Effects of soil deformation and saturation on elastic wave velocities in relation to prediction of rain-induced landslides. Eng. Geol. 230, 84–94. https://doi.org/10.1016/j.enggeo.2017.09.024

Tao, S., Uchimura, T., Fukuhara, M., Tang, J., Chen, Y., Huang, D., 2019. Evaluation of Soil Moisture and Shear Deformation Based on Compression Wave Velocities in a Shallow Slope Surface Layer. Sensors 19, 3406. https://doi.org/10.3390/s19153406

CHAPTER 7

MONITORING ELASTIC WAVE IN NATURAL SLOPE

7.1 INTRODUCTION

To investigate the behavior of elastic wave propagation in the natural slope surface layer, elastic wave monitoring has been conducted at a slope located at Aso-shi, Kumamoto, Japan. This slope was suffered from the 2016 Kumamoto Earthquakes and some big cracks appeared on the slope surface (Figure 7.1). It is a typically unstable slope. The depth of the crack is near 1m (Figure 7.2). Some monitoring researches using tilt sensors, extensometer, rain gauge, and soil moisture sensors also conducted on this unstable slope(Figure 7.4).

In this study, the seismic refraction method has been applied to measure the thickness of the slope surface layer and compared to the results of the dynamic cone penetrometer test (DCPT). Elastic wave velocities and attenuation have been analyzed with different exciter energy. Exciter energy is generated by a 5kg hammer vertically free dropping down from difference high like 10cm, 20cm, 30cm, 40cm and 50cm. Elastic wave frequency characteristics are also compared with different exciter energy and different distance on this slope.

The physical properties of an undisturbed soil sample from Aso natural slope are shown. An elastic wave monitoring system including one exciter and several revivers have been developed and installed in a natural unstable slope. Two cases are shown in this section. Case 1 shows that wave attenuation behaviors with soil moisture. The sensors layout and sampling rate are improved in case2 so the wave velocity changes with soil moisture can be observed. The results On-site are compared to laboratory experiments.

Figure 7.1 A typically unstable slope located at Aso-shi, Kumamoto, Japan.

Figure 7.2 The depth of the crack is near 1m.

Figure 7.3 Soil layers underground.

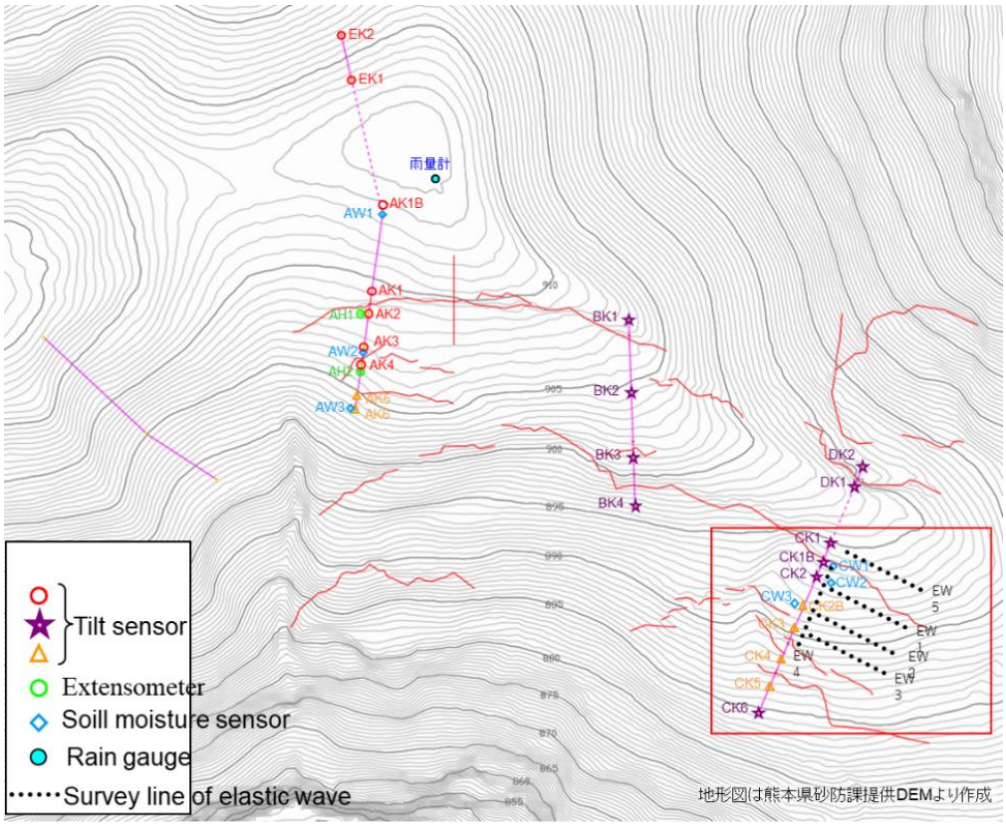

Figure 7.4 Layout of monitoring devices

7.2 MEASURE THE THICKNESS OF SLOPE SURFACE LAYER

7.2.1 Portable Dynamic Cone Penetrometer Test

Portable dynamic cone penetrometer test (DCPT) is a simple method for shallow in-situ investigation and light field exploration, shown in Figure 7.5. It is performed by driving a metal cone into the ground by repeated striking it with a 5 Kg weight hammer vertically free dropping down from a height of 50cm. The count of drops is recorded when the penetration of the lower shaft cone inserted into the soil per 5cm (called Nd-value).

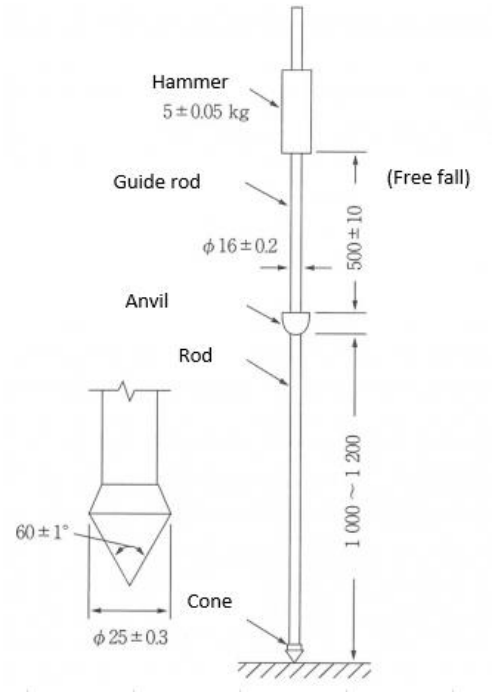

Figure 7.5 Portable Dynamic cone penetrometer (JGS)

7.2.2 Seismic Refraction Method

The seismic refraction method can be described by Snell's Law, which shows that wave energy changes direction whenever it crosses a boundary between different media which transmit at different velocities.

Commonly the surface lay is weathering so it is soft than the subsurface layer, so V1 (elastic wave propagation in the surface layer) is slower than V2 (Elastic wave propagation in the subsurface layer). The energy source is usually a hammer's hitting,

and the elastic wave is detected by an array detector and recorded by the data recorder. From the arrival times and distances plotted in the time-distance graph the V1 and V2 can be calculated. The thickness of the surface layer h is calculated by the following formula,

$$h = \frac{x}{2}\sqrt{\frac{V_2 - V_1}{V_2 + V_1}} \tag{7-1}$$

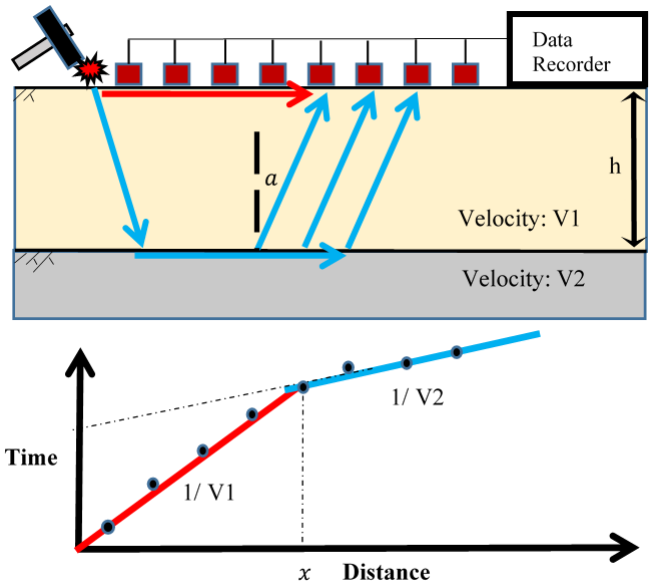

Figure 7.6 Simplified case of seismic refraction method

The seismic refraction method uses a linear spread, exciter and detectors (8 geophones) are located along a single survey line and layout with the same interval distance 1.5m on the slope surface shown as Figure 7.8 and 7.9.

Figure 7.7 Seismic refraction test. Energy source a drop of hammer. The receivers are 8 geophones which set up with 1.5m of interval distance.

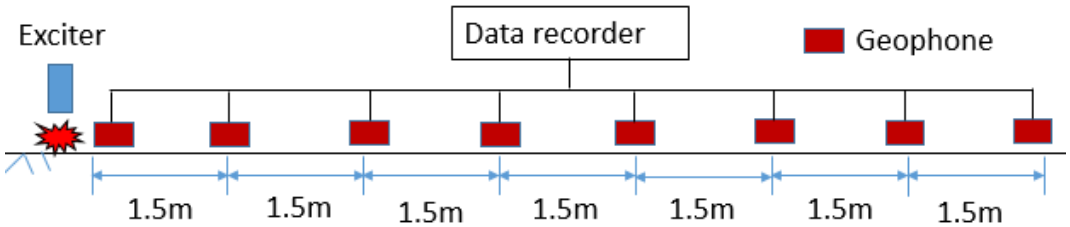

Figure 7.8 Arrangement of the devices

7.2.3 The Thickness and strength of Surface Layer

The results of the portable dynamic cone penetrometer test are shown in Figure 7.10. Near the position of CK1, there is a hard layer at a depth of 2.2-2.5m. Between CK2 and CK4, the soil hardness did not increase remarkably even when the depth exceeded 2.5 m. In other words, there is a discontinuous surface like the old ground surface at a depth of about 2.5m. From CK5 to CK6, it became slightly hard at a depth of 1 to 1.5m, but the soil hardness decreased again at a deeper point. In particular, the soil hardness did not increase, so the test was completed at a depth of 3 m.

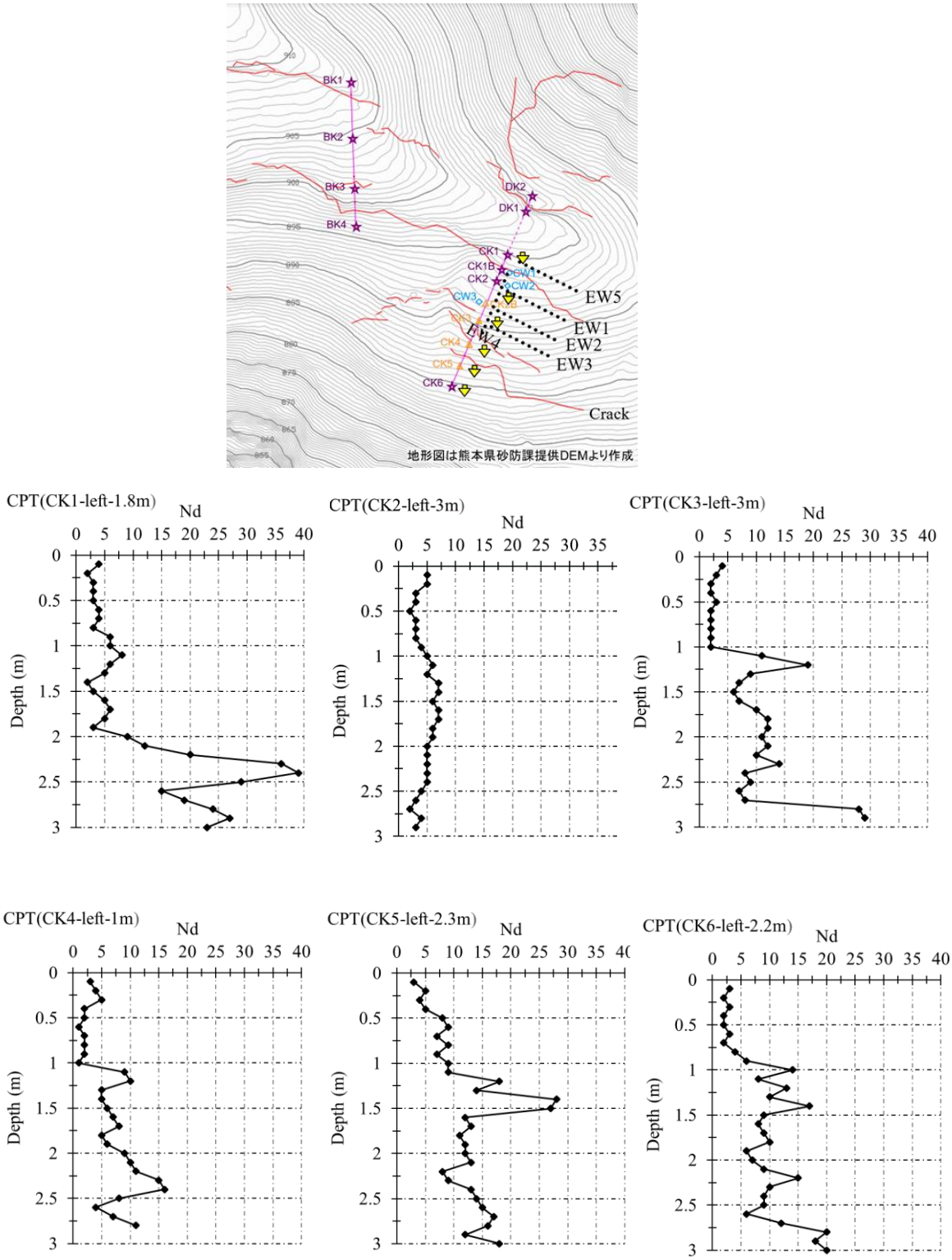

Figure 7.10 The results of portable dynamic cone penetrometer tests at six different positions.

The thickness of the slope surface layer has been investigated by the seismic refraction method with different exciter energy and compared with the dynamic cone penetrometer test. The thickness of the slope surface layer is around 1m at position1 (near ew2 and DCPT1). The dynamic cone penetrometer test also shows that from the depth of 1m at position1 the soil becomes hard, shown in Figure 7.11.

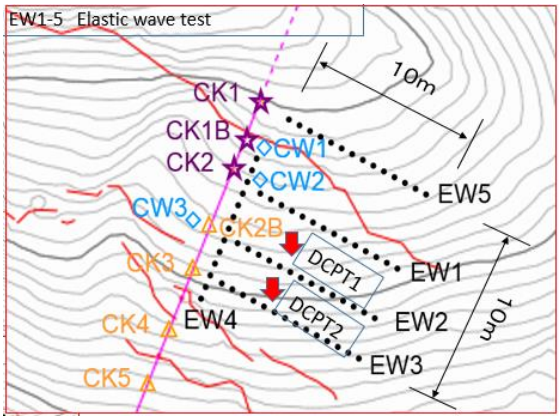

Figure 7.11 The position of DCPT and seismic refraction test.

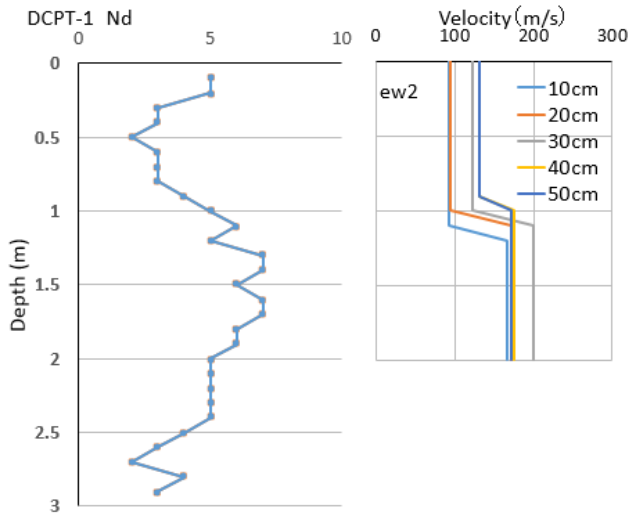

Figure 7.12 The comparison of DCPT and seismic refraction method (position 1)

The thickness of the slope surface layer is around 2m at position2 (near ew3 and DCPT2). Dynamic cone penetrometer test also shows that from the depth of 2m at position2 the soil becomes hard, shown in Figure 7.13.

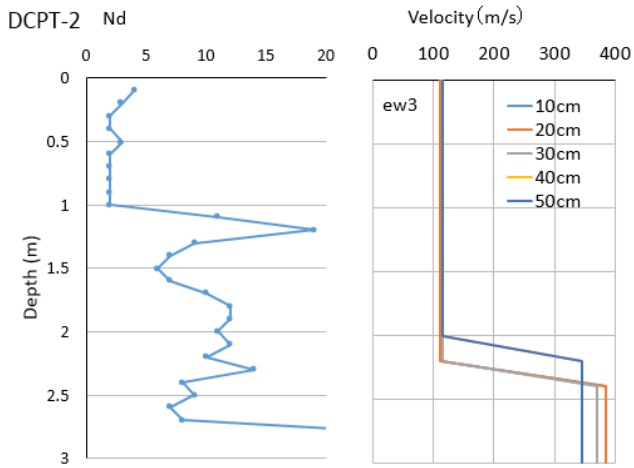

Figure 7.13 The comparison of DCPT and seismic refraction method (position 2)

Thickness not changes with exciter energy. DCPT shows that the soil of the subsurface layer at position 2 is harder than position 1. V2 (Elastic wave propagation in the subsurface layer) at position 2 is over 350m/s but less than 200m/s at position 1, it shows that the harder subsurface layer has faster wave velocity. V1 (elastic wave propagation in the surface layer) is around 100m/s at both position 2 and position 1.

7.3 WAVE ENERGY ATTENUATION WITH DISTANCE

This section outlines an experimental analysis of the elastic wave generated by dropping a hammer from some fall heights at a natural slope. Laboratory tests included triaxial tests and slope model tests show that elastic wave velocity continuously decreases in the response of moisture content and deformation, it can apply to predict slope failure(Irfan and Uchimura, 2013). For the purpose of developing an elastic wave monitoring system installed in a natural slope, field investigation is necessary to know the relationship of wave propagation distance and exciter energy. To understand the behavior of elastic wave propagation in natural slope surface, a field investigation has been conducted.

7.3.1 Elastic Wave Energy

The wave signal is a period of time waveform, it can be converted to its frequency components by the algorithm of fast Fourier transform (FFT).

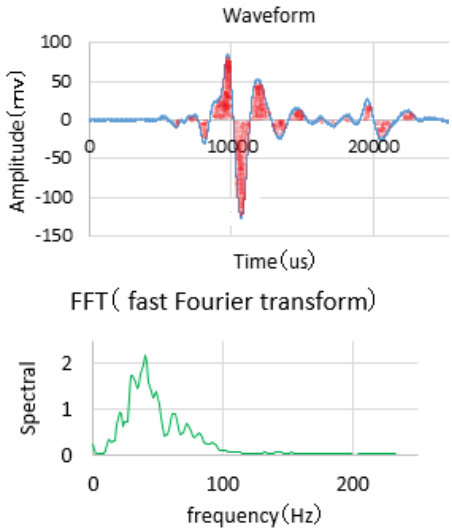

Figure 7.14 Elastic waveform and its FFT

Wave energy E contained in elastic wave may be expressed as

$$E = \sum_{f=1}^{f=3000} \left(\frac{1}{2}\right) * 4\pi^2 \rho (f * A_f)^2, \tag{7-2}$$

where ρ is the density of material, f is frequency, A_f is the amplitude of wave. Frequency is resolved from 1~3000Hz.

The elastic wave attenuation is defined by the wave energy ratio, calculated by

$$\text{Energy ratio } = E_n / E_0 (\text{n=1,2, …,7}), \tag{7-3}$$

where E_0 is energy of the receiver near the exciter (r0), E_n is others receiver' energy which far away from exciter(r1~r7).

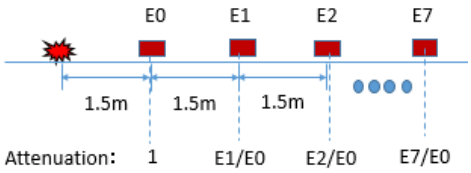

Figure 7.15 Elastic wave energy attenuation

7.3.2 Exciter Energy

Exciter energy is generated by a 5kg hammer vertically free dropping from difference high (h) like 10cm, 20cm, 30cm, 40cm and 50cm.

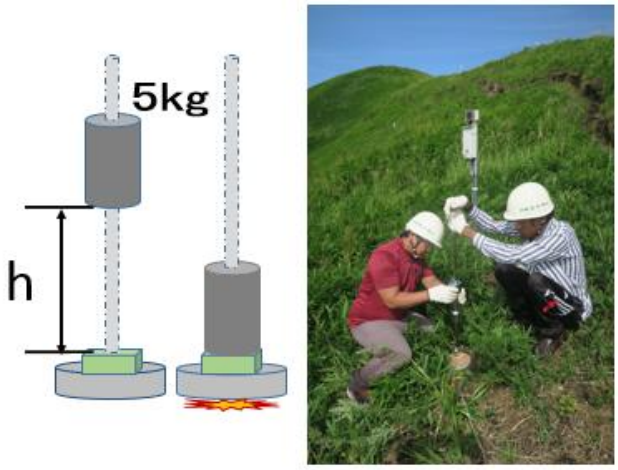

Figure 7.16 Exciter energy generator

Exciter energy is calculated by the following formula, where m is 5kg, g is 9.8 m/s^2,

$$Energy = mgh \tag{7-4}$$

Table 7.1 The energy of source exciter

High(cm)	10	20	30	40	50
Energy(J)	4.9	9.8	14.7	19.6	24.5

7.3.3 The Results

A 5kg hammer vertically free drops from the high 10cm, 20cm, 30cm, 40cm and 50cm to generate the elastic wave. The higher energy impact, the stronger wave signal can be detected. And the nearer the exciter, the stronger signal can be detected. Elastic wave attenuation has been analyzed at three survey lines (EW1, EW2, and EW3). At the same survey line, Elastic wave attenuation is almost the same with different exciter energy, shown in Figure 7.17.

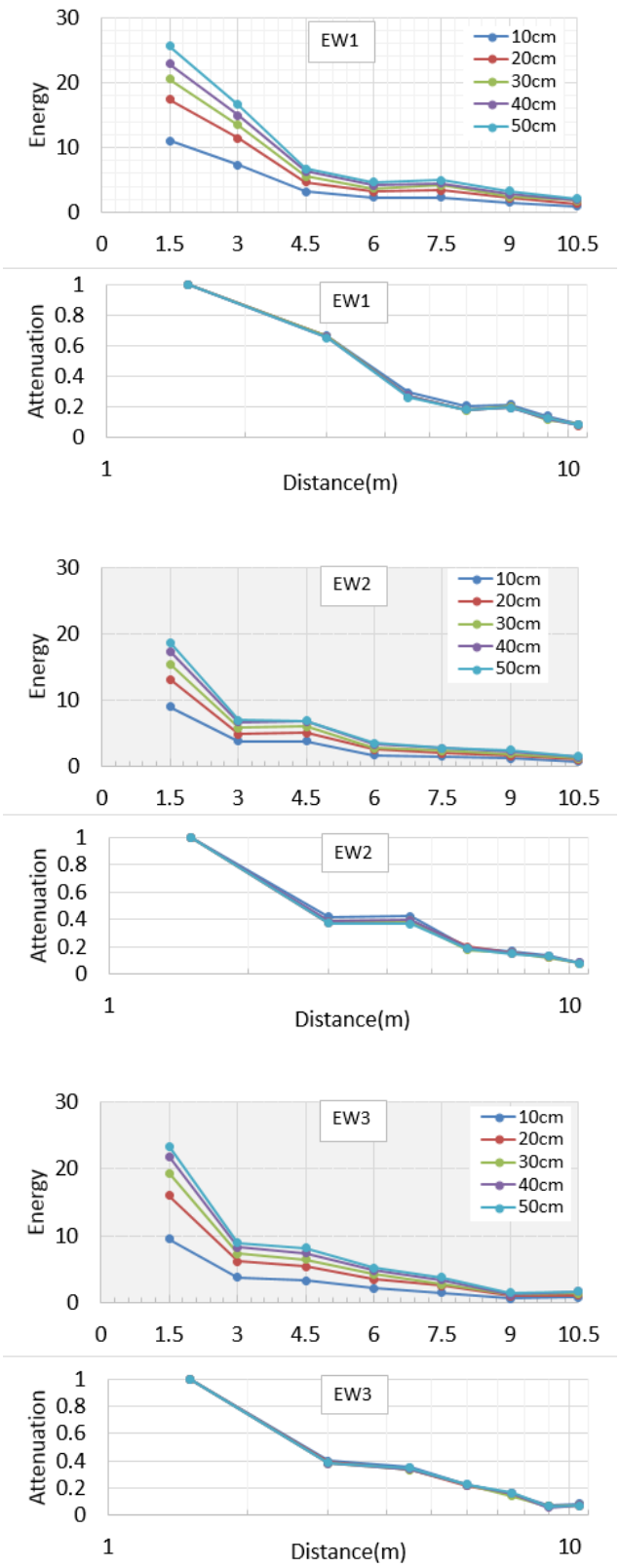

Figure 7.17 Elastic wave energy attenuation with distance

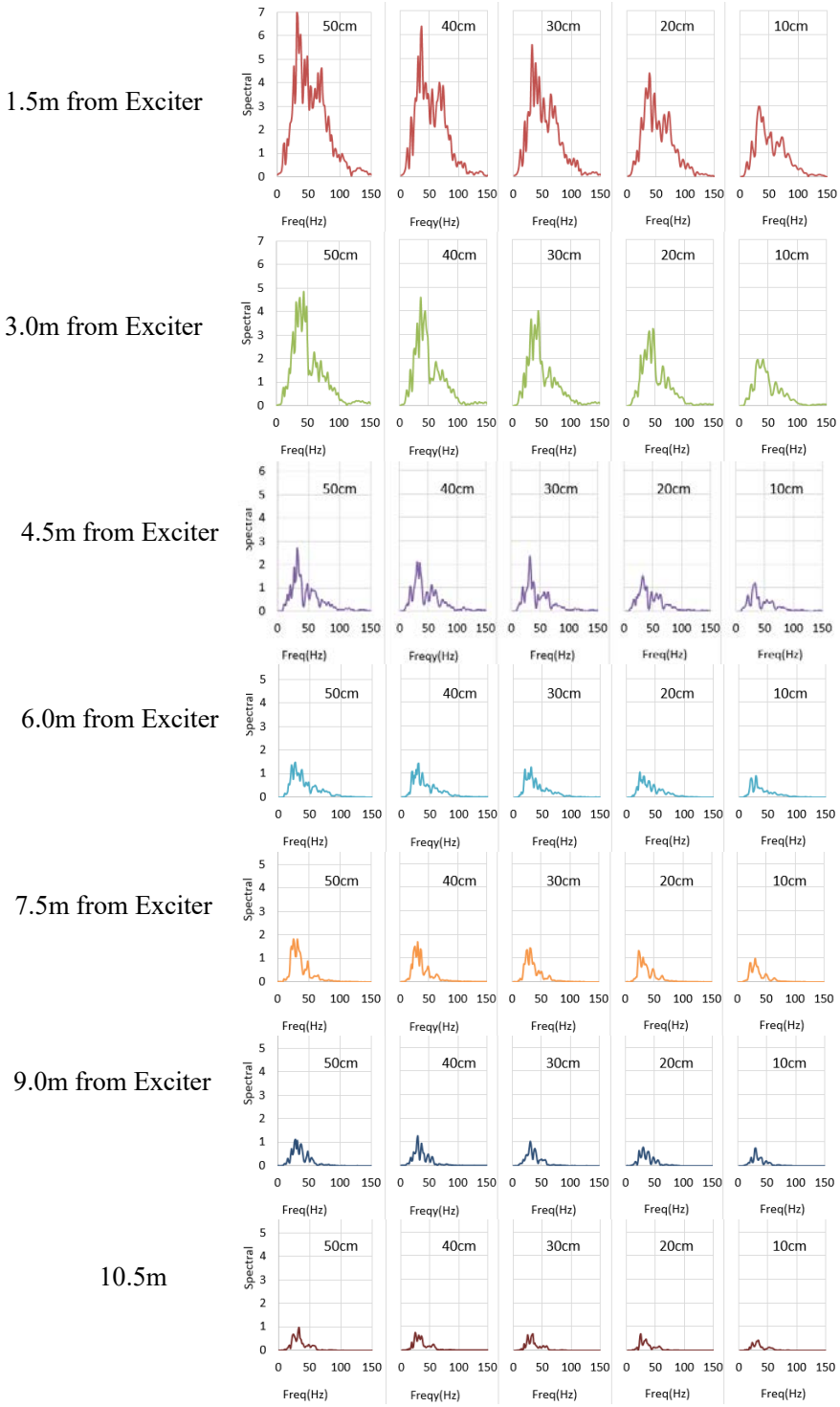

Figure 7.18 Frequency with different energy and distance

Figure 7.18 shows the frequency characteristics change with different exciter energy and distance. The high frequency disappears quickly when far away from the exciter. For example, on the 50cm free drop impact, the frequency decreases from 150Hz ~100Hz ~ 50Hz from distance changes from 1.5~4.5~10.5m.

7.4 PHYSICAL PROPERTIES

An undisturbed soil sample from a depth of 0.4m in Aso natural slope(Figure 7.19). It had a wet density of around 1.70 g/cm^3 and a dry density of around 0.57 g/cm^3. High Moisture Content was 226% shown in Table 7.2. About the disturbed soil sample, its minimum and maximum dry density were found to be 0.686 g/cm^3 and 0.821 g/cm^3. Figure 7.20 shows the grain size accumulation curve of the sample.

Figure 7.19 Undisturbed soil sample from a depth of 0.4m

Table 7.2 Undisturbed soil sample

No	Physical properties	Value
1	Dry density (ρ_d)	$0.57 g/cm^3$
2	Wet density(ρ_t)	$1.70 g/cm^3$
3	Moisture Content	226%

Table 7.3 Disturbed soil sample

No	Physical properties	Value
1	Maximum dry density (ρ_{dmax})	0.821 g/cm^3
2	Minimum dry density (ρ_{dmin})	0.686 g/cm^3

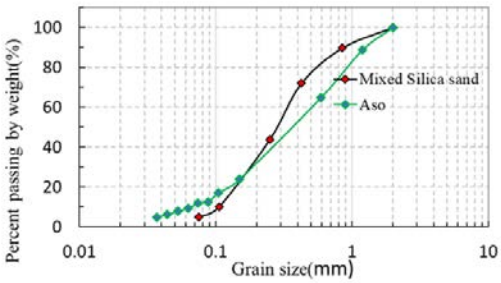

Figure 7.20 Grain size accumulation curve of the sample

7.5 ELASTIC WAVE MONITORING ON-SITE

An elastic wave monitoring system including one exciter and several revivers have been developed and installed in nature unstable slope. Two cases are shown in this section. Case 1 shows that wave attenuation behaviors with soil moisture. The sensors layout and sampling rate are improved in case2 so the wave velocity changes with soil moisture can be observed.

7.4.1 Case 1 Wave Attenuation Behaviors with Soil Moisture

Figure 7.21 shows elastic wave monitoring devices. It has a fully automatic to generate elastic wave by the exciter, measure the wave signal by receivers. It includes a controller and data collection device, an exciter, 4 receivers, and a VWC sensor. Exciter is made with a Solenoid Electromagnet, which is controlled by the controller, it can generate pulse elastic wave per 10 minutes. Receivers are 3- axis MEMS accelerometers, ADXL354, a production of Analog Devices. The controller and data collection device control the timing of exciter, handle the wave data received by the receiver with a 7kHz of sampling rate, and store wave data into the SD card. The VWC sensor is a soil moisture sensor EC-5 to measure the volumetric water content in the soil. The power is supplied by the arrangement of the lead-acid battery, which is charged by a solar panel (Figure 7.22), to be continually running for a long term.

Figure 7.22 shows the elastic wave monitoring system installed on an unstable slope. The dotted line in the photo shows the survey line of elastic wave. Sensors and exciter were set in the underground. The exciter and VWC sensors were installed at a depth of 0.2 m. The receiver (CH1) was set at a horizontal distance of 0.01 m and a depth of 0.1 m from the exciter. Receiver (CH3) has a horizontal distance of 0.2 m from the exciter and a depth of 0.1 m; receiver (CH5) has a horizontal distance of 0.2 m from the exciter, a depth of 0.4 m; receiver (CH6) was installed at a depth of 0.1 m at a horizontal distance of 1.5 m from the exciter.

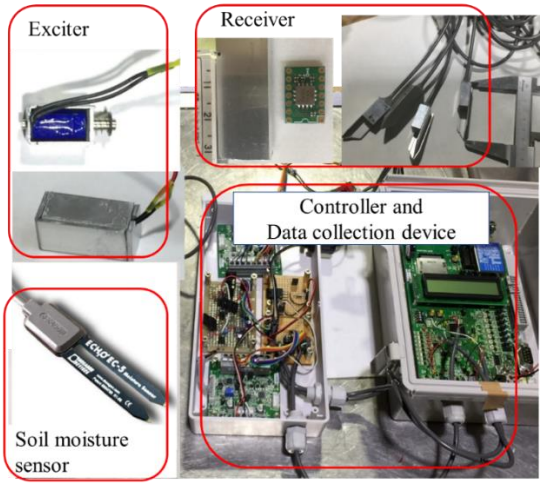

Figure 7.21 Elastic wave monitoring devices

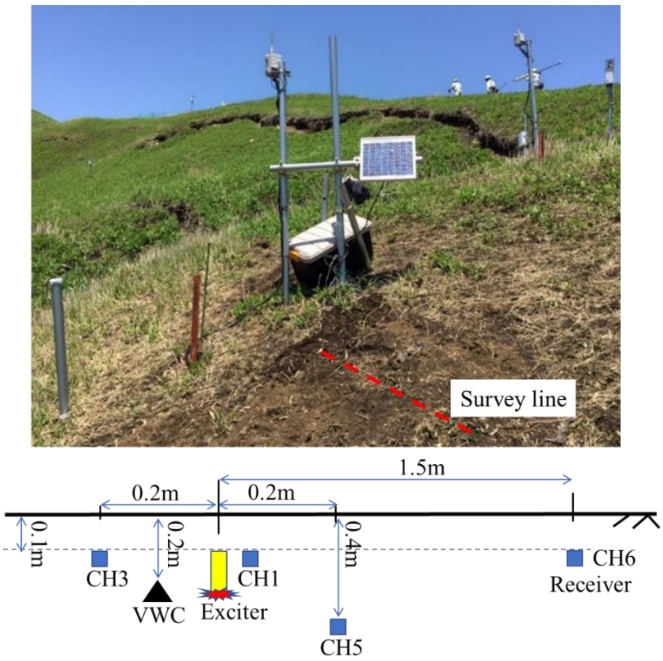

Figure 7.22 Elastic wave monitoring system installed on an unstable natural slope. The dotted line shows the survey line of elastic wave. The layout of sensors and exciter underground.

Figure 7.23 shows the examples of waveforms of a pulse elastic wave observed by each acceleration sensor. CH1, the nearest with exciter, could detect the strongest signal around 30 cm/s2, whereas CH6, the farthest from the exciter, detected the weakest signal around 1 cm/s2. It indicates that wave amplitudes reduced quickly with distance.

Figure 7.24 shows VWC and energy ratio plot in time series from 2018/9/24 to 2018/12/20. In the dry process, the energy ratio of the elastic wave tends to increase with the decrease of VWC. On the contrary, in the wet process (rainfall events), the energy ratio of the elastic wave tends to decrease with the increase of VWC.

Figure 7.25 shows energy ratio response with VWC. Wet process is the cases of rain event, the dry process is a drain event. In CH5/CH1, wave energy ratio dropped down 60% when VWC increased from 0.39 to 0.41 m^3/m^3. In CH3/CH1, wave energy ratio dropped down 70% when VWC increased from 0.39 to 0.44 m^3/m^3. Whereas CH6, the farthest from the exciter, not clear changes trend. Hysteresis had been observed in CH3/CH1, that is similar to the results in laboratory experiments.

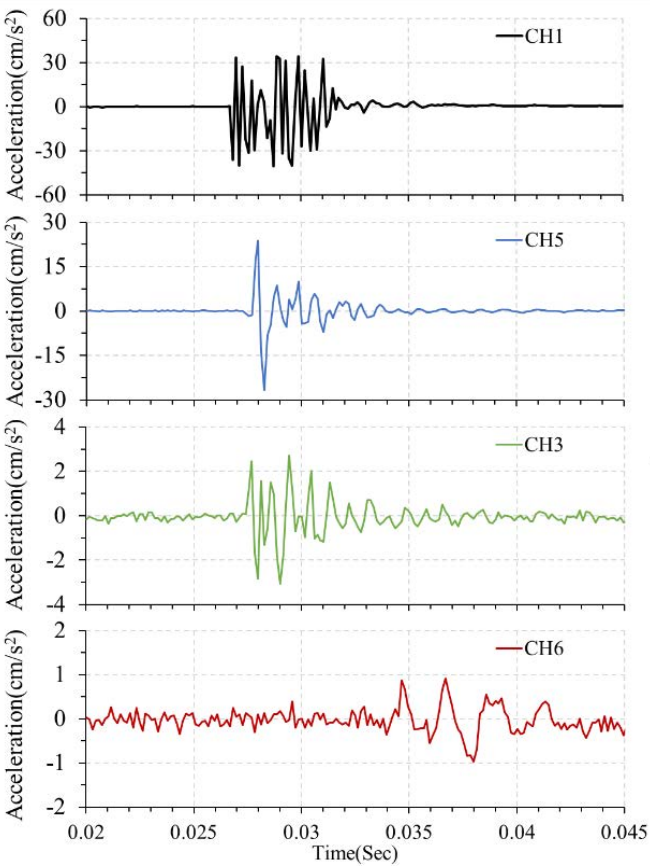

Figure 7.23 Examples of waveforms of a pulse elastic wave observed by receivers.

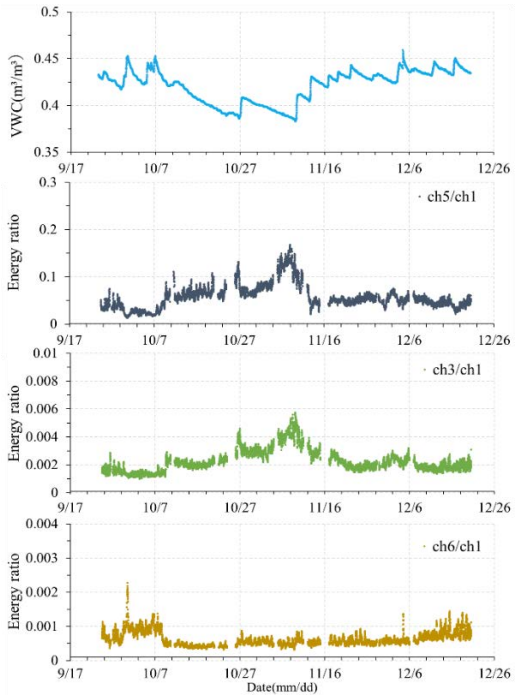

Figure 7.24 VWC and energy ratio plot in time series. Elastic wave data was collected from 2018/9/24 to 2018/12/20 on-site.

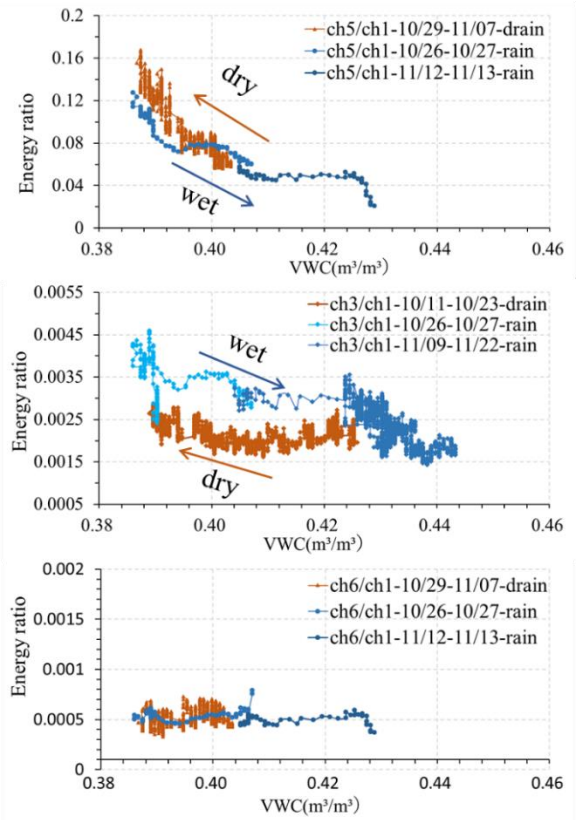

Figure 7.25 Energy ratio responses with VWC. Wet and dry process are the cases of rain event and drain event.

7.4.2 Case 2 Wave Velocities Behaviors with Soil Moisture

In case 2, The sampling rate has been improved from 7kHz to 100Khz. Figure 7.26 shows the elastic wave monitoring devices. It includes an exciter, several receivers, a controller and a data collection device. Exciter is made with a Solenoid Electromagnet, which is controlled by the controller, it can automatically generate pulse elastic wave per 10 minutes. Receivers are 3- axis MEMS accelerometers, ADXL354, a production of Analog Devices. The controller and data collection device control the timing of exciter, handle the wave data received by the receiver with a 100kHz of sampling rate, and store wave data into the SD card. The soil moisture sensor is EC-5 to measure the volumetric water content in the soil. The pressure sensor is LPS33HW (STMicroelectronics).

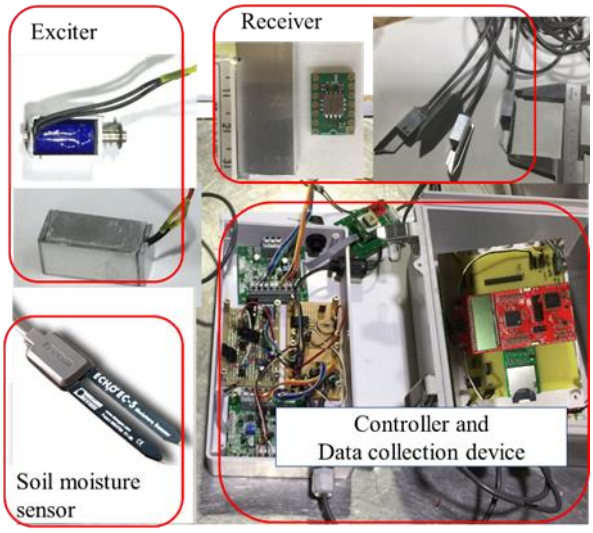

Figure 7.26 The new elastic wave monitoring devices

Figure 7.27 shows the elastic wave monitoring system installed on an unstable slope. The dotted line in the photo shows the Y survey line of the elastic wave. Sensors and exciter were set in the underground. The exciter was installed at a depth of 0.5 m. The receiver (A1) was set near the exciter. At the vertical survey line, Receiver A2 and A3 were set at the depth of 1m and 1.5m. At a horizontal survey line, Receiver A4 and

A5 were set at a distance of 0.3 m and 0.6m. Receiver (CH6) has a horizontal distance of 0.6 m from the exciter and a depth of 1 m; A tilt sensor was set near the exciter with a distance of 1m, use to measure the deformation of the slope, angle X was the direction of the slope. The soil moisture sensors were placed at a different depth from 0.2m to 0.8m underground. One of the pressure sensors was set up in the box on the ground and the other one was set at a depth of 0.4m underground, the pressure and temperature data were collected for the pressure sensors. A rain gauge was also set on this slope to collect the precipitation.

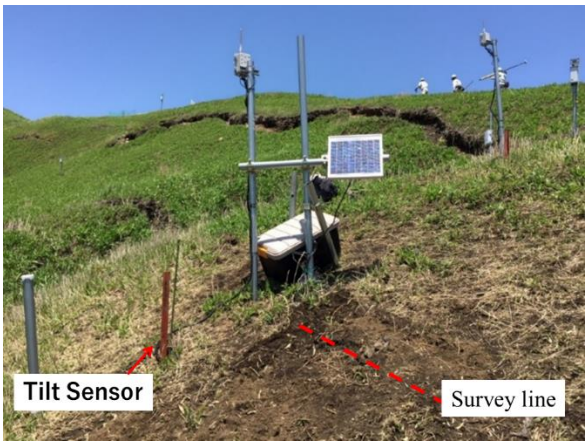

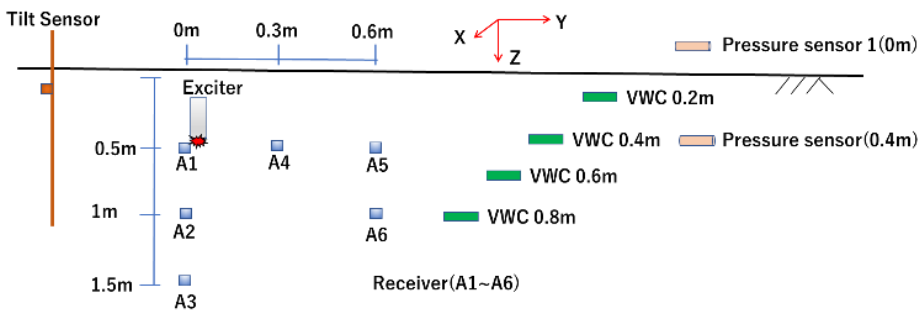

Figure 7.27 Elastic wave monitoring system installed on an unstable natural slope. The dotted line shows the Y survey line of elastic wave. The layout of sensors and exciter underground.

Figure 7.28 a) shows daily precipitation from 5/15 to 6/30. several rainfall events over 20mm recorded. the volume matrix water content increased quickly with the rainfall event, and slowly decreased during the dry period, shown in Figure 7.28 b). The pressure is higher than the pressure in the air. The temperature difference in the air

between day and night is intense, while the temperature underground is stable, shown in Figure 7.28 c).

Figure 7.29 shows the changes of the tilt sensor. The tilt angle X was found that it started to move with a very slow rate (1 degree/ 20 day) after heavy rainfall, whereas the tilt angle Y had no changes. Figure 7.30, Figure 7.31, and Figure 7.32 show the effects of soil moisture on elastic wave velocities. Since the deformation is very small, the results of on-site showed that the elastic wave velocities mainly change with the soil moisture. It is similar to the result of the laboratory experiment.

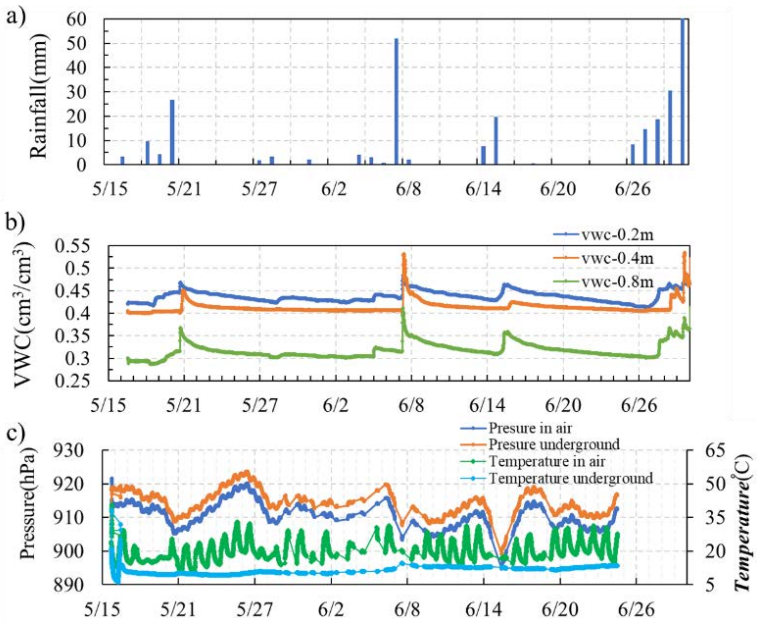

Figure 7.28 a) daily precipitation, b) volume matrix water content in the soil, c) pressure and temperature in air and underground.

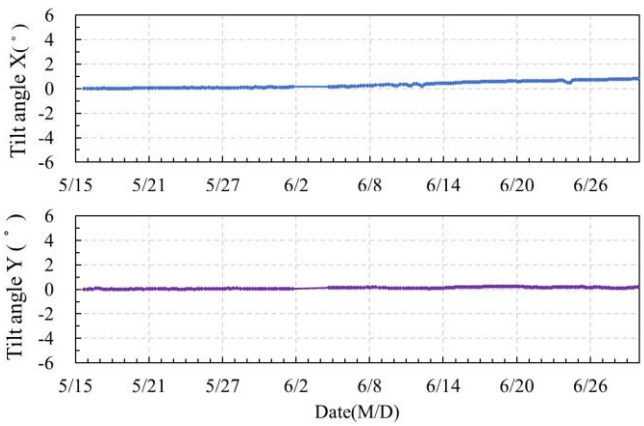

Figure 7.29 The data of tilt sensor, X is the slope direction

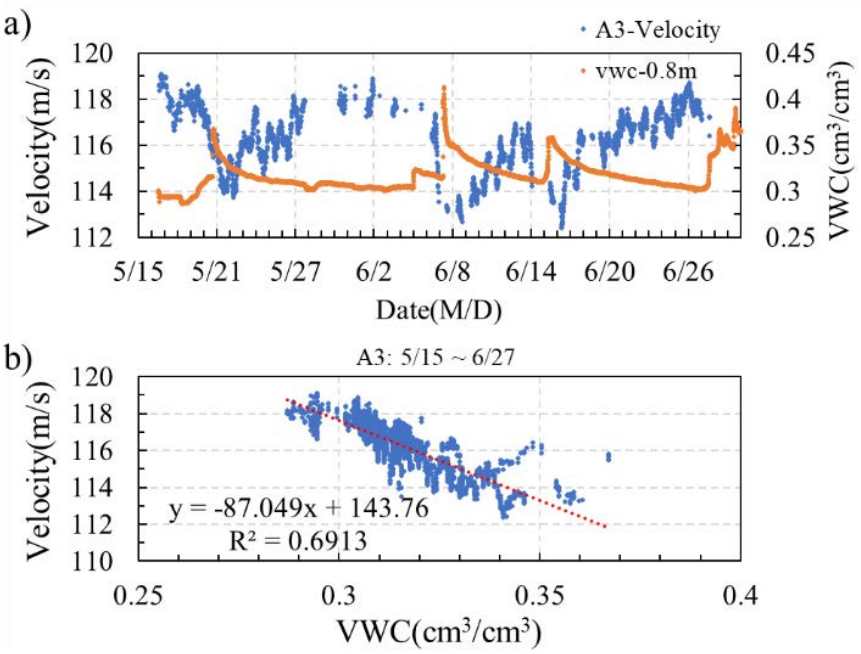

Figure 7.30 The effects of soil moisture on elastic wave velocities between A1-A3.

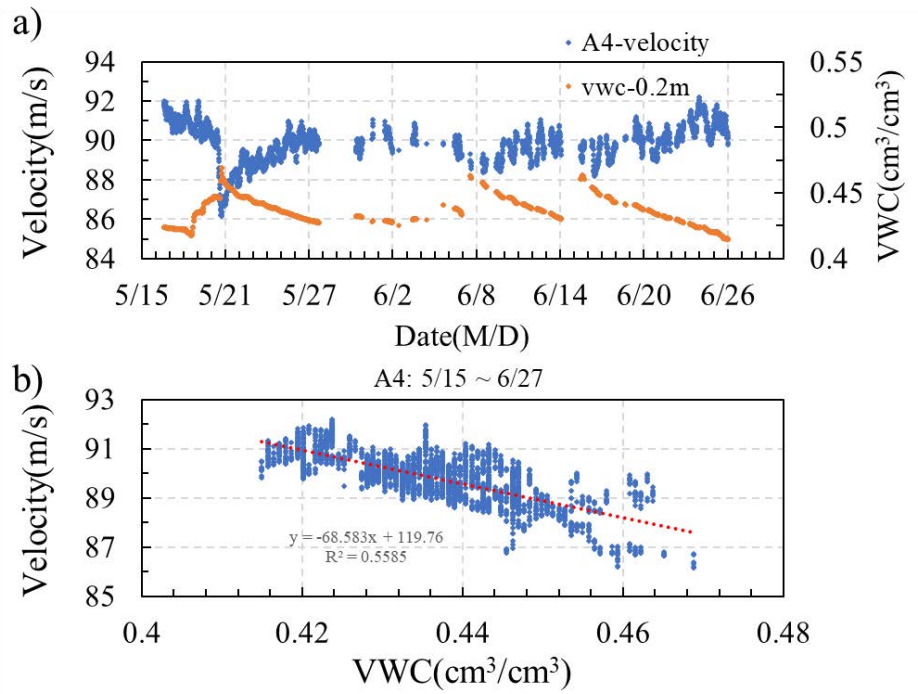

Figure 7.31 The effects of soil moisture on elastic wave velocities between A1-A4.

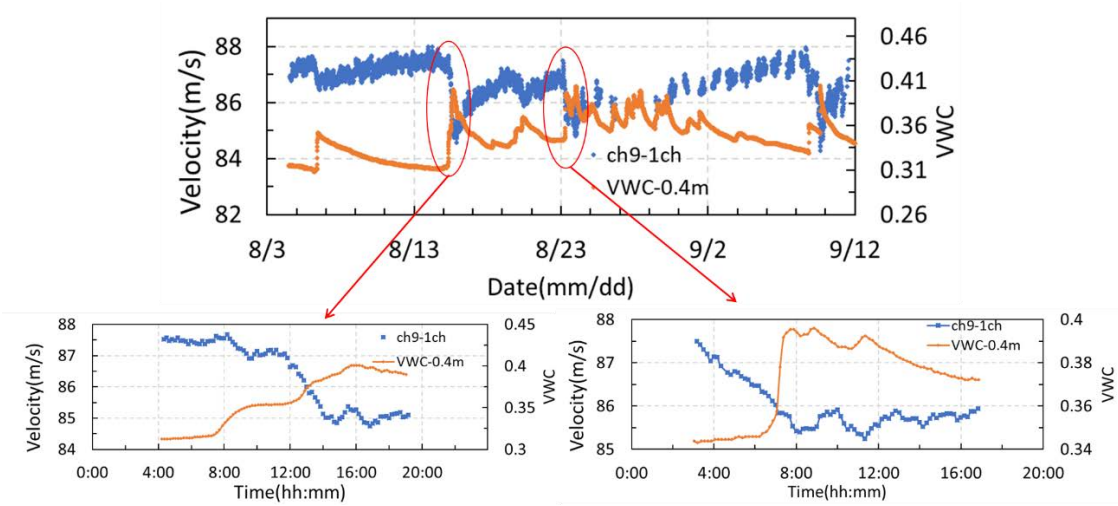

Figure 7.32 The effects of soil moisture on elastic wave velocities between A1-A5.

7.6 SUMMARY

Field investigation has been conducted to understand the behavior of elastic wave propagation in nature slope surface. The seismic refraction method and DCPT have been applied to measure the thickness of the surface layer. Attenuation and Frequency characteristics have been analyzed with differed exciter energy and distance. Based on the experiment results, the conclusions can be summarized as the following:

1)Thickness calculated by the seismic refraction method is not affected by different exciter energy.

2)At the same survey line, elastic wave attenuation is almost the same with different exciter energy.

3)The higher energy exciter, the higher frequency and spectral can be detected. The high frequency disappears quickly when far away from the exciter.

An undisturbed soil sample from a depth of 0.4m in this natural slope, the physical properties such as wet density, Moisture Content, and dry density was analyzed.

An elastic wave monitoring system including one exciter and several revivers have been developed and installed in nature unstable slope. The results of case 1 show that

wave attenuation behaviors with soil moisture are similar to laboratory experiments. The results of case 1 show that wave attenuation behaviors with soil moisture is similar to laboratory experiments. The results of case 2 show that the changes of wave velocities with soil moisture are also similar to laboratory experiments.

7.7 REFERENCE

Irfan, M., Uchimura, T., 2013. Effects of soil moisture on shear and dilational wave velocities measured in laboratory triaxial tests. Fifth Int. Young Geotech. Eng. Conf.

CHAPTER 8

CONCLUSIONS & RECOMMENDATIONS

8.1. INTRODUCTION

Rainfall-induced landslides commonly occur and cause severe human and infrastructural damage around the world. landslide early warning systems are an alternative soft countermeasure that can provide an efficient and economical way to reduce the damage of landslides. The key of early warning systems is giving enough time to let people know the dangerous status of slope, so variation of different slope parameters such as soil moisture, normal stress, shear stress, shear deformation and so on are used to determine the status of slope when these parameters approach their respective critical values to issue a warning. The purpose of this study is to propose a method to predict the instabilities of slope by elastic wave propagation in soil. Laboratory model experiments are designed to investigate the factors affecting on elastic wave, and on-site monitoring is conducted to verify this method. Laboratory experiments using a multi-layer shear model simulating shallow slope failure were conducted to observe the changes in elastic wave velocities and attenuation in a slope surface layer. A series of experiments were designed to reproduce the slope failure. The detailed behavior of elastic wave over a wide range of soil moisture, shear stress, and shear deformation was analyzed. The factors affect on elastic wave velocity have been confirmed. An elastic wave monitoring system had been developed and installed in nature unstable slope. The layout of sensors and exciter underground and the monitoring parameters such as velocities, soil moisture, deformation from the sensors were discussed. Major conclusions derived from these studies are summarized in the following section.

8.2. CONCLUSIONS

8.2.1 Factors Effect on Wave Velocities in a Slope Surface Layer

A new type of exciter and receiver have been developed by assembling a MEMS accelerometer and using the AIC algorithm, which can automatically calculate the elastic wave travel time with accuracy and reliability. Laboratory experiments using a multi-layer shear model simulating shallow slope failure were conducted to observe the changes in elastic wave propagation in a slope surface layer. The results can be concluded as follows:

The soil moisture, normal stress, shear stress, shear deformation are the main parameter of the status of an unstable slope or slope failure. These parameters can be evaluated by elastic wave velocities. The change of velocity is presented as the following formula

$$\begin{aligned} V &= F(\sigma, VWC, \Upsilon) \\ &= g(\sigma) * f(VWC) * k(\Upsilon) \\ &= \left(a * (\sigma)^{m/2}\right) * (b * VWC) * (c * (\Upsilon)^{d}) \end{aligned}$$

Where σ is normal stress, VWC is volumetric water content, Υ is the shear strain, coefficient a, m, b, c, and d are constants, and they are determined from experiments.

Based on the results of experiments, the coefficient a, m, b, c and d in the formula are determined (a = 157.36, m = 0.43; b = - 235.89; c = 45.17; d = - 0.21).

The elastic wave velocities calculated by the coefficient and the input soil moisture and shear stresses were compared to the measured velocities, it showed they were the similar trend.

1) The wave velocities increased with increasing normal stress.

2) Effects of soil moisture on elastic wave velocities. The wave velocities decreased

with increasing soil moisture in the rain event and increased during the drain stage. The wave velocity ratio reduced by 0.1–0.2 when the volume of water content increased from 0.1 to 0.27 m^3/m^3.

3) Effects of shear stress on elastic wave velocities. The stronger the shear force applied, the lower the velocities observed. When loading a shear stress corresponding to slope angles of 24, 27, 29, and 31 degrees, a drop wave velocity of 0.2–0.3 was observed at the middle layer, and near 0.5 at the bottom layer.

4) Effects of shear displacement on elastic wave velocities. Increasing the displacement caused the wave velocities to also increase. The wave velocity ratio dropped by 0.2 after 3 mm of displacement.

8.2.2 Wave Attenuation Changes in a Shallow Slope

Laboratory experiments using a multi-layer shear model simulating shallow slope failure were conducted to observe the changes in elastic wave propagation in a slope surface layer. By applying the Fast Fourier Transformation (FFT), the elastic wave signals can be converted from the time domain into the frequency domain, and the frequency component with maximum amplitude in the spectrum was defined as the dominant frequency. Elastic wave attenuation is the wave energy ratio, which mainly relates to wave frequency and amplitude. The results can be concluded as follows:

1) Elastic wave attenuation is sensitive to soil moisture, due to the amplitude of high frequency decreases sharply with the increase of soil moisture. the wave energy reduced by 20%~50% when the VWC grew up from 0.1 to 0.25 m^3/m^3.

2) The stronger shear force applied, the lower energy ratio observed. Wave energy ratio reduced 20%~40% when shear force increases from 27 to 31degrees

3) With increasing the displacement, the wave attenuation also increased. Wave energy ratio dropped by 50% during a 3 mm of displacement.

8.2.3 Elastic Wave Monitoring on Natural Slope Surface layer

Before the application of the elastic wave, field investigation has been conducted to understand the behavior of elastic wave propagation in nature slope surface. The seismic refraction method and DCPT have been applied to measure the thickness of the surface layer. Attenuation and Frequency characteristics have been analyzed with differed exciter energy and distance.

An undisturbed soil sample from a depth of 0.4m in this natural slope, the physical properties such as wet density, Moisture Content, and dry density was analyzed.

An elastic wave monitoring system including one exciter and several revivers have been developed and installed in nature unstable slope.

Based on the experiment results, the conclusions can be summarized as following:

1) Thickness calculated by the seismic refraction method is not affected by different exciter energy.

2) At the same survey line, elastic wave attenuation is almost the same with different exciter energy.

3) The higher energy exciter, the higher frequency and spectral can be detected. The high frequency disappears quickly when far away from the exciter.

4) Wave attenuation behaviors with soil moisture are also similar to laboratory experiments. In the dry process, the energy ratio of the elastic wave tends to increase with the decrease of VWC. On the contrary, in the wet process (rainfall events), the energy ratio of the elastic wave tends to decrease with the increase of VWC.

5) From the data of the tilt sensor, the deformation of the slope is very small, the elastic wave velocities mainly affected by the soil moisture. Elastic wave velocities changes with soil moisture are also similar to laboratory experiments.

8.3. RECOMMENDATIONS FOR FUTURE RESEARCH

Due to the limitation of time, apparatus and the scope of the current study, the finding of this study may be further extended in several aspects. Some recommendations for future researches are summarized below;

1. The scope of the present study was limited to Silica sand of silica sand No. 4, No. 5, No. 7 and No. 8 mixed at a ratio of 1:1:3:1 and a natural slope only. It is maybe better to confirm other soil types such as clayey soils and colluvial deposits in the Laboratory experiments. This can be expanded to other aspects which may better represent the in-situ ground conditions, such as anisotropy and lack uniformity.

2. Laboratory experiments using a multi-layer shear model were conducted to reproduce the slope failure, can simulate the rainwater infiltrate from the ground surface. However, it cannot simulate the increase of the groundwater level. Some slope failure occurs after the rainfall maybe is the result of the increase of groundwater level.

3. Installed an elastic wave monitoring system in the actual field required to clear the following factors, firstly, well in-situ investigation and understand the conditions of the slope surface, it is ideal to find out the sliding surface. Secondly, make sure the system can run continually not stop for the runout battery. Finally, the more range of wave propagation the more wave energy is required.